

144-564

NASA CR.

144-564

SKYLAB PROGRAM

EARTH RESOURCES EXPERIMENT PACKAGE

SENSOR PERFORMANCE EVALUATION FINAL REPORT VOLUME III (S192) -

(NASA-CR-144564) SKYLAB PROGRAM EARTH

N76-13563

RESOURCES EXPERIMENT PACKAGE SENSOR
PERFORMANCE EVALUATION, VOLUME 3, (S192)

Final Report (Martin Marietta Corp.). 106 p

Unclas

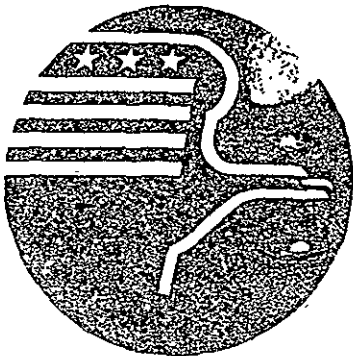
HC \$5.50

CSCI 05B G3/43 03899

MAY 5, 1975

CONTRACT NAS8-24000

AMENDMENT JSC-14S



National Aeronautics and Space Administration
LYNDON B. JOHNSON SPACE CENTER
Houston, Texas

JSC-05546

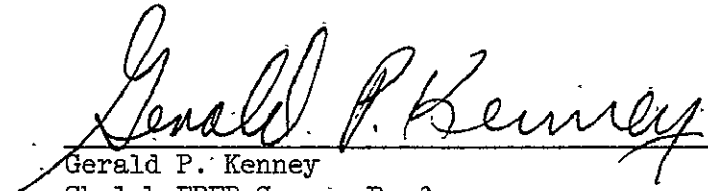
EARTH RESOURCES EXPERIMENT PACKAGE

SENSOR PERFORMANCE REPORT
VOL. III (S192)

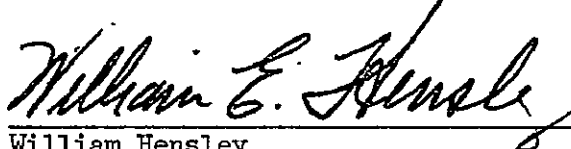
FINAL REPORT

MAY 5, 1975


Submitted by:


Gerald P. Kenney
Skylab EREP Sensor Performance
Evaluation Manager, JSC/HC

Technical
Review by:


William Hensley
S192 Project Scientist, JSC/TF

Approved:


Richard A. Moke
Manager, Systems Analysis and
Integration Office, JSC/HC

Contract NAS8-24000
Amendment JSC-14S

Skylab Program
Lyndon B. Johnson Space Center

MSC-05546 Volume III

FOREWORD

This volume is Section III of six sections of document MSC-05546, submitted by Martin Marietta Corporation, in accordance with the requirements of Annex I to Exhibit A, Statement of Work, Part I, Data Requirements List, of Contract NAS8-24000, Amendment JSC-14S, Line Item 295; and was prepared under WBS 02216.

CONTENTS

Section	Page
1.0 INTRODUCTION	III-1
1.1 Purpose	III-1
1.2 Scope	III-1
1.3 Usage Guide	III-1
1.4 Abstract	III-2
2.0 APPLICABLE DOCUMENTS	III-3
3.0 SUMMARY OF SENSOR PERFORMANCE EVALUATION INTERIM REPORT	III-4
3.1 Function/Limit Verification	III-4
3.2 Data Interference	III-7
3.3 Response versus Scan-Angle Determination	III-8
3.4 Absolute Radiometric Accuracy and Stability	III-17
3.5 System Frequency Response	III-25
3.6 Geometric Distortion	III-32
3.7 Noise Analyses	III-33
3.8 Pointing Accuracy and Field-of-View Determination	III-38
3.9 Photographic Image Adequacy for Site Location	III-40
3.10 Geometrical Band-to-Band Registration Error	III-41
4.0 SUPPLEMENTARY ANALYSES	III-43
4.1 Supplementary Analysis of Scan-Related System Response	III-43
4.2 Supplementary Analysis of System Noise	III-48
4.3 S190A, S191, and S192 Radiometric Comparison	III-49
5.0 CONCLUSIONS	III-57
6.0 RECOMMENDATIONS	III-57

Section	Page
7.0 NOTES	III-58
7.1 Acknowledgements	III-58
7.2 Abbreviations	III-59
APPENDIX A — TECHNIQUES ADDENDUM	III-A-1

TABLES

Table	Page
3.1.1-1 CONTROLLED HOUSEKEEPING FUNCTION SUMMARY	III-5
3.1.1-2 UNCONTROLLED HOUSEKEEPING FUNCTION SUMMARY	III-6
3.1.2-1 CALIBRATION DATA STATUS	III-6
3.7.1-1 STANDARD DEVIATIONS, ATTENUATORS OUT	III-33
3.7.1-2 STANDARD DEVIATIONS, ATTENUATORS IN	III-34
3.7.1-3 NOISE-EQUIVALENT SPECTRAL RADIANCES (NESR), ATTENUATORS IN	III-37
3.7.1-4 NOISE-EQUIVALENT SPECTRAL RADIANCES (NESR), ATTENUATORS OUT	III-38
3.7.2-1 THERMAL-BAND NOISE	III-39
3.8.1-1 MAXIMUM LATITUDE AND LONGITUDE DIFFERENCE BETWEEN S192 DATA AND POINTING ESTIMATES DETERMINED FROM SKYLAB ATTITUDE TELEMETRY	III-39
3.10-1 EXTRACT FROM LC1 DATA (NORMALIZED)	III-42
4.2-1 S192 MULTISPECTRAL SCANNER SENSITIVITY (NOISE)	III-50
4.3-1 S190A, S191, S192 SPECTRAL BANDS FOR RADIOMETRIC COMPARISON	III-51
4.3.1-1 S191 SPECTRAL RADIANCE FOR S190A AND S191 COMPARISON SITES	III-52
4.3.1-2 S190A, S191, AND GROUND-TRUTH RADIOMETRIC COMPARISON . . .	III-53
4.3.2-1 S190A, S192, AND GROUND-TRUTH RADIOMETRIC COMPARISON . . .	III-54
4.3.3-1 S191 SPECTRAL RADIANCE OF RIO GRANDE RESERVOIR FOR COMPARISON OF S191 TO S192	III-55
4.3.3-2 S191, S192, AND GROUND-TRUTH RADIOMETRIC COMPARISON . . .	III-56
A.11-1 SAMPLE OF TABLE CONSTRUCTED TO FACILITATE CALCULATION OF MEAN LUNAR RADIANCE BY BAND	III-A-17
A.11-2 ESTIMATED LUNAR RADIANCE NORMALIZED BY BAND, L	III-A-17

FIGURES

Figure		Page
3.3.2-1	Scan response	III-10
3.3.2-2	Scan response (continued)	III-11
3.3.2-3	Scan response (continued)	III-12
3.3.2-4	Scan response (continued)	III-13
3.3.2-5	Scan response (continued)	III-14
3.3.2-6	Scan response (concluded)	III-15
3.3.3-1	Residual effects (Z_j')	III-16
3.3.3-2	Response versus scan angle	III-17
3.4.1-1	Comparison of equivalent calibration lamp radiances . . .	III-20
3.4.1-2	Band 13-1 Y-3 CDDP thermal band calibration	III-21
3.4.1-3	Band 13-2 X-5 CDDP thermal band calibration	III-21
3.4.2-1	Geometry of data utilized in off-axis rejection determination	III-22
3.4.2-2	Off-axis rejection across track	III-23
3.4.2-3	Off-axis rejection along track	III-23
3.4.3-1	SL3 spectral response determination	III-24
3.5.2-1	Average response versus distance from lunar edge for band 1, SL3	III-27
3.5.2-2	Average response versus distance from lunar edge for band 2, SL3	III-27
3.5.2-3	Modulation transfer function (MTF) for band 1, SL3 . . .	III-28
3.5.2-4	Modulation transfer function (MTF) for band 2, SL3 . . .	III-28
3.5.2-5	Idealized modulation transfer function (MTF)	III-29
3.5.3-1	Frequency response for SL4, Y3, LC4, band 1	III-30

Figure		Page
3.5.3-2	Frequency response for SL4, Y3, LC4, band 2	III-31
3.7.1-1	Data-word histogram, band 1	III-35
3.7.1-2	Power spectral density plot, band 7	III-36
4.1-1	Scene data minus calculated real offset	III-44
4.1-2	Comparison of SL3 scene (Sahara Desert) with prelaunch data for band 3	III-44
4.1-3	Comparison of S192 data product and S190A densitometry data	III-46
4.1-4	S190A computed scene radiance variation for Sahara Desert	III-47
4.1-5	Comparison of S192 data for Sahara Desert corrected for S190A scene radiance variation with prelaunch data for band 3	III-47
4.3.1-1	S191 spectral radiance plot for S190A and S191 comparison sites	III-53
4.3.3-1	S191 spectral radiance of Rio Grande Reservoir, SL3 . . .	III-55
A.I-1	Sample determination of ground-truth atmospheric and target radiance for an S192 band	III-A-5
A.II-1	Geometric albedo of the Moon	III-A-11
A.II-2	Correction for lunar phase angle	III-A-15
A.II-3	Selection of lunar data	III-A-19
A.II-4	A-trace of averaged scan line centered on lunar diameter (LC 1, band 6)	III-A-19
A.III-1	Correction curves for clipped mean values	III-A-22
A.VIII-1	Reflection from water surface at 0, 60, and 80° incidence angles	III-A-37
A.VIII-2	Reflectivity and emissivity of water verses incidence angle	III-A-37
A.VIII-3	Upwelling radiance calculation	III-A-38

1.0 INTRODUCTION

1.1 Purpose

This document reports the final results of the sensor performance evaluation for the multispectral scanner (S192) of the Skylab Earth Resources Experiment Package (EREP) and is based on data and evaluations reported in the interim performance evaluation report (MSC-05528, Volume III, dated September 6, 1974).

1.2 Scope

This document summarizes the results of S192 sensor performance evaluation based on data presented by all contributors (Martin Marietta Corporation, the Environmental Research Institute of Michigan, and the Science and Applications Directorate of the Lyndon B. Johnson Space Center) to the sensor performance evaluation interim reports, provides the result of additional analyses of S192 performance, and describes techniques used in sensor performance evaluation (Appendix A). The summarization includes significant performance changes identified during the Skylab missions, S192 and EREP system anomalies that affected S192 performance, and the performance achieved, in terms of pertinent S192 parameters. The additional analyses include final performance analyses completed after submittal of the SL4 interim sensor performance evaluation reports, including completion of detailed analyses of basic performance parameters initiated during the interim report periods and consolidation analyses to reduce independent mission data (SL2, SL3, and SL4) to determine overall performance realized during all three Skylab missions.

1.3 Usage Guide

The basic task outline for the EREP sensor performance evaluation was specified EREP Mission Data Evaluation Requirements, JSC-05529, August 31, 1973. The results of these evaluations were subsequently reported in MSC-05528, Earth Resources Experiment Package, Sensor Performance Report, Volumes I through VII, as follows:

Volume I (S190A)	Multispectral Photographic Camera
Volume II (S191)	Infrared Spectrometer
Volume III (S192)	Multispectral Scanner
Volume IV (S193 R/S)	Radiometer/Scatterometer
Volume V (S193 Alt)	Altimeter
Volume VI (S194)	L-Band Radiometer
Volume VII (S190B)	Earth Terrain Camera

These volumes were issued after prelaunch testing at KSC and updated after each mission. The single exception is Volume VII (S190B), which was originally issued after SL3, with a single update after SL4.

This document is based on the data and analyses in the first six volumes of the sensor performance report, MSC-05528 (Volume VII, S190B, is not included). The same volume designation used for MSC-05528 has been retained for the individual sensor volumes, with the individual volumes bound in a single cover and identified as MSC-05546. The individual volumes are designed so they can be used independently of the full six-volume report, if desired.

1.4 Abstract

A prelaunch and flight performance evaluation of the multispectral scanner (S192) has been made and a summarization is provided. The following aspects of S192 performance are among those discussed--absolute radiometric calibration, noise, system frequency response, and scan-related response. The primary performance problem was signal noise, especially in the thermal band when the Y-3 detector was in use. Final results regarding achieved performance, significant performance changes, and anomalies are presented.

S192 accomplished its primary objective to simultaneously gather quantitative radiance values suitable for image reconstruction in 13 spectral bands.

Techniques used for sensor performance evaluation are described.

2.0 APPLICABLE DOCUMENTS

- MSC-05528 Earth Resources Experiment Package, Sensor Performance Report, Volume III (S192), Engineering Baseline, SL2, SL3, and SL4 Evaluation; Lyndon B. Johnson Space Center, Houston, Texas, September 6, 1974.
- MSC-05531 Ground Truth Data for Test Sites (SL2); Lyndon B. Johnson Space Center, Houston, Texas, August 15, 1974.
- MSC-05537 Ground Truth Data for Test Sites (SL3); Lyndon B. Johnson Space Center, Houston, Texas, March 29, 1974.
- MSC-05543 Ground Truth Data for Test Sites (SL4); Lyndon B. Johnson Space Center, Houston, Texas, April 30, 1974.

3.0 SUMMARY OF SENSOR PERFORMANCE EVALUATION INTERIM REPORT

After preflight testing of EREP experiments at Kennedy Space Center and after each Skylab mission, raw data from preflight tests and each mission were reduced to provide performance data for each EREP sensor. These data were presented by mission in interim sensor performance evaluation reports entitled EREP Sensor Performance Report (Engineering Baseline, SL2, SL3, and SL4 Evaluation), MSC-05528, Volumes I through VII. Preflight test data and selected qualification test data were the engineering baseline, and flight data were added after each Skylab mission. This section summarizes the sensor performance report, MSC-05528, Volume III (S192), Change 3, September 6, 1974, paragraph by paragraph. To provide traceability, applicable interim report paragraphs in the summary are referenced.

3.1 Function/Limit Verification

Analysis of sensor performance properly began with an evaluation of those parameters that indicated the relative "health" of the instrument. These were instrument oriented measurements with expected values or limits. Evaluation of the S192 multispectral scanner included verification of four such indicators of sensor operation--housekeeping values, calibration data status, data loss rate, and alignment history. The following paragraphs summarize the data analyzed with respect to these indicators during evaluation of the performance of the S192, during ground test, SL2, SL3, and SL4. The detailed evaluation is in Section 3 of MSC-05528, Volume III, dated September 6, 1974.

3.1.1 Housekeeping Functions

S192 housekeeping parameters were monitored throughout the prelaunch and orbital operations. All parameters indicated proper operation of the S192. Maximum and minimum values observed during these operations are summarized in Tables 3.1.1-1 and 3.1.1-2.

Table 3.1.1-1 summarized the operation of those parameters that were regulated. These data indicate that, throughout testing and the Skylab missions, these parameters were controlled to within 0.3°K in temperature and less than 1 milliampere variation in calibration lamp current. The cold blackbody temperature was the only parameter to show a larger variation, and that was only 1.5°K.

Table 3.1.1-2 summarizes housekeeping temperatures that were not controlled. The in-flight range of values is divided into two columns. The first column gives the range of values that occurred during the first eight passes of SL2. During this time, the Skylab wall heaters were not used due to power constraints. The low wall temperatures caused several sensor temperature to go below expected limits. The second column summarizes the range of temperature noted throughout the rest of the SL2, SL3, and SL4 missions. During this

TABLE 3.1.1-1.- CONTROLLED HOUSEKEEPING FUNCTION SUMMARY

PARAMETER	DATA WORDS	EXPECTED RANGE	TEST RANGE	IN-FLIGHT RANGE
Hot Blackbody Temperature	109	318 - 322 °K	Not applicable in ambient conditions	321°K
	126	318 - 322 °K		321°K
Cold Blackbody Temperature	110	258 - 262 °K	Not applicable in ambient conditions	260.0 - 260.5 °K
	127	258 - 262 °K		260.5 - 261.5 °K
100% Earth Cal Lamp Current	111	Cal 3 HI 0- 20 mA	0 mA	0 mA
		Cal 3 LO 180-220 mA	184 mA	184 mA
200% Earth Cal	113	Cal 3 LO 0- 20 mA	186 mA	186 mA
		Cal 3 HI 180-220 mA		
Detector Array Temperature	114	95°K	94°K	94°K

time, all temperatures were within expected limits, except for the door temperature and scan-motor temperature. The door temperature dropped below expected limits only during lunar calibration passes, while the scan-motor temperature exceeded expected limits during most passes. The scan motor's nominal operating temperature range was from 316 to 320°K. This was not considered an anomaly but an error in determining the expected operating temperature based on theoretical functioning of the heat pipe.

3.1.2 Calibration Data Status

Calibration data are the sensor outputs in counts when viewing the calibration sources inside the sensor. Table 3.1.2-1 summarizes the maximum and minimum mean values of the six calibration words from a few example data sets for each band in eight configurations. Where a range of values is not given, only one data set was available. The output values given for the automatic gain control bands (i.e., bands 4 through 13 without attenuation, and bands 6 and 9 through 13 with attenuator installed) are mean values of the six calibration words (which vary in count value due to the variation from uniformity of the internal calibration source radiance) one or more of which are usually clipped at 255. The six calibration words vary from 255 because the radiance of the internal calibration source is non-uniform and each of the six values is taken from a different portion of the source as the instantaneous field of view scans across it. The automatic gain control systems attempt to make the value on the analog-to-digital converters either 254 or 255 after the sixth calibration source value has been sampled. The last word is usually clipped at 255 and the fifth word is frequently 255, but the first four words are seldom 255. The randomness is due to the noise on the signals.

TABLE 3.1.1-2.- UNCONTROLLED. HOUSEKEEPING FUNCTION SUMMARY

PARAMETER	DATA WORDS	EXPECTED RANGE (°K)	TEST RANGE (°K)	IN-FLIGHT RANGE (°K)	
				SL2 Passes 1-8	SL2 Passes 9-11, SL3 & SL4
Primary Mirror Temperature	115 117	289 - 311	296 - 301	286.0 - 292.0	290.5 - 294.0
Secondary-Mirror Temperature	116	289 - 309	298 - 301	286.5 - 292.0	289.0 - 294.5
Aspheric-Mirror Temperature	118	288 - 312	296 - 299	286.0 - 292.0	290.0 - 293.0
Door Temperature	119	284 - 322	297 - 300	284.0 - 289.0	279.5 - 289.5
Scan-Motor Temperature	120	289 - 316	304 - 306	302.0 - 320.0	300.0 - 324.0
Cooler-Case Temperature	121	289 - 311	304 - 306	292.0 - 300.0	298.0 - 303.5
Internal-Scanner Assembly Temperature	122	289 - 329	305 - 307	292.0 - 300.0	300.0 - 304.5
Monochromator Temperature	123	289 - 311	299 - 307	288.0 - 292.5	293.0 - 298.0
Digital-Electronics Assembly Temperature	124	289 - 329	304 - 311	*Less than 304.5	*Less than 304.5

* Temperature was usually less than 303.16°K, the zero digital count output.

TABLE 3.1.2-1.- CALIBRATION DATA STATUS

Band	SYSTEM RESPONSE TO HIGH CALIBRATION SOURCE (Counts)							
	Pre-launch		SL2		SL3		SL4	
	With Attenuator	Without Attenuator	With Attenuator	Without Attenuator	Preattenuator Adjustment	Postattenuator Adjustment	Y-3	X-5
1	NA	29.3	32.7 - 40.8	43.4	29.3 - 33.2	29.0 - 32.1	29.9 - 32.1	8.1 - 9.9
2	38.8	34.3	32.8 - 39.6	40.8	27.2 - 28.2	27.2 - 33.8	27.9 - 31.9	5.6 - 7.3
3	59.5	80.4	45.8 - 48.6	44.9	44.6 - 45.6	45.1 - 48.5	42.2 - 49.6	17.8 - 20.4
4	95.6	249.8	72.6 - 79.5	249.0	83.4 - 83.8	97.8 - 101.5	82.5 - 89.7	246.5 - 247.8
5	102.9	251.5	71.2 - 80.3	250.7	73.8 - 75.4	159.9 - 168.4	130.8 - 140.3	Inoperative
6	253.8	253.4	246.1 - 254.1	254.2	245.7 - 246.1	245.5 - 247.2	244.8 - 246.4	250.0 - 252.5
7	159.9	251.5	137.1 - 148.3	254.5	152.0 - 156.9	153.1 - 162.6	183.5 - 204.5	82.1 - 96.3
8	184.4	253.0	177.5 - 185.1	254.3	172.3 - 175.9	177.6 - 187.3	185.8 - 201.3	252.4 - 254.9
9	253.6	253.7	253.1 - 253.3	253.9	248.8 - 249.7	249.6 - 250.1	247.9 - 249.7	216.6 - 218.4
10	253.1	253.3	252.8 - 253.9	254.5	244.7 - 245.1	244.7 - 246.4	243.2 - 246.6	Inoperative
11	254.4	251.7	254.6 - 254.8	254.9	248.3 - 248.5	247.5 - 248.8	246.6 - 250.3	253.0 - 254.2
12	253.9	251.4	254.5 - 254.7	254.8	239.2 - 239.5	236.7 - 240.7	236.4 - 241.4	239.2 - 247.2
13-1	NA	NA	238.8 - 242.0	241.6	242.0 - 242.7	241.5 - 242.4	241.5 - 243.0	242.2 - 243.9
13-2	NA	NA	253.1 - 255.0	255.0	259.0 - 255.0	255.0 - 255.0	255.0 - 255.0	255.0 - 255.0

3.1.3 Data Loss

Data loss rate was evaluated by analysis of the frame synchronization pattern and housekeeping data. The frame synchronization pattern was a fixed digital output in which errors could be detected. Housekeeping temperature data were evaluated for the percent of erroneous data presented. Due to the predictable nature of thermistor networks, anomalies were easily identified and a loss rate was determined. Since the synchronization patterns were inserted into the data stream at the output register of the S192 electronics assembly the data losses due to faulty synchronization patterns were almost certainly due to the data handling systems (probably in the Miller encoding/decoding operation or in reformatting). The faulty housekeeping temperature words could have arisen at any point in the data path--within S192 or without.

Loss rates were determined for prelaunch, SL2, SL3, and SL4 data. For prelaunch data; the average loss rates were as high as 0.35%. The Skylab data average loss rates varied from 0.001 to 0.01 percent.

There were data losses certainly not attributable to S192. As a result of inconsistencies in cleaning the tape recorder heads and the high temperature environment experienced by tapes launched on SL1, data were lost from bands 3 and 11. Because both of these bands were doubly sampled, the data loss was minimized. These were most notable on SL4 passes 44, 47, 48, 49, and LC6.

3.1.4 Alignment History

The alignment of the detector array to the incoming radiation was a crew procedure. Voice transcripts of crew comments recorded while performing the detector alignment verifications were reviewed to determine whether the proper alignment was achieved. During SL2, the cooler/dewar/detector/preamplifier assembly was improperly mounted to the optical bench, causing difficulties in alignment. A good alignment was not achieved until before pass 4. Alignments for the remainder of SL2 and during all of SL3 and SL4 were considered good.

3.2 Data Interference

An analysis was performed to determine any effects of interference from external sources detectable in the S192 data. The basic approach used was to evaluate S192 data taken while other EREP sensors and module systems were in various modes of operation. The data analyzed for comparison were the frame synchronization pattern, detector output data taken of a uniform scene, and the noise characteristics of the data.

Data from prelaunch testing and SL2 were analyzed in detail. The results indicated that S192 data were not susceptible to interference from potential sources in its operating environment. A detailed analysis was not performed on data from SL3 and SL4; however, the results of the noise analysis (See Section 3.7.) did not indicate the presence of interference.

Details of the data interference analysis were presented in Section 4 of MSC-05528, Volume III, September 6, 1974.

3.3 Response versus Scan-Angle Determination

S192 scan-related system response was determined using the techniques presented in Sections III and IV of Appendix A of this volume. Detailed results are presented in Section 5 of MSC-05528, Volume III, September 6, 1974.

3.3.1 Scan-Related Signal Offset Bands 1 through 12

To determine S192 response as a function of scan angle, it was necessary to first determine the response to a zero radiance level as a function of scan angle, that is, signal offset. Using the technique described in Appendix A, Section III, the mean value was determined from clipped digital data values on a pixel-by-pixel basis across the scan. Deep-space data from the lunar passes were used as an effective zero radiance input. Results from the six lunar passes performed during the Skylab missions indicated that the offsets were not constant. For five of the lunar passes, the offsets showed similar characteristics of shape. The other lunar passes yielded offsets with the same frequency characteristics but shifted in phase. Additionally, it was noted that, for a given lunar calibration, all bands had the same shaped offset function, with the major difference band-to-band being a larger amplitude for the fixed-gain bands than for the variable-gain bands. It was concluded that the offset was due to scan synchronous electrical pickup where the phase of the components varied. Examples of these characteristics are given in Section 4 of this volume.

3.3.2 Scan-Related System Response Bands 1 through 12

Scan-related system response was determined using the techniques described in Section IV of Appendix A. The response was evaluated for prelaunch and each of the three Skylab missions.

3.3.2.1 Prelaunch - Prelaunch testing was performed using the optical functional checkout unit as the external radiance source. This provided a "scene" known to be a uniform function of scan angle. The curves determined for scan-related system response were therefore the S192 response to a uniform input as a function of scan angle. Figures 3.3.2-1 through 3.3.2-6 present the normalized prelaunch curves for bands 1 through 12 as well as the flight results. Band 13 could not be determined before launch due to constraints on thermal band operation in a ground environment. Except for band 1, attenuator-in curves are shown for prelaunch results; however, as would be expected, insertion of the Attenuator Assembly makes no significant difference to scan-related system response.

3.3.2.2 Scan-Related System Response Band 1-12

The prelaunch and flight results are given in Figures 3.3.2-1 through 3.3.2-6.

The extent to which the flight curves are in fact affected by scene details is uncertain, so some subjective judgment is required in deciding whether significant changes have occurred. The undulations in many of the SL4/X5 results are probably due to scene details but the X5 curves do appear significantly changed from the Y3 results, particularly in the lower numbered bands. For Bands 4 through 8 the flight and prelaunch data tend to cluster about a common mean, though individual flight curves may look significantly different from their prelaunch counterparts. In Band 9 the flight curves slope down to the right a good deal more than do the prelaunch curves. The same effect occurs to a lesser extent for the SL2 and SL4/Y3 curves in Band 11. In addition, the prelaunch curves for Band 9 are much flatter than for 7, 8 and 10, and it has been suggested that the Band 9 prelaunch curves contain an error. It is, however, difficult to see how such an error could have been introduced. The Band 1 flight curves appear much less arched and overall have a steeper slope up to the right than prelaunch. This effect repeats to a reduced extent in Band 2 and perhaps, but hardly significantly, in Band 3. The SL4/X5 data are an exception in that the slope up to the right is continuous with only a little abatement through Band 3. For Bands 10, 11 and 12 the SL2 and to a lesser extent the SL4/Y3 data depart increasingly from prelaunch, becoming more arched and steeper downwards at the right end.

There seems little doubt that the scan angle effects have changed in some details from prelaunch and throughout the missions. However, particularly for the middle bands, the evidence of change is not substantial and selection of the best description of these effects is a difficult and inevitably subjective one.

It should also be remembered that each of the flight curves is formed by averaging 4 to 6 curves, each derived from individual scenes observed during the mission in question. Thus when making a decision as to whether the flight results should be used in place of the prelaunch curves, the spread of these individual curves was compared with the difference between their mean and the prelaunch curves. Complete details will be found in the individual evaluations for each mission, MSC-05528.

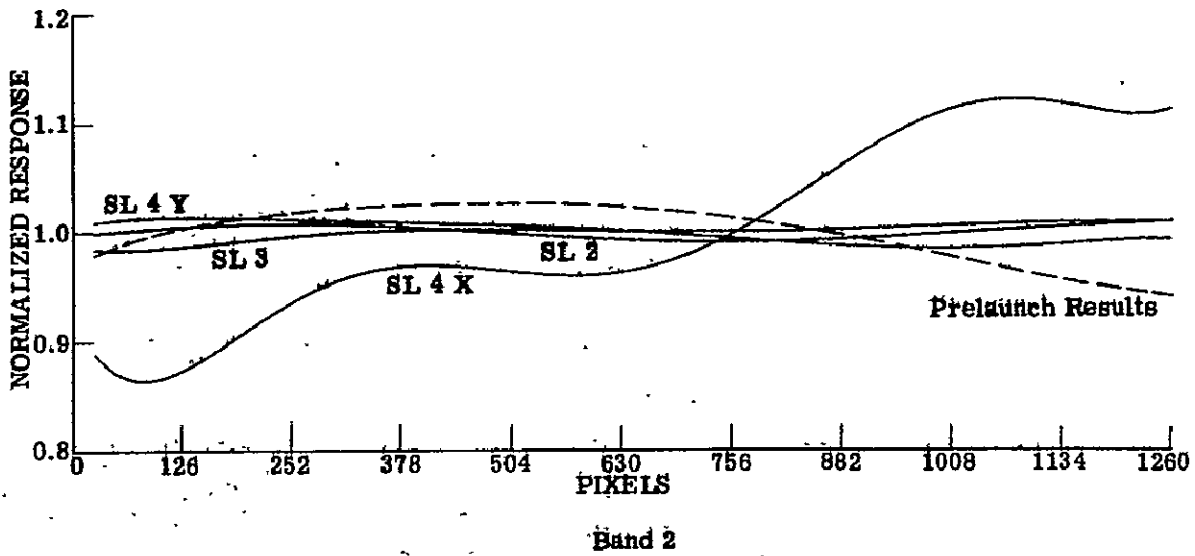
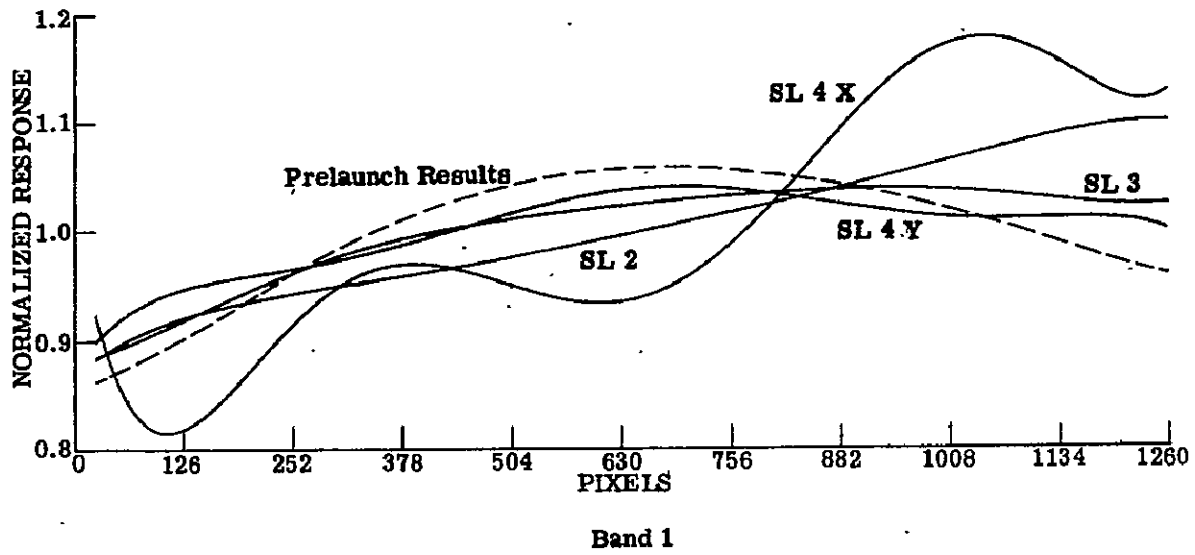


Figure 3.3.2-1.4 Scan response.

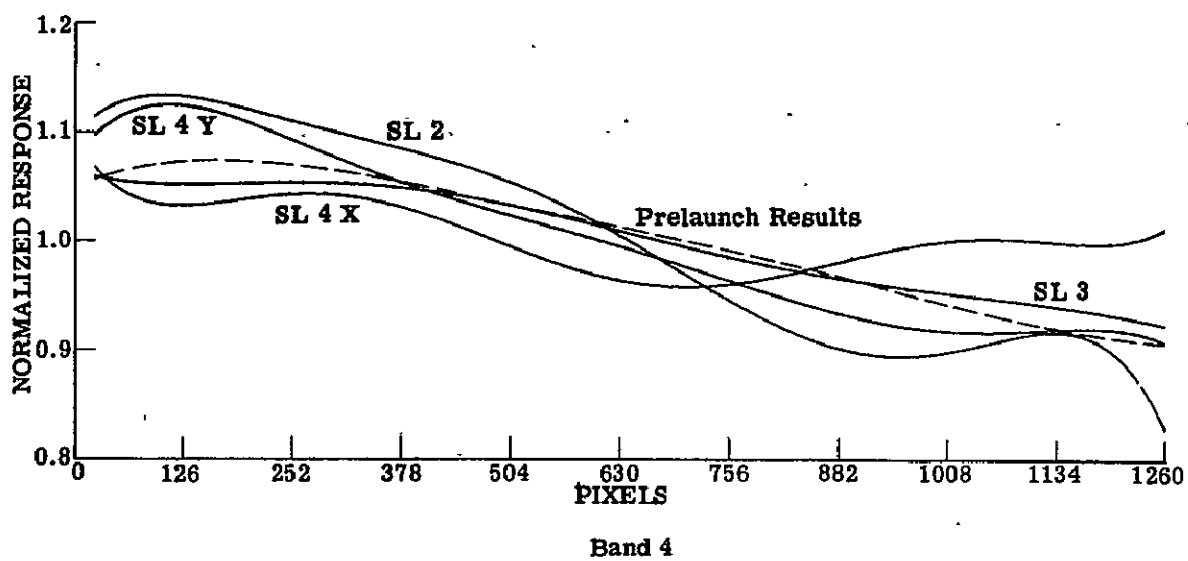
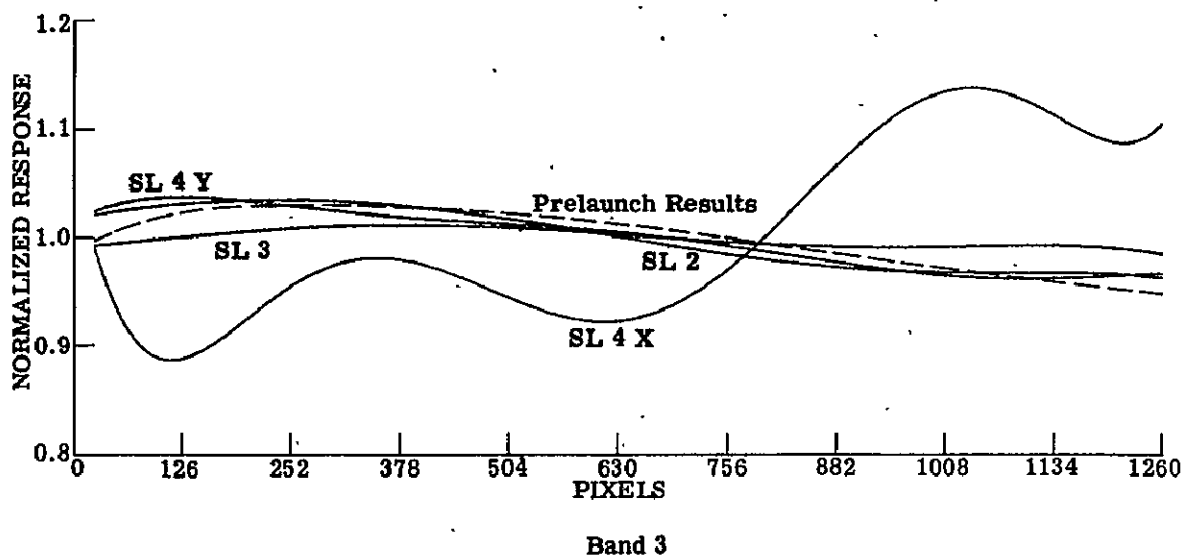


Figure 3.3.2-2.- Scan response (continued).

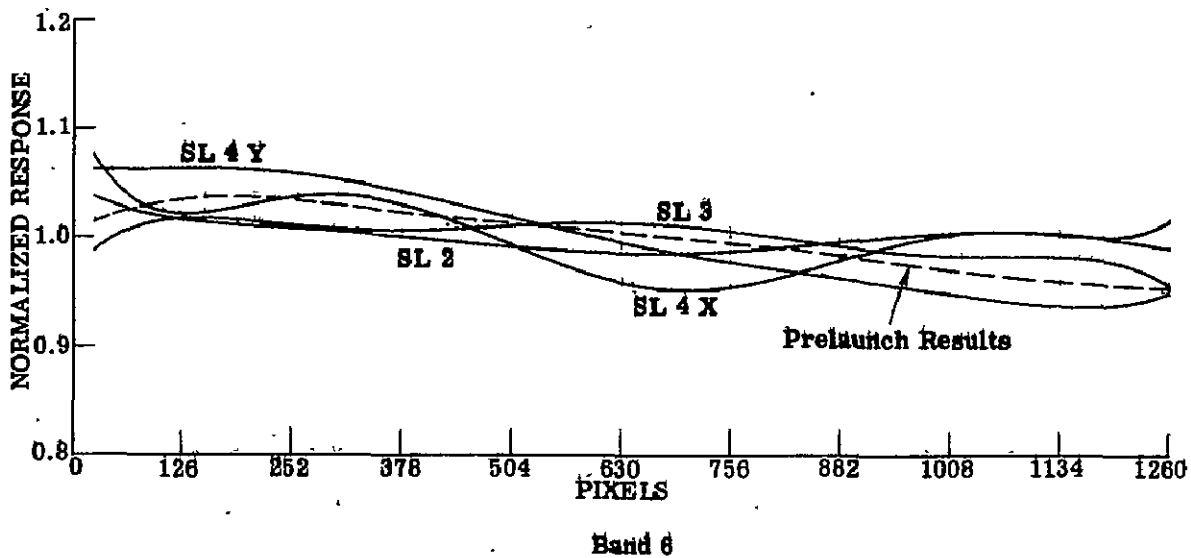
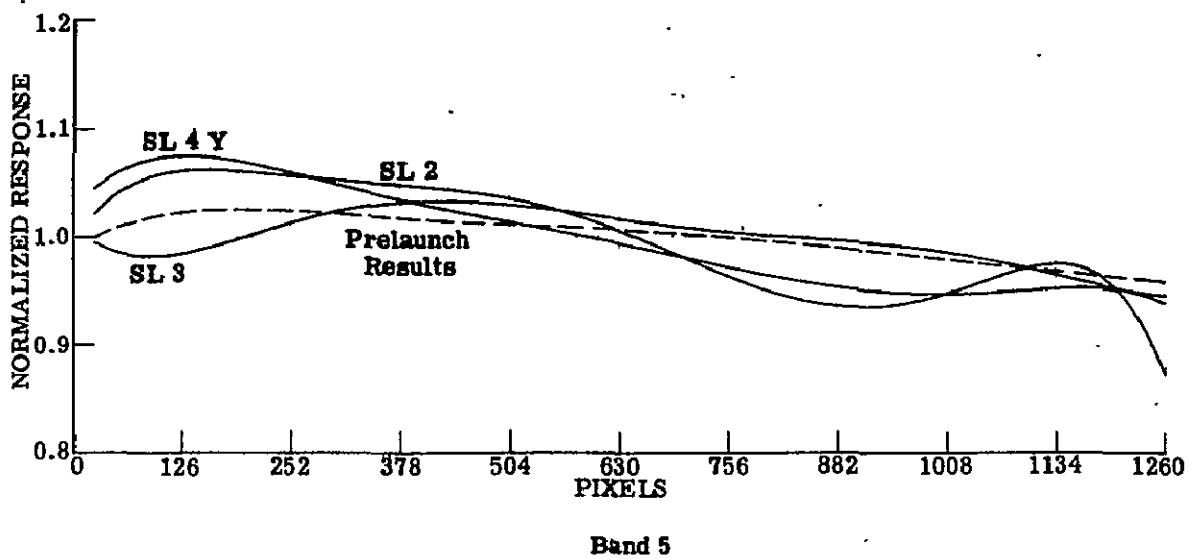


Figure 3:3.2-3:- Scan response (continued).

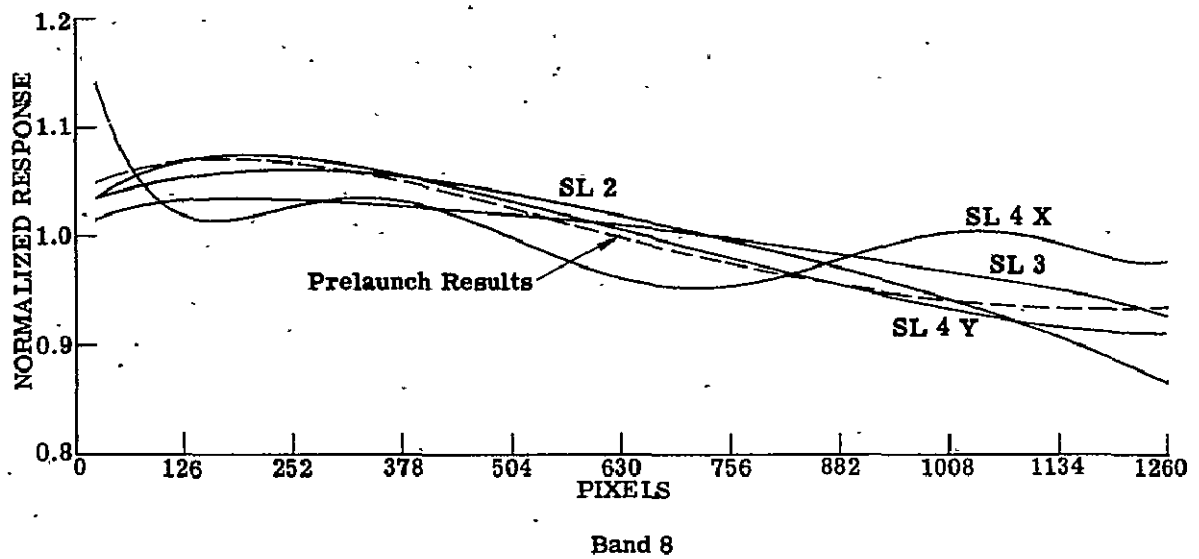
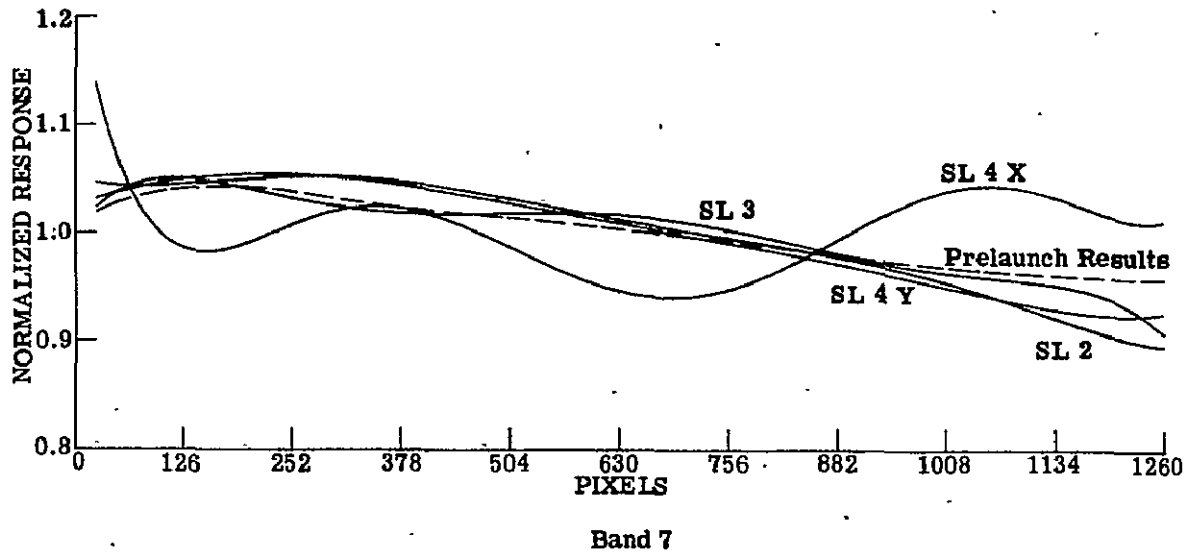


Figure 3.3.2-4.- Scan response (continued).

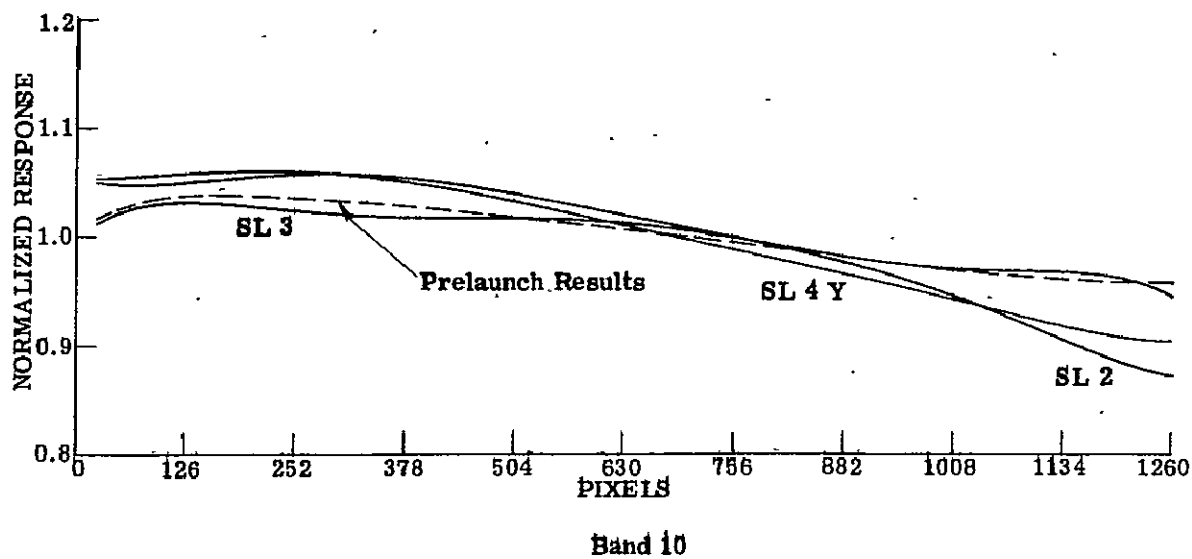
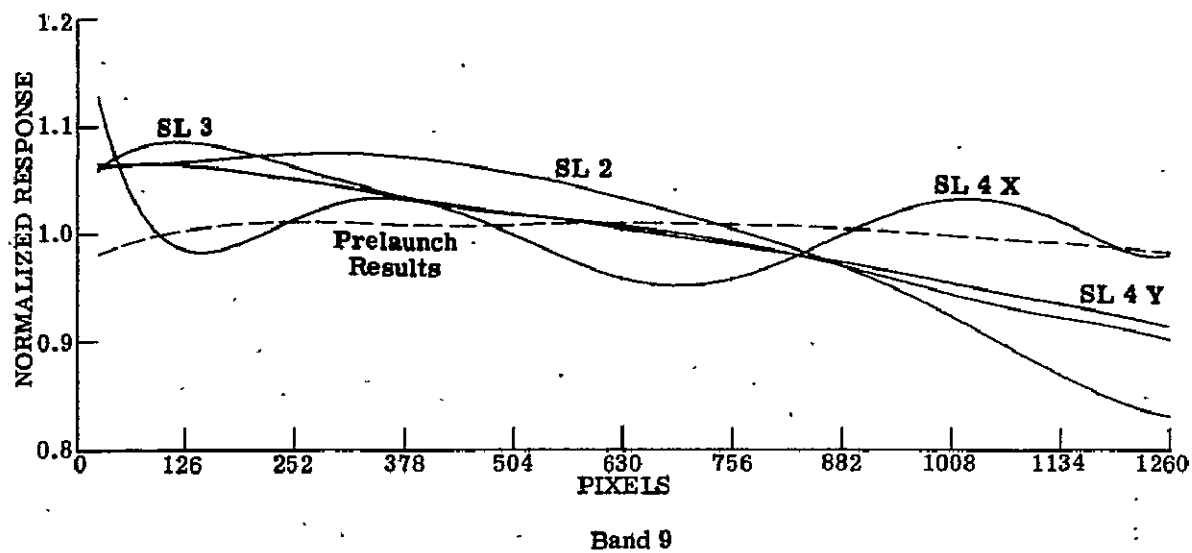


Figure 3.3.2-5.- Scan response (continued).

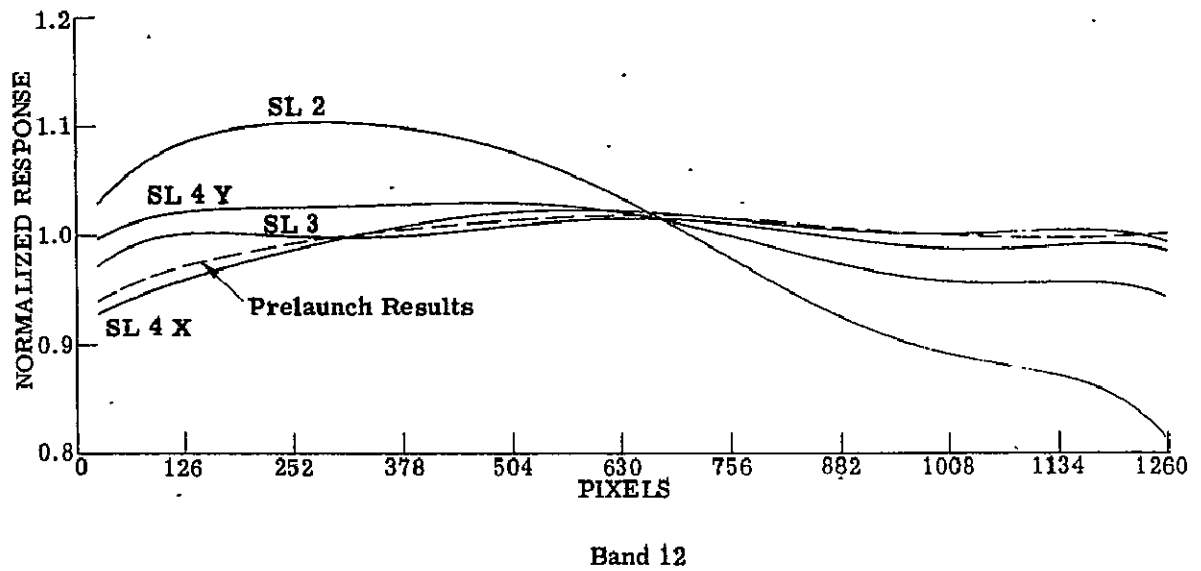
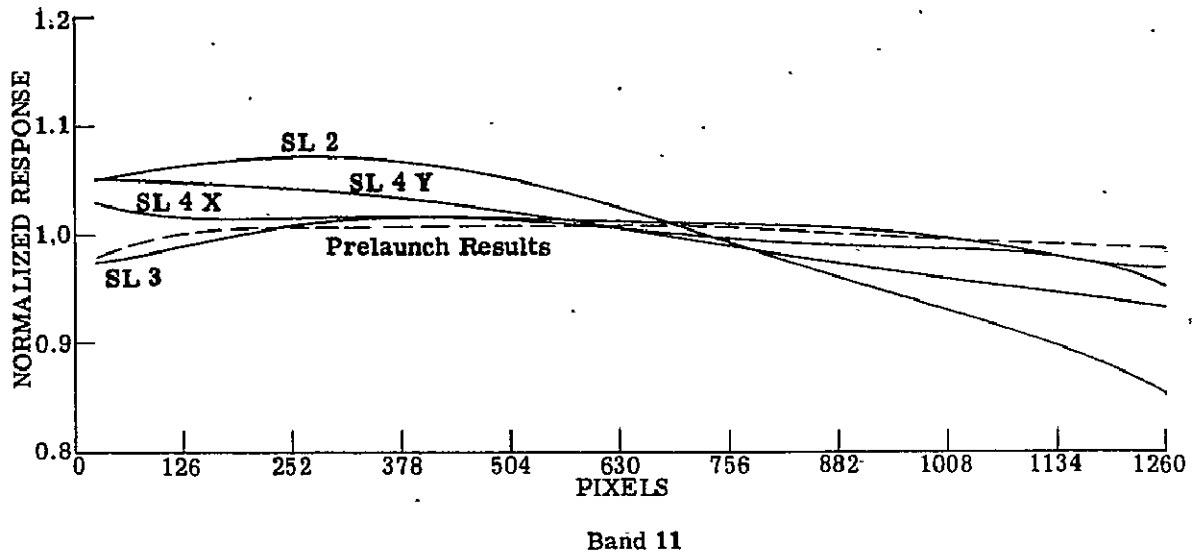


Figure 3.3.2-6.- Scan response (concluded).

3.3.3 Scan Related Signal Offset and System Response - Band 13

The response vs scan angle (R) and residual effects (Z_j) as defined in Appendix A, Section IV, are given in Figures 3.3.3-1 and 3.3.3-2. Bands 13-1 and 13-2 are equivalent but have different calibration source offsets and gains, so that 13-1 has an extended dynamic range. No prelaunch data are available for comparison. The results for the Y3 detector for the three missions are quite similar, though as might be expected the results for the X5 detector are significantly different.

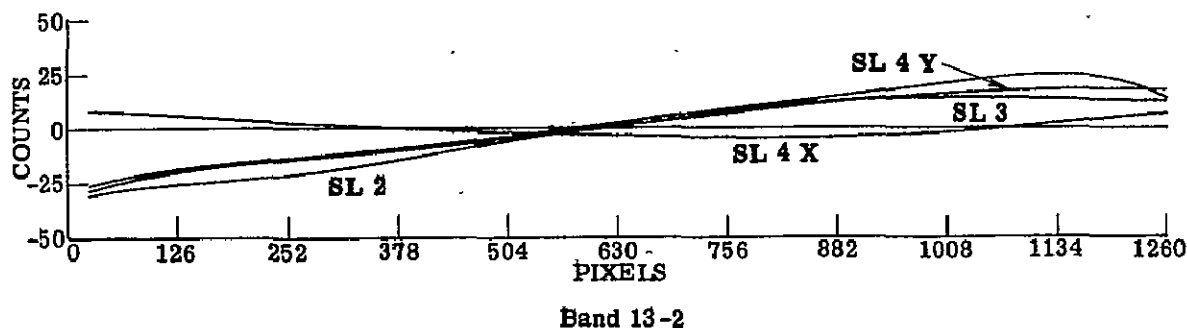
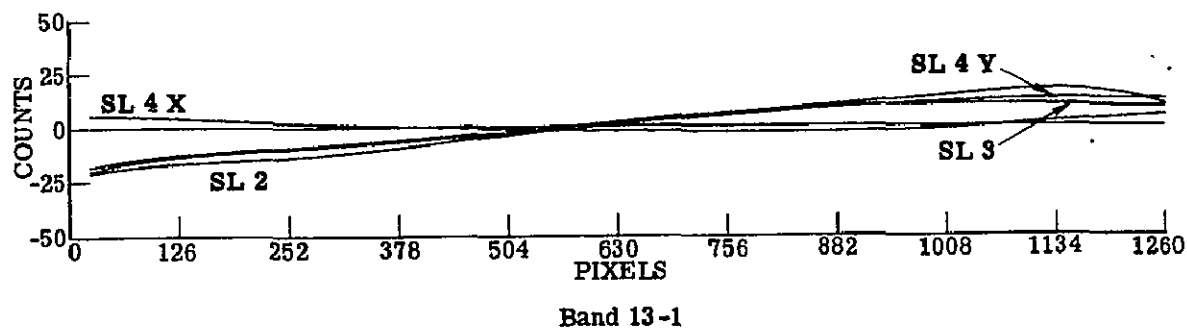
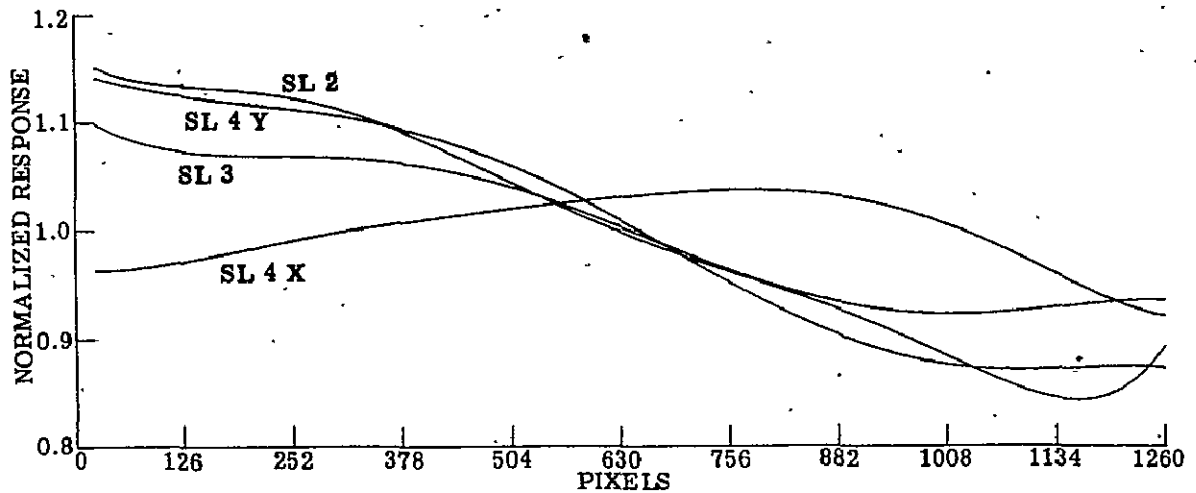
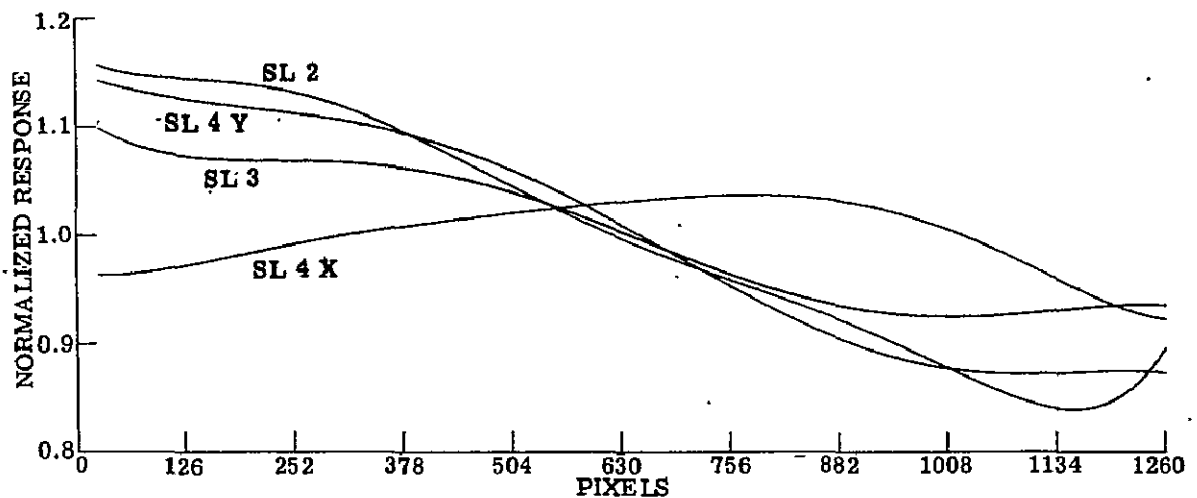


Figure 3.3.3-1.- Residual effects (Z_j).



Band 13-1



Band 13-2

Figure 3.3.3-2.- Response versus scan angle.

3.4 Absolute Radiometric Accuracy and Stability

S192 radiometric accuracy and stability was determined by analysis of the radiometric calibration of the S192 reflective bands (1 through 12) and the thermal band (13). The rejection of radiation reflected from sources off-axis to the S192 was evaluated, as was the stability of band locations. Details of these analyses were presented in Section 6 of MSC-05528, Volume III, September 6, 1974.

3.4.1 Radiometric Calibration

Radiometric calibration of SL92 was performed in two parts. The reflective bands were calibrated using prelaunch response to a test target, ground truth data, and lunar radiances. The thermal band was calibrated using ground truth data from lakes used as thermal targets.

3.4.1.1 Reflective Bands (1 through 12) - Data were evaluated from prelaunch testing, five lunar calibration data passes, and the Great Salt Lake Desert (with ground truth data) on the SL3 mission. The evaluations were performed using the techniques described in Sections I, II, and III of Appendix A. Calibration lamp radiances consistent with these data sets were determined and are plotted in Figure 3.4.1-1.

The ground data results are not self-consistent and differ from the lunar data results. The lunar data results are quite self-consistent, but both lunar and ground data results differ noticeably from the prelaunch results. A critical examination of these various results does not identify specific causes for the differences but does identify candidate sources for some error. For example, the ground data results are based upon a single data set from each instrument which would permit undetected systematic instrument error, and the transfer to the spacecraft requires correction for atmospheric effects which is still a subject for research. The lunar data results also must include correction for atmospheric effects in the results from the literature, and the Irvine* & McCord** data are combined and extrapolated to cover the SL92 range. Although the final prelaunch calibrations were performed under far from optics lab conditions, the external source used was a well understood test target which was recalibrated after launch. For these reasons, the prelaunch values for calibration source radiance were used for SL92 production data processing although the possibility of sensor change following the last prelaunch calibration cannot be dismissed. There can be little questions that the sensor response in Band 1 changed before the first SL4 lunar calibration pass, but with that exception the lunar calibrations indicated good radiometric stability.

Ground truth data in Figure 3.4.1-1 were derived from two separate instruments. Data that determined curve G were taken with an interference-wedge spectral-scanning spectroradiometer, manufactured by Instrumentation Specialties Company, Lincoln, Nebraska (I.S.C.O.). Data that determined curve B were taken with a Bendix Model 100 Radiant-Power Measuring Instrument (RPMI). Ground truth radiance data resulting from these two instruments differed in magnitude by about 20% on the average with the radiances derived from the RPMI

*Adair P. Land & William M. Irvine: "Monochromatic Phase Curves and Albedos for the Lunar Disk," Astronomical Journal, April 1973.

**T. B. McCord & T. V. Johnson: "Lunar Spectral Reflectivity (0.30 to 2.50 microns) and Implications for Remote Mineralogical Analysis," Science, August 8, 1970.

being the higher. These results are reflected in the calculated lamp radiance values plotted. This deviation in magnitude, while spectral shape is similar, can be considered to indicate systematic errors.

The lunar calibration data shown in Figure 3.4.1-1 were determined from data sets taken with the S192 scanner by orienting and rotating the spacecraft so that the moon was viewed and scanned. The spacecraft pitch rate was such that the scan-line advance rate was only about 5% of that normally used for terrestrial scenes, thus nearly 1000 scans of the moon were made on each lunar calibration pass. Using lunar radiance characteristics from the literature*, the radiance of the S192 internal calibration lamp was calculated. These results demonstrate significant changes in the calibration of Band 1 over the missions and indicate changes in the calibration of the lower numbered bands between LC 1 and the later missions. Otherwise the results indicate that the S192 was quite stable during those parts of the three missions when the Y3 detector array was in use. Discrepancies of up to 50% between corresponding KSC and flight results for Bands 2 through 11 are not too surprising in view of the many uncertainties involved in both sets of measurements and particularly in interpreting the radiometric data available for the moon. These problems are particularly severe for Band 12, but the 100% discrepancy for this band appears too large to be accounted for in this way, so the results may indicate a real change in performance. In fact, the changes in the radiance profile of the high (internal) calibration source do suggest real changes in calibration in all bands following the prelaunch calibration.

3.4.1.2 Thermal Band Calibration - Calibration of the thermal band was verified by using lakes as ground truth targets, as described in Section VIII of Appendix A. Data were evaluated for the Y-3 from SL2 and SL3 and the X-5 from SL4. The results indicated that a linear fit between the hot- and cold-temperature blackbodies could be used to determine the radiometric temperatures of ground targets to within approximately 1°K. Figures 3.4.1-2 and 3.4.1-3 show the results obtained. Figure 3.4.1-2 is a linear plot between the radiances of the hot and cold blackbodies for band 13-1. The band 13-1 output from the cold blackbody was set to approximately 60 counts and the hot blackbody to 240 counts. Results of ground truth measurements of radiance versus S192 counts for the Great Salt Lake on SL3 are also plotted. Figure 3.4.1-3 presents similar data for the X-5 data of Laguna Reservoir on SL4. This is an example of the results obtained for the smaller dynamic range band 13-2, where the hot- and cold-blackbody radiances are set to 255 and 0 counts, respectively.

3.4.2 Off-Axis Rejection

The rejection of off-axis radiation by the S192 was evaluated using the technique described in Section V of Appendix A. Using the lunar calibration pass data, adjacent scan-line data were evaluated as the S192 instantaneous field of view (FOV) was rotated onto the moon, and adjacent pixels were evaluated as the S192 scanned across the moon as shown in Figure 3.4.2-1. Data were

*Ibid.

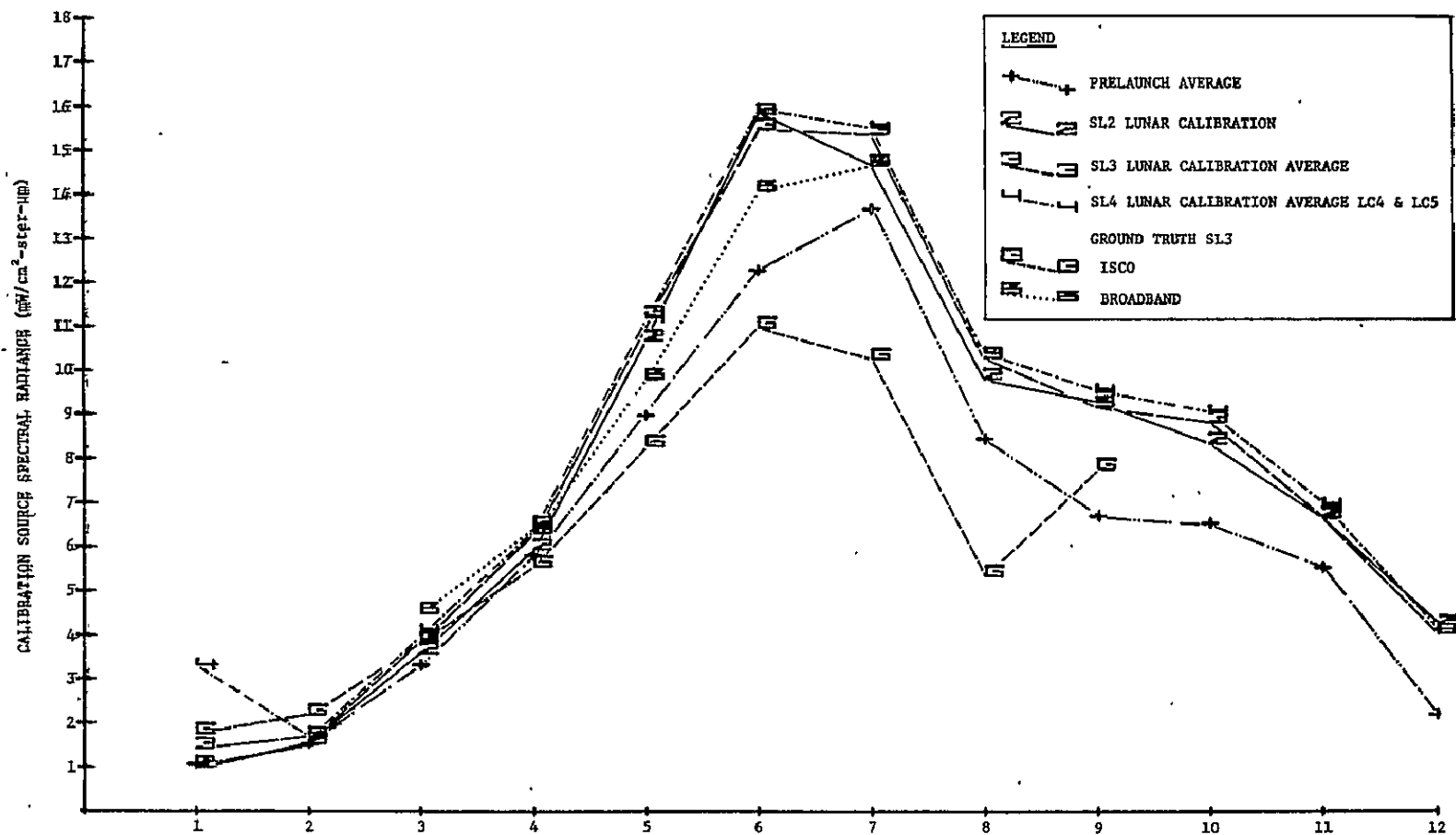


Figure 3.4.1-1.- Comparison of equivalent calibration lamp radiances.

MSC-05546

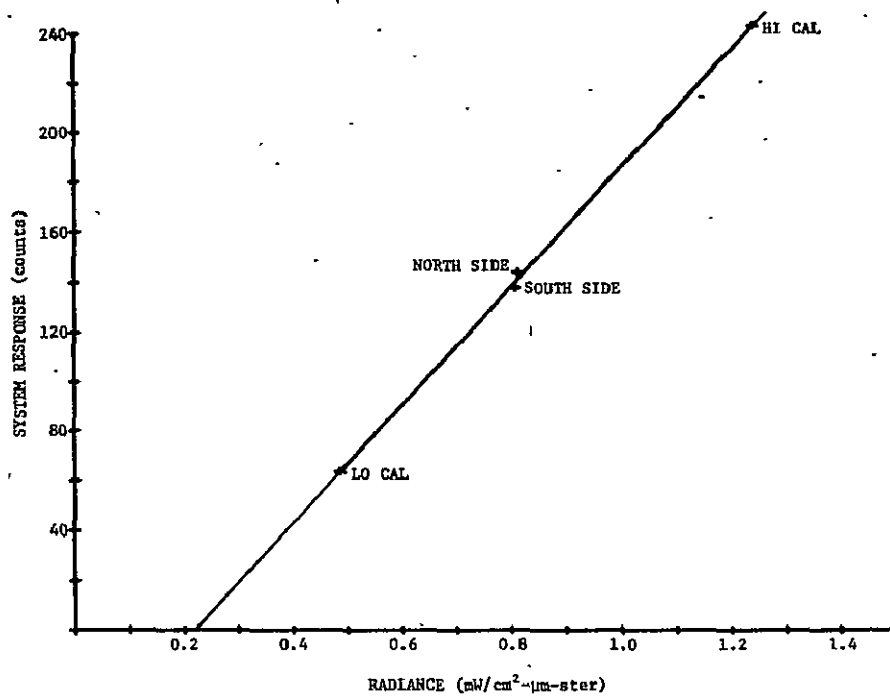


Figure 3.4.1-2.- Band 13-1 Y-3 CDDP thermal band calibration.

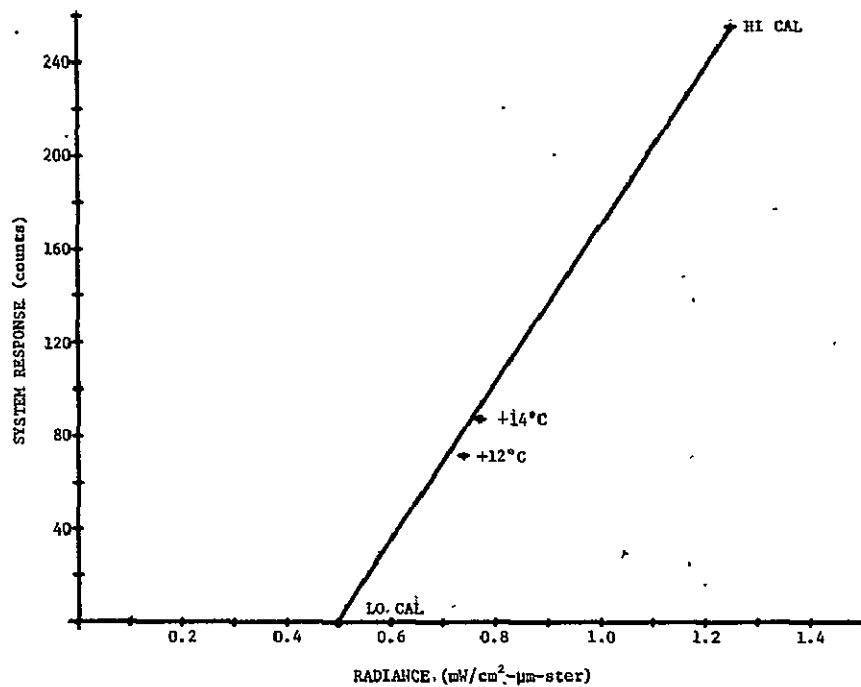


Figure 3.4.1-3.- Band 13-2 X-5 CDDP thermal band calibration.

evaluated for the five lunar calibration passes, using the Y-3 assembly. Figures 3.4.2-2 and 3.4.2-3 are sample plots of the data obtained. Figure 3.4.2-2 is a plot of cross-track pixels versus counts. The distinct rise as the S192 scans across the lunar limb, with no detectable scattered radiation in the deep space data before the moon, indicates excellent off-axis rejection. Figure 3.4.2-3 is a similar plot for the along-track data. Due to the slow rate of Skylab rotation of the S192 field of view onto the moon, the scan lines overlapped extensively. The pixel scale on the abscissa is the actual S192 instantaneous FOV accounting for this overlap. As in Figure 3.4.2-2, the indication is that the off-axis rejection is excellent.

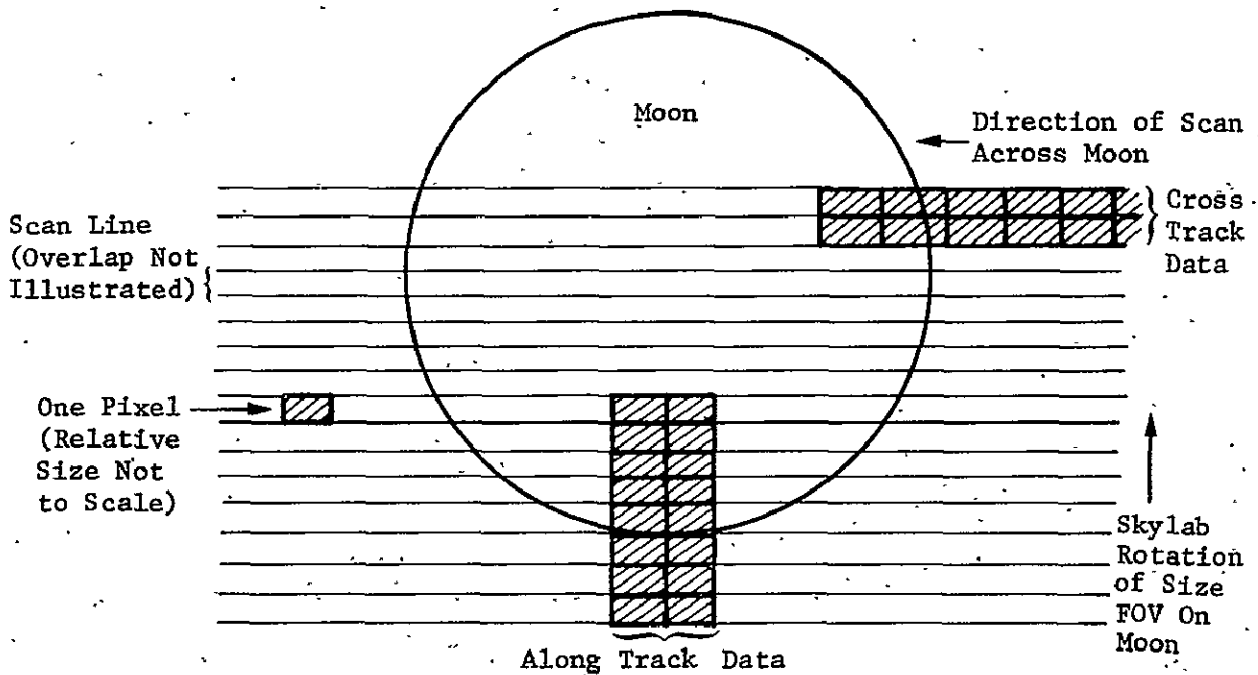


Figure 3.4.2-1.- Geometry of data utilized in off-axis rejection determination.

3.4.3 Spectral Band Locations

Spectral band locations were verified by the Environmental Research Institute of Michigan. The technique used was to compare the S192 response to an agricultural scene with the "predicted response" for that scene. The S192 response was determined by taking the average counts for each band from a block of pixels taken over an agricultural area. These averaged counts were made comparable by using the radiometric calibration results of the lunar calibrations (See paragraph 3.4.1.1). The "predicted response" was derived by multiplying a textbook "green vegetation" reflectance spectrum by a terrestrial solar illumination spectrum for two air masses, then integrating over the S192 bands.

Figure 3.4.3-1 is an example of the results obtained. The dips at bands 5 and 9 show the chlorophyll absorption band and the 1.13-micrometer water-vapor absorption band, respectively. The relatively high signal at shorter wavelengths compared to the predicted curve is due to path radiance.

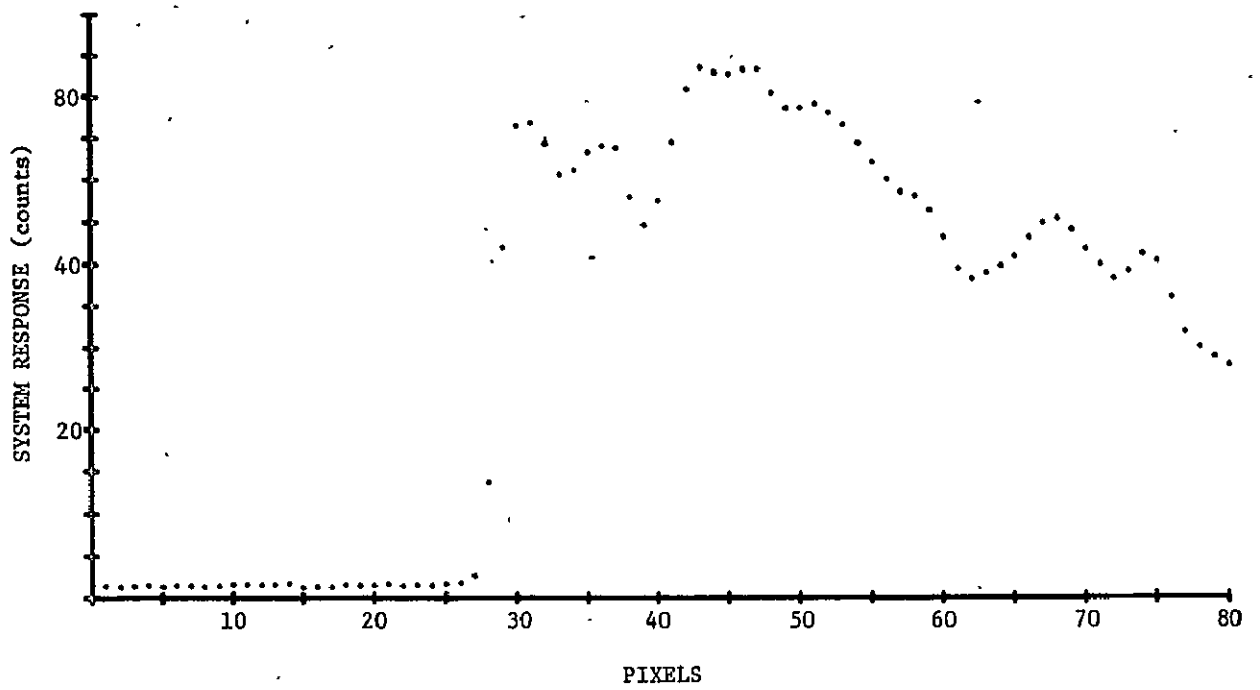


Figure 3.4.2-2.- Off-axis rejection across track.

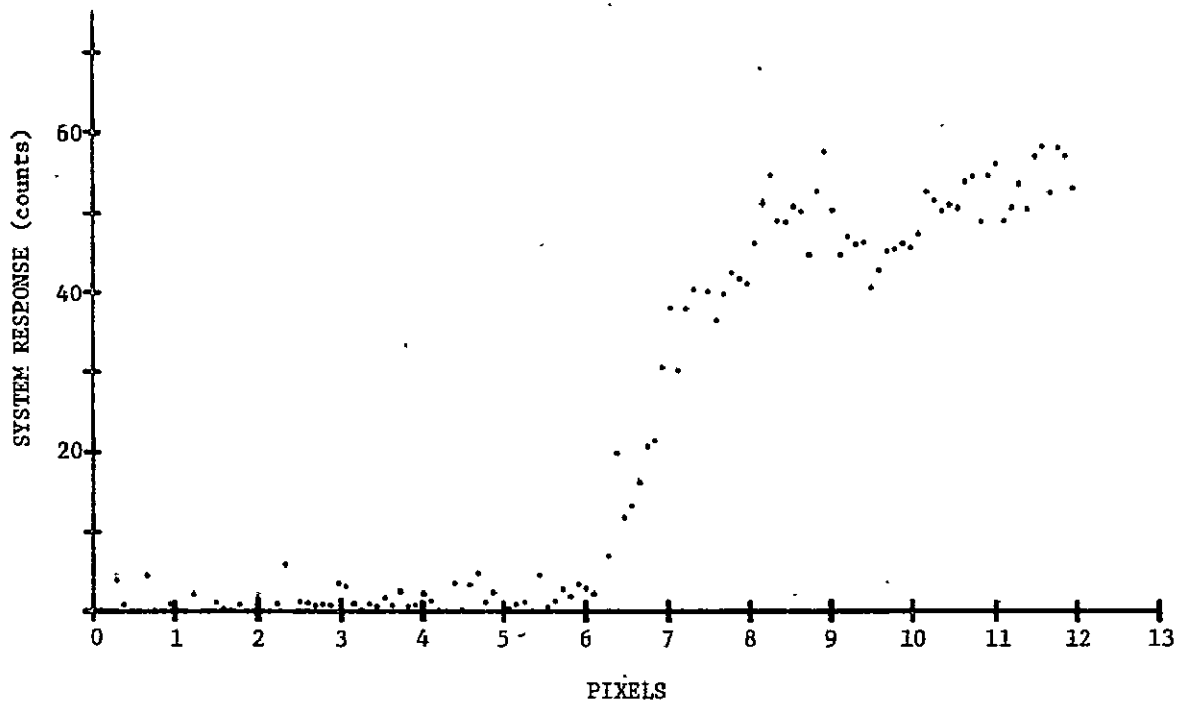


Figure 3.4.2-3.- Off-axis rejection along track.

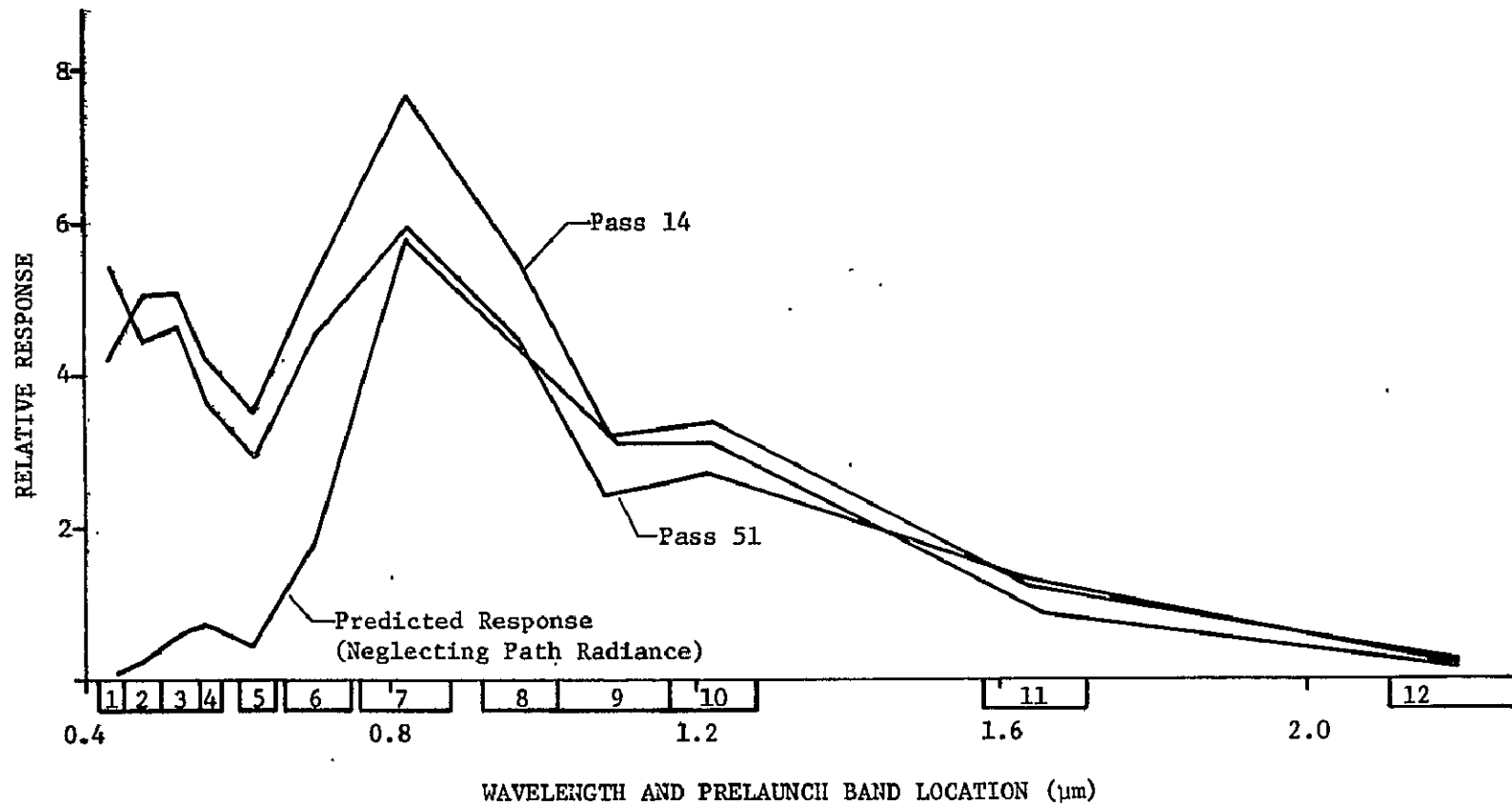


Figure 3.4.3-1.- SL3 spectral response determination.

Data were evaluated from the three Skylab missions. The location of the two absorption bands previously mentioned indicates that the band locations were essentially as measured before launch.

3.4.4 Dynamic Range

During prelaunch testing the internal calibration source for the reflective bands (1 through 12) was discovered to have a radiance too low to give the necessary dynamic range in bands 1, 4, 5, 7, and 8. Since it was too close to scheduled launch to make changes in the basic hardware, an attenuator assembly (installed on the connector of the signal output cable of the preamplifiers and containing voltage dividers including adjustable trim-potentiometers) to reduce the signals from the detectors in those bands and thereby increase the dynamic range. The attenuation in band 1 caused adverse frequency response characteristics (see paragraph 3.5.1), so the trim-potentiometer was adjusted to its lowest resistance making the dynamic range too small in band 1.

Since the Attenuator Assembly was not launched in place but was stowed elsewhere in the MDA and since the Attenuator Assembly had been exercised in the system minimally, EREP passes (1, 2, and 3) taking S192 data without the attenuation were flown before the Attenuator Assembly was installed between passes 3 and 4. As expected, a large amount of signal saturation (i.e., clipped at 255) on ground scenes was experienced in bands 1, 4, and 5 and lesser amounts in bands 7 and 8. With the Attenuator Assembly installed only band 1 still saturated on ground scenes at high sun elevation angles.

Since the increase in dynamic range was produced by a reduction in signal, it reduced S/N (signal-to-noise ratio). In bands 4 and 5 the decrease in signal was found to be greater than required, so between passes 24 and 25 the attenuation in those bands was adjusted with an accompanying change in dynamic range.

The Attenuator Assembly was also determined to have increased the noise level by permitting more "pick-up" of electronic noise. A new Attenuator Assembly with a modified grounding scheme was sent up with the SL4 crew and installed before pass 53. This new voltage divider network changed the attenuation and therefore the dynamic range in each attenuated band but not significantly.

The X-5 C/D/P (Cooler/Dewar/Preamplifier Assembly) was installed in place of the Y-3C/D/P on January 15, 1974, between passes 83 and 84. This C/D/P had different detectors and preamplifiers so that the Attenuator Assembly was not installed with it. The dynamic ranges in bands 1, 2, 3, and 7 were drastically increased by factors of 4, 5, 2.5, and 2, respectively, with commensurate changes in S/N. Bands 5 and 10 were inoperative.

3.5 System Frequency Response

S192 system frequency response evaluation determined the ability of the sensor to respond as a function of ground spatial frequency. The following is a summary of this evaluation. This task is described in detail in Section 7 of MSC-05528, Volume III, September 6, 1974.

3.5.1 System Frequency Response - Prelaunch

A characteristic apparently inherent in the high performance HgCdTe detector material used in S192 is frequency response that varies non-linearly with incident radiance level. Fixed radiance levels (called optical bias) were applied to the detectors to adjust frequency response. Since sensitivity also varies inversely with incident radiance level a trade-off was made between optimum frequency response and sensitivity in setting the optical bias levels. The preamplifiers were then trimmed to give optimum performance in each channel in the range of radiance levels for each spectral band expected from terrestrial scenes of greatest interest. At radiance levels different from the trim levels frequency response changed from that existing at the trim levels.

In prelaunch testing at the Honeywell Radiation Center, bar targets (with uniformly spaced bright and dark bars giving different spatial frequencies) were used to determine the frequency response characteristics of bands 1 through 12 at three illumination levels (trim level, 1.5 trim and 0.5 trim). These results are presented in MSC-05528, Volume III (S192)* and showed frequency response in several bands to be significantly different from that desired but in no case to be unsuitable for use.

In prelaunch testing at Kennedy Space Center the voltage divider network of the Attenuator Assembly when combined with the capacitive coupling of the alignment signal circuit in band 1 destroyed the frequency response of that band. There was not sufficient time to change the Attenuator Assembly other than to set the band 1 adjustable resistance to minimum. This left band 1 with such poor frequency response with the Attenuator Assembly installed that the data are generally unusable.

3.5.2 System Frequency Response - SL2, SL3

The technique used to obtain S192 system frequency response in orbit is described in Section V of Appendix A. The modulation transfer function (MTF), which is a measure of that response, was determined from S192 output as the sensor scanned from the moon to deep space.

Results for SL2 and SL3 were very similar. For bands 3 through 13, the system frequency response was satisfactory. As expected, band 1 was very poor at all frequencies; band 2 was also poor but to a much lesser extent. Average responses of band 1 and 2 as S192 scanned off the trailing lunar edge during SL3 are shown in Figures 3.5.2-1 and 3.5.2-2. These average responses are a pixel-by-pixel average of 20 scan lines. The corresponding MTF curves are presented in Figures 3.5.2-3 and 3.5.2-4. An idealized MTF curve is shown for comparison in Figure 3.5.2-5.

*Skylab Program Earth Resources Experiment Package Sensor Performance Report, Volume III (S192), Engineering Baseline, SL2, SL3, and SL4 Evaluation, MSC-05528, dated September 6, 1974.

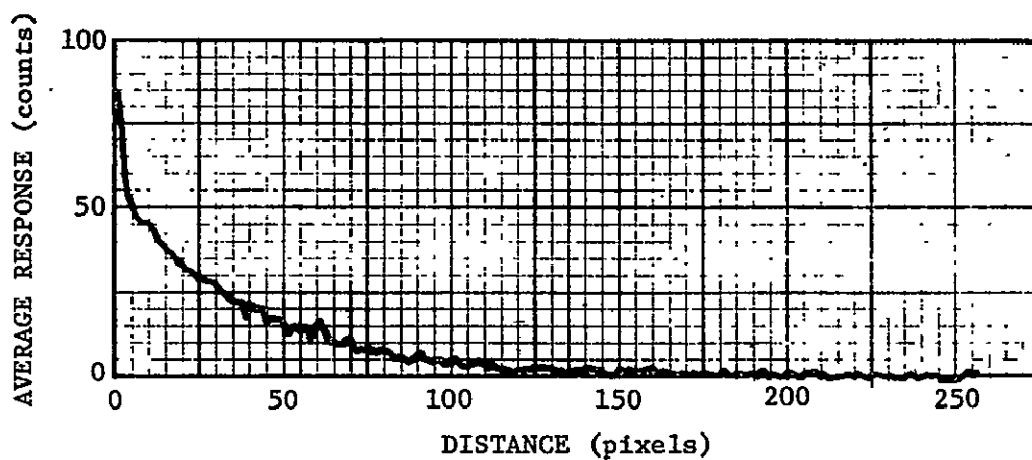


Figure 3.5.2-1.- Average response versus distance from lunar edge for band 1, SL3.

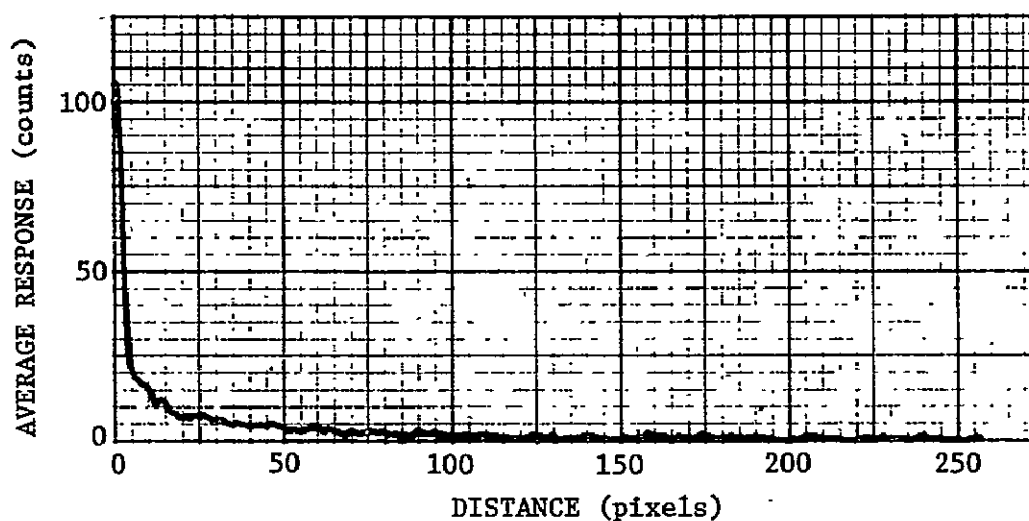


Figure 3.5.2-2.- Average response versus distance from lunar edge for band 2, SL3.

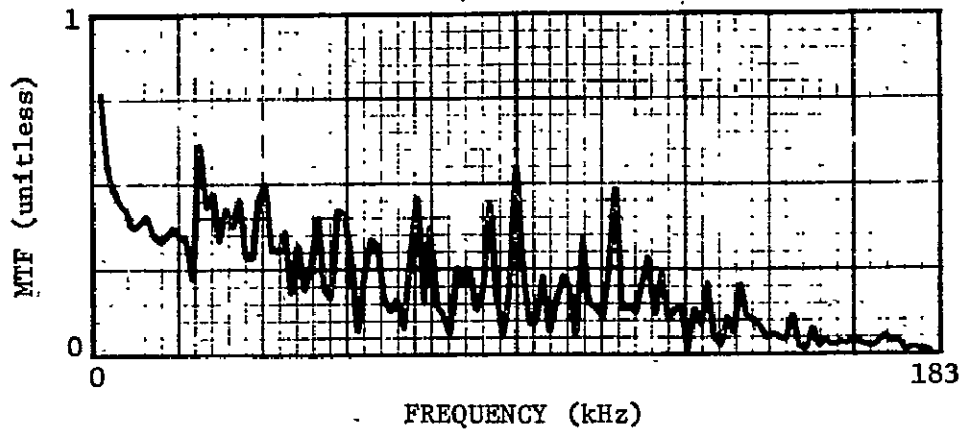


Figure 3.5.2-3.- Modulation transfer function (MTF)
for band 1, SL3.

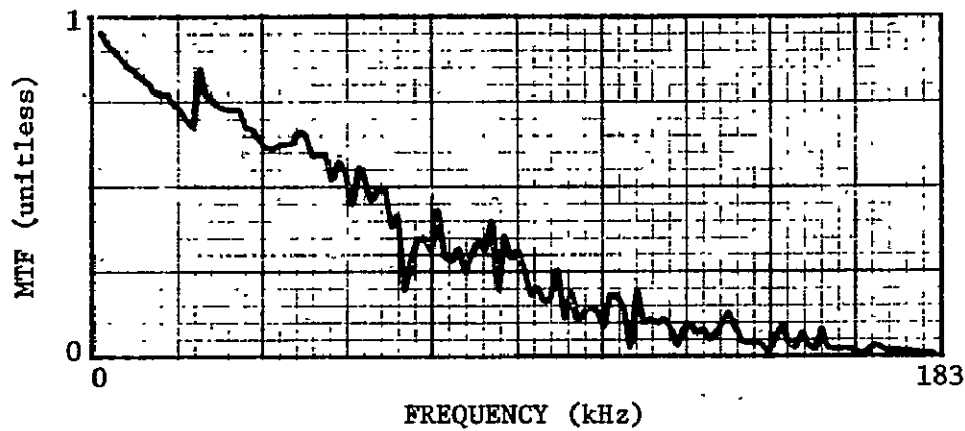


Figure 3.5.2-4.- Modulation transfer function (MTF)
for band 2, SL3.

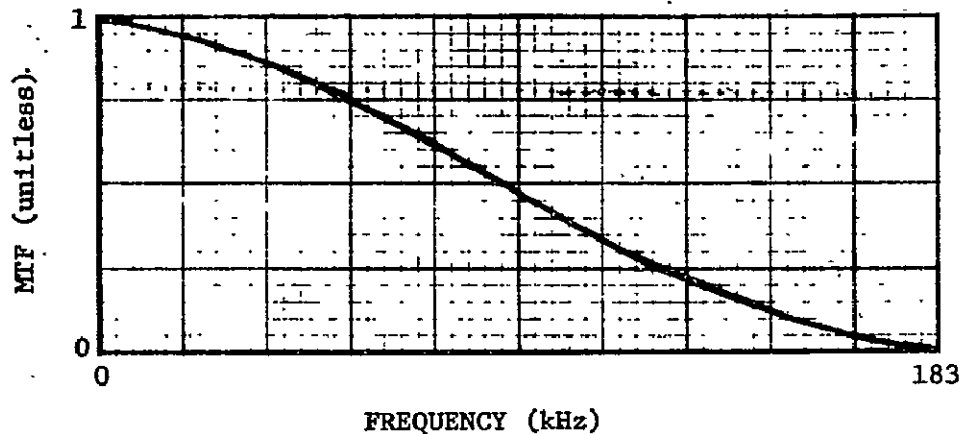


Figure 3.5.2-5.- Idealized modulation transfer function (MTF).

3.5.3 System Frequency Response - SL4

An improved attenuator was installed in S192 at the start of SL4. This considerably improved the system frequency response for band 1 but caused some overshoot in bands 2, 3, and 4 and decreased the signal-to-noise ratios in bands 1 and 2. Figures 3.5.3-1 and 3.5.3-2 show the average response when scanning off the trailing lunar edge and the MTF curve for bands 1 and 2 during SL4 before the Y-3 detector array was replaced with the X-5 detector array.

System frequency response for the X-5 detector array caused extensive overshoot for many bands following the trailing lunar edge so that the digital output was completely clipped. This meant that the true shape of the average response could not be determined. An estimated MTF was obtained by fitting a series of exponentials to the signals at the trailing edge of the moon, using the positive overshoot at the leading edge as a guide. The resulting MTFs showed that most bands have considerable frequency boost in the lower half of the frequency range. Filters have been developed to permit improvement of the reflective region data (bands 1 through 12) taken with the X-5 array. This study was not completed in time for inclusion in this report but will be published under separate cover.

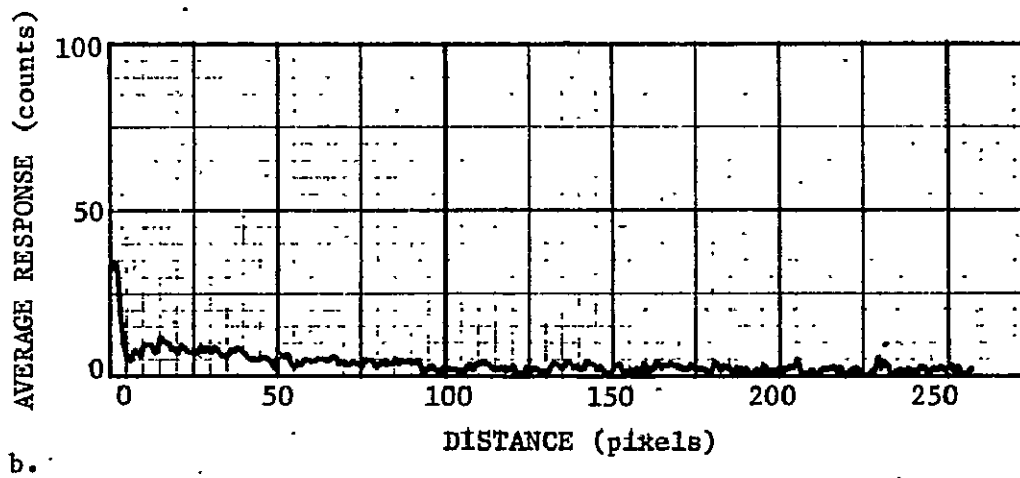
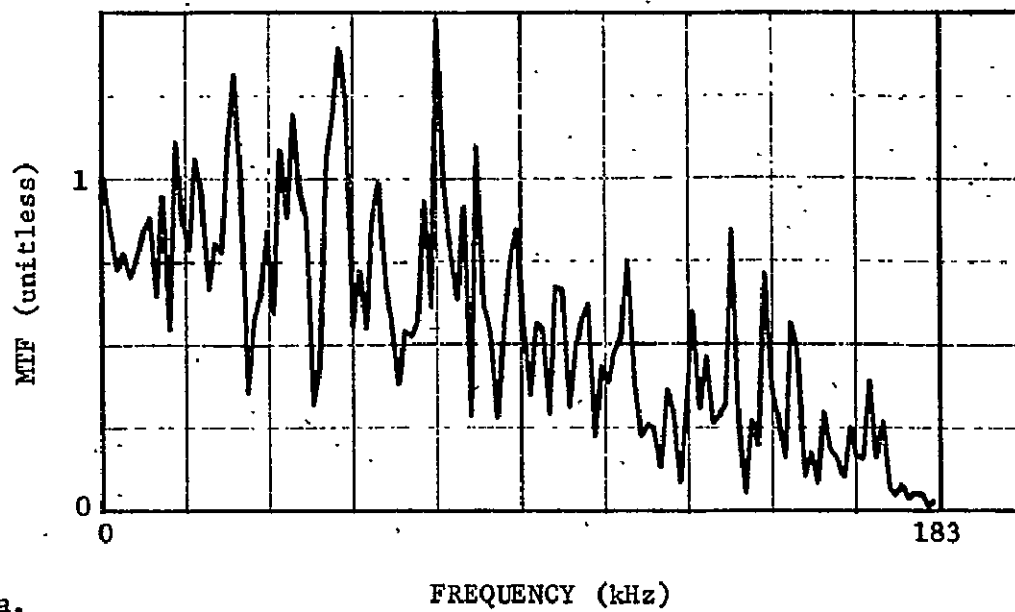


Figure 3.5.3-1.- Frequency response for SL4, Y3, LC4, band 1.

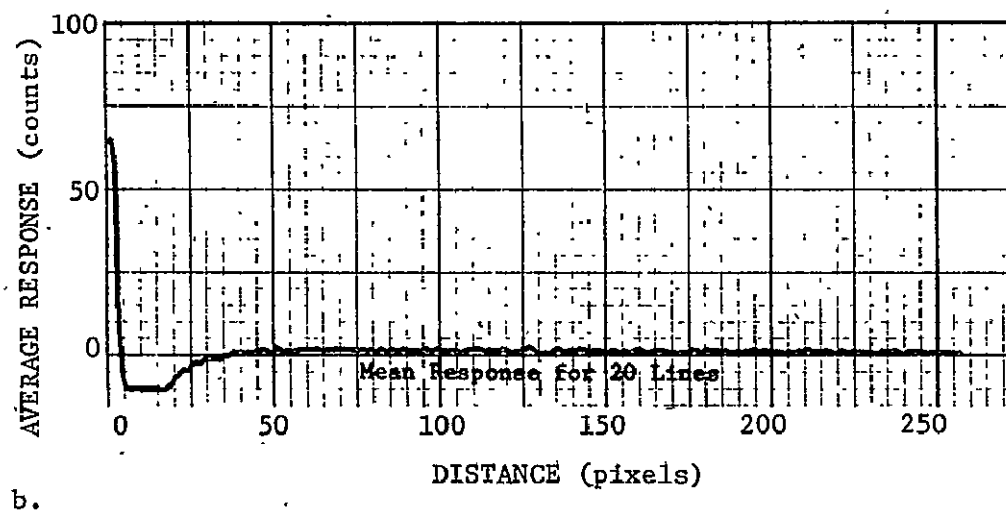
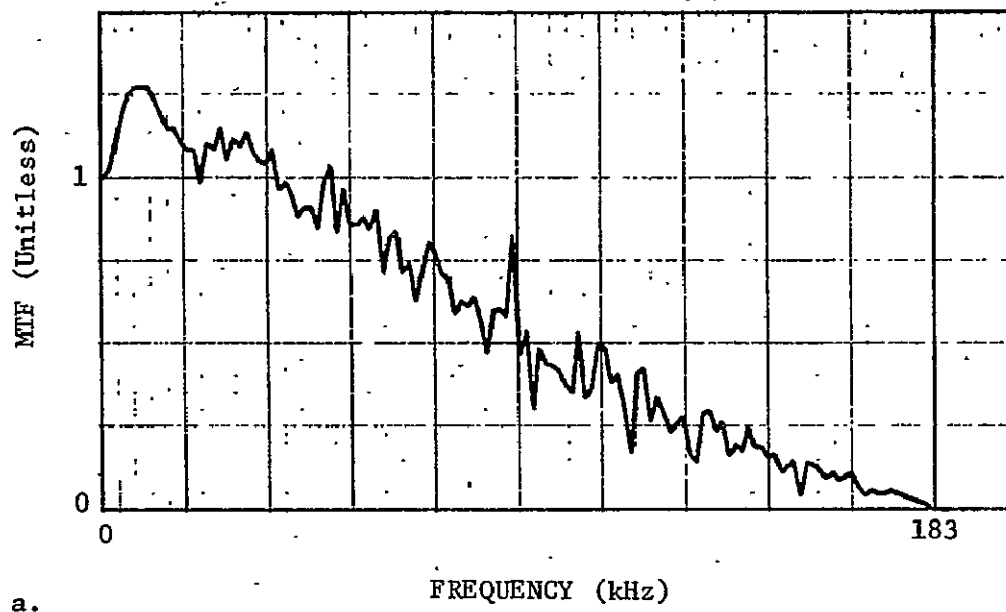


Figure 3.5.3-2.- Frequency response for SL4, Y3, LC4, band 2.

3.6 Geometric Distortion

The geometric fidelity of SL92 data was evaluated by:

- 1) Mathematical modeling of the data acquisition system to determine positional correction parameters;
- 2) Determination of the geometric distortion in the screening film.

The evaluations are presented in detail in MSC-05528, Volume III, September 6, 1974, Section 8, and are summarized below.

3.6.1 Geometric Distortion from Mathematical Modeling

The approach used to evaluate the geometric distortion is described in Appendix A, Section VII. For SL2, SL3, and SL4, the mathematical model was successful in handling time-dependent systematic errors through a determination of the positional correction parameters. Residual errors (after eliminating the systematic errors) were random, with a standard deviation of 4 pixels. No prelaunch evaluation was made.

3.6.2 Geometric Distortion in Screening Film

Screening films were generated on a JSC production film processor by using an algorithm that generated conical scan lines on the film. These scan lines were obtained on the special raster that was guided by knowledge of the length of the scan-line arc in degrees, velocity of the spacecraft in meters per second, altitude of the spacecraft in meters, scans per second and degrees of drift angle due to the earth's rotation. The width of the image was constrained to be 5 inches which fixed the number of raster positions available in the y-direction at a number that did not permit placing the pixel dot at its exact computed location. Screening films thus generated were evaluated for along- and cross-track scales (S_x and S_y) and nonorthogonality between X and Y axes. The scales S_x and S_y differed by as much as 12 percent, and were nonorthogonal by approximately 0.055 radian. All of the screening film had been produced by the time these geometric imperfections were identified. Since these imperfections did not prevent or even detract from the use of the screening film for its intended purpose of previewing sensor data and correlating data acquisition time with an investigator's area of interest, no screening film was generated with improved geometric quality. The scale of the screening film provided on 5-inch film was found to be in the neighborhood of 1:800,000.

There were many other film products to be made for investigators so the pixel placing program of the production film converter was corrected by inserting more exact values for scan-line arc length and scan rate, adding 3.15° (0.055 radians) to the ephemeris drift angle, and not requiring the image width to be exactly five inches. This resulted in reducing the difference between across-track and along-track scales to about 1% and in reducing nonorthogonality to less than 0.005 radian.

3.7 Noise Analyses

Noise analyses were performed on S192 prelaunch and flight data. Detailed results are presented in section 9 of MSC-05528, Volume III, September 6, 1974.

3.7.1 Noise Analyses - Prelaunch

Prelaunch raw data were evaluated for noise by five methods. The performance data derived by each method are summarized below.

3.7.1.1 Standard Deviation - Standard deviations were determined for each band at the center of the scan line from 1000 consecutive scan lines. Representative values are given in Table 3.7.1-1, when the attenuators were not installed and Table 3.7.1-2 when they were installed.

TABLE 3.7.1-1.- STANDARD DEVIATIONS,
ATTENUATORS OUT

BAND	STANDARD DEVIATIONS (counts)	
	Prelaunch	SL2
1	6.9	*
2	4.1	4.7
3	3.3	3.5
4	15.6	*
5	11.4	12.7
6	4.9	6.3
7	4.4	4.8
8	4.9	4.9
9	4.2	3.7
10	6.1	6.0
11	2.6	3.2
12	4.2	3.2

* Insufficient data

3.7.1.2 Strip-Chart Recordings - Strip-chart recordings for each of three points in the scan line as a function of scan line, or time, were examined. A very low-amplitude, low-frequency modulation was found. Additional evaluation indicated that this modulation was 1/f noise (flicker noise) generated by the detector where f was the noise frequency.

3.7.1.3 Data Histograms - Data histograms for all bands were made using the data word at the center of the scan line for 1000 consecutive scan lines. Figure 3.7.1-1 shows a histogram for band 1 and is typical of all the S192 bands.

TABLE 3.7.1-2.- STANDARD DEVIATIONS, ATTENUATORS IN

BAND	STANDARD DEVIATIONS (counts)				
	PRELAUNCH	SL2	SL3		SL4
			Before Attenuator Change	After Attenuator Change	
1		7.7	7.2	7.2	*
2	4.1	4.2	4.0	4.0	3.9
3	3.3	3.2	3.1	3.1	3.2
4	7.8	8.2	7.7	9.2	9.4
5	6.1	5.1	5.9	8.2	8.0
6	5.0	6.5	5.6	6.0	5.7
7	2.8	3.0	3.5	4.3	4.2
8	5.6	*	4.7	4.7	6.2
9	3.3	*	4.5	3.7	3.6
10	5.4	*	6.6	6.0	5.8
11	2.6	*	2.7	2.7	2.7
12	3.6	*	3.1	3.1	3.3

* Insufficient data

3.7.1.4 Power Spectral Density - Power spectral density (PSD) plots (described in Section VI of Appendix A) exhibited low-frequency broadband noise. Figure 3.7.1-2 shows a typical power spectral density plot for frequencies less than 100 hertz. The $1/f$ noise can be seen between 1 and 10 hertz. The spike between 20 and 30 hertz corresponds to the cooler piston frequency.

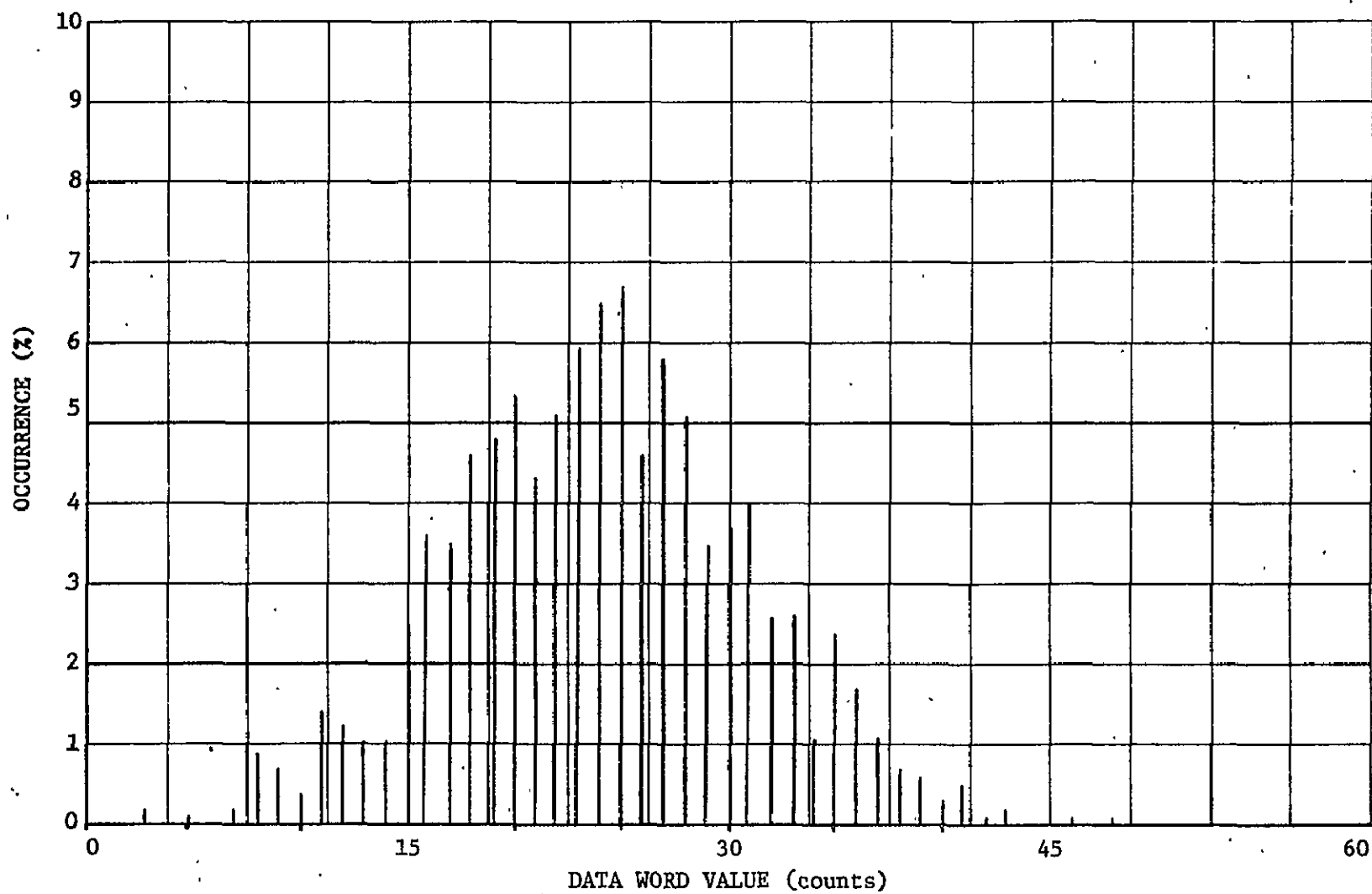
3.7.1.5 Noise-Equivalent Spectral Radiance - Noise-equivalent spectral radiances (NESR) were determined by converting the standard deviation in counts for each band to spectral radiance by means of the radiometric calibration. Tables 3.7.1-3 and 3.7.1-4 give the noise-equivalent spectral radiance corresponding to the standard deviations of Tables 3.7.1-1 and 3.7.1-2.

3.7.2 Noise Analyses - SL2, SL3, and SL4

Standard deviations and noise-equivalent spectral radiances for bands 1 through 12, for SL2, SL3, and SL4 are shown in Tables 3.7.1-1, 3.7.1-2, 3.7.1-3 and 3.7.1-4. The values listed are from the Y-3 detector array only. The X-5 detector array noise levels averaged about 50% higher than the Y-3 array.

The thermal band, band 13, was not given a full system test before launching, so no prelaunch standard deviations and noise-equivalent temperature differences (NEAT) were available to compare with the flight values summarized in Table 3.7.2-1. There were two outputs from band 13, labeled 13-1 and 13-2, which differed from each other by scale and reference level. Table 3.7.2-1 shows the noise values for both. The values from the Y-3 detector array and its replacement, the X-5 detector array, are given under SL4.

III-35



MSC-05546

Figure 3.7.1-1.- Data-word histogram, band 1.

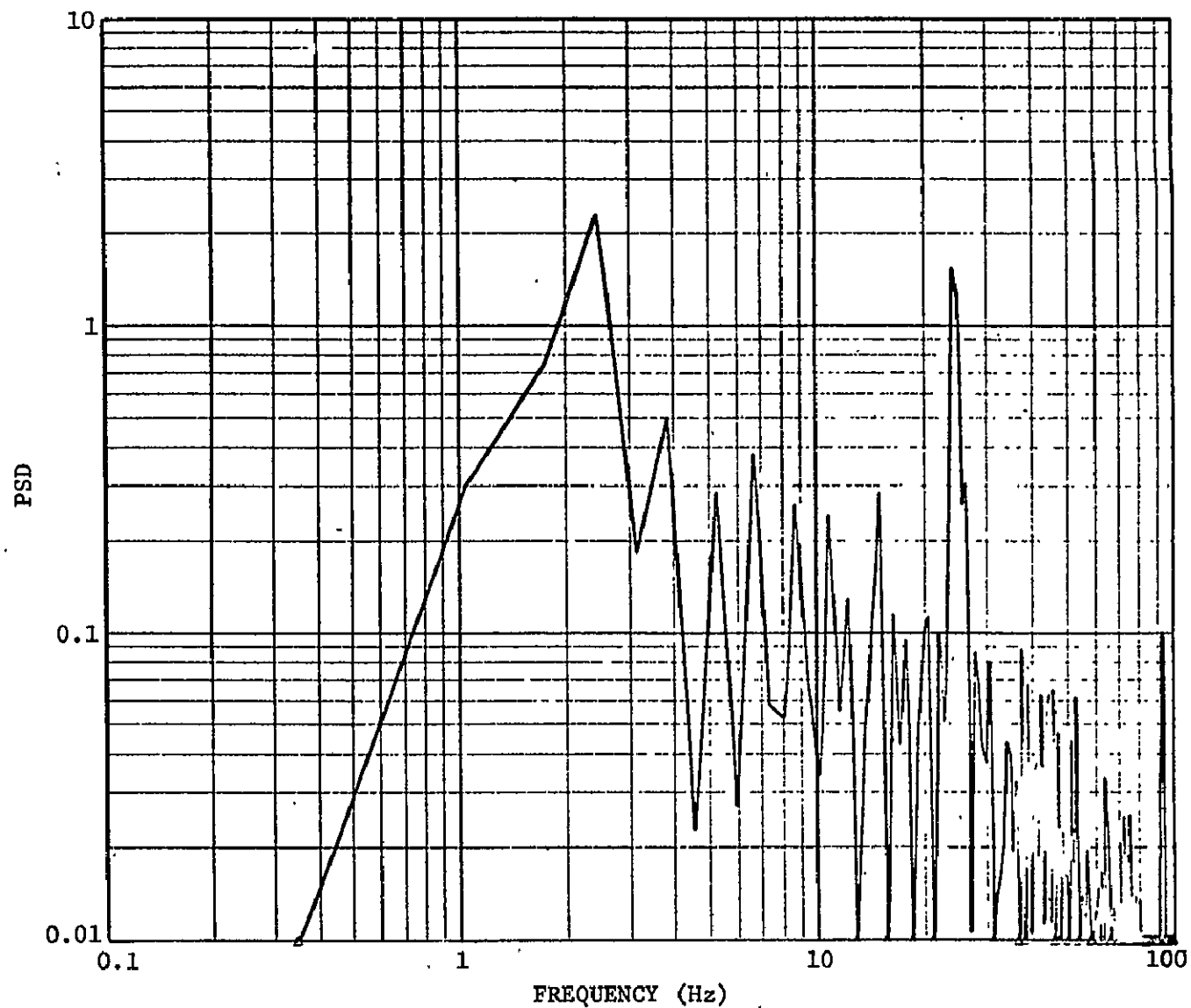


Figure 3.7.1-2.- Power spectral density plot, band 7.

TABLE 3.7.1-3.- NOISE-EQUIVALENT SPECTRAL RADIANCES (NESR),
ATTENUATORS IN

NESR (mW/cm ² -μm-ster)					
BAND	PRELAUNCH	SL2	SL3		SL4
			Before Attenuator Change	After Attenuator Change	
1	*	0.3	0.23	0.24	*
2	0.2	0.2	0.2	0.2	0.40
3	0.2	0.3	0.2	0.2	0.26
4	0.5	0.6	0.5	0.5	0.66
5	0.6	0.8	0.72	0.46	0.58
6	0.3	0.3	0.3	0.3	0.27
7	0.25	0.3	0.3	0.35	0.27
8	0.3	*	0.22	0.21	0.27
9	0.08	*	0.12	0.10	0.09
10	0.14	*	0.17	0.15	0.15
11	0.05	*	0.06	0.06	0.06
12	0.03	*	0.025	0.025	0.027

* Insufficient data

TABLE 3.7.1-4.- NOISE-EQUIVALENT SPECTRAL RADIANCES (NESR),
ATTENUATORS OUT

BAND	NESR (mW/cm ² -μm-ster)	
	Prelaunch	SL2
1	0.3	*
2	0.2	0.2
3	0.2	0.3
4	0.4	*
5	0.4	0.6
6	0.2	0.4
7	0.2	0.4
8	0.2	0.2
9	0.1	0.1
10	0.1	0.2
11	0.05	0.07
12	0.03	0.03

* Insufficient data

The imagery produced from flight data had two types of structured noise. One was low frequency and appeared as banding or streaking in the direction of scan. The other was high frequency and appeared as a "herringbone pattern" in the image. Sections 9.2, 9.3, and 9.4 of MSC-05528, Volume III, September 6, 1974 include descriptions of these noises and how they were suppressed.

3.8 Pointing Accuracy and Field-of-View Determination

A valuable aspect of the Skylab earth resources multispectral scanner imagery was its ability to record the left, center, and right geographic coordinates of a scan line. These data were based on spacecraft attitude and position telemetry and the geometry of the S192 system. To determine the accuracy of these coordinates, an evaluation was performed to determine the pointing direction of S192 relative to S190A and the error between the actual coordinates observed on the imagery and those predicted from attitude data.

TABLE 3.7.2-1.- THERMAL-BAND NOISE

	STANDARD DEVIATION (counts)		NOISE-EQUIVALENT TEMPERATURE DIFFERENCE (°K)	
	Band 13-1	Band 13-2	Band 13-1	Band 13-2
SL2	13.0	18.5	4.3	4.3
SL3	7.6	10.8	2.3	2.3
SL4 (Y-3)	7.0	9.7	2.2	2.2
SL4 (X-5)	3.0	4.2	0.9	0.9

3.8.1 Pointing Accuracy

The pointing accuracy of S192 was evaluated for each of the three Skylab missions. Using the technique described in Section VII of Appendix A, the S192 data were registered with respect to latitude and longitude determined from identifiable geologic features in the data. These coordinates were compared with those resulting from spacecraft attitude telemetry. It was found that the difference varied with time, indicating that the source of the error originated in the drift of the rate gyros.

For the times analyzed, Table 3.8.1-1 shows the maximum differences at the center of the scan.

TABLE 3.8.1-1.- MAXIMUM LATITUDE AND LONGITUDE DIFFERENCE
BETWEEN S192 DATA AND POINTING ESTIMATES DETERMINED
FROM SKYLAB ATTITUDE TELEMETRY

	Latitude	Longitude	MAXIMUM DIFFERENCES			
			Latitude		Longitude	
			min	s	min	s
SL2, Pass 7	39°20'N	87°50'W	5	21.9	3	26.5
SL3, Pass 52	30°10'N	90°30'W	2	5.7	0	50.6
SL4, Pass 90	40°50'N	89°W	4	13.8	7	24.5

3.8.2 Field-of-View Determination

Determination of the actual S192 Field of view was performed by locating geologic features taken from S192 imagery on Geologic Survey maps. The nominal S192 swath width (i.e., exactly in Z-LV attitude and at 235 n.mi. altitude) is 38.61 n.mi. The results of the flight data determination showed S192 swath width to be 39.6 ± 0.5 n.mi.

3.9 Photographic Image Adequacy for Site Location

S192 screening film served to locate sites so particular digital data or high-quality film can be specified and ordered. Evaluation of this film is detailed in Section 11 of MSC-05528, Volume III. No prelaunch screening film was made from which image adequacy could be evaluated.

3.9.1 Image Adequacy - SL2

The standard 5-inch screening film was not made for SL2 because the screening film equipment was not operational in time. As a substitute, 35-millimeter SL2 screening film was made with a temporary facility. Screening film for bands 2, 7, and 11 was compared with S192 data analysis station (DAS) imagery and with "Printed gray maps."

The primary image-quality factor noted in the screening film was the lack of contrast. High-contrast objects were easily detected, but objects that produced small changes in contrast were not detectable. Objects with sufficient contrast had resolutions comparable to those obtained from an area with about 3.5 S192 pixels on a side combined into one pixel. The granularity of the screening film was also a significant source of degradation, making scan-line counting difficult in some areas and impossible in most.

3.9.2 Image Adequacy - SL3

S192 screening film for SL3 was 5-inch film made by the JSC production film converter. The film was considerably superior in resolution, contrast, time-mark location accuracy, and convenience. Screening film for bands 2, 7 and 11 were examined.

The most serious limitation of the imagery was the quantization of the levels by reducing the number of 256 counts to 64 density levels. Low-contrast information below a four-count difference was suppressed. This caused an absence of fine shades of gray and an uniform appearance on large water and desert areas.

The resolution along the scan direction was obviously less than the resolution perpendicular to it. The distance for a detectable change was a single pixel perpendicular to the scan direction and 1 to 2 pixels in the scan direction.

When medium- or high-contrast targets were used, the screening film was excellent for locating targets and specifying the scan-line number (in terms of time) and the pixel number along the scan line.

3.9.3 Image Adequacy - SL4

There was little difference between the SL3 and SL4 screening film. The X-5 detector array was installed in place of the Y-3 array on January 16, 1974 and was used for the rest of the mission. The screening film from the X-5 detector appeared somewhat better to the eye but quantifying this improvement was impractical.

3.10 Geometrical Band-to-Band Registration Error

Band-to-band data registration was studied by analysis of scan lines and pixel traces crossing the edges of the moon. The single field stop design of the instrument makes it extremely unlikely that there could be detectable misregistration perpendicular to the scan lines. Comparison of corresponding pixel traces for the several bands did not disclose any such misregistration.

Along the scan lines, however, misregistration could occur due to lags in the analog electronics or data displacements in the digital electronics either on-board or during ground processing. Comparison of averaged scan lines crossing the moon showed that any along-line misregistrations were small. However analysis of the tabulated data used in carrying out the lunar calibrations showed some minor effects. To explore these more thoroughly five or six pixels covering the leading and trailing edges of the moon were selected and the averaged data for these pixels in each band in the LG tabulations were normalized by dividing by the peak signal recorded. An example of the results is shown in Table 3.10-1.

Generally only odd SDO data were used from the double-sampled bands. However, due to poor CCT data in the odd SDO, whenever even SDO data were used the signals in the even SDO's appear to lead the odd SDO's by about 1/2 pixel. This is to be expected, as in these high-data-rate bands alternate samples go to odd and even SDO's. In each LC SDO 20 appears in registration with the odd high-rate data while in LCs 2 through 5 SDO's 17 and 19 lag the odd SDO's by about 1/2 pixel and are thus 1 pixel behind the even high-rate SDO's. However, in LC 1 SDO's 17 and 19 appear to be in registration with the odd high-rate SDO's while SDO's 18 and 20 lag 1/2 pixel to become about 1 pixel behind the even high-rate SDO's. Finally, for LCs 4 and 5, SDO 1 leads the odd high-rate SDO's by 1/2 to 1 pixel so that it is then more than 1 pixel ahead of SDO's 17 and 19.

The results given above were based on the rise at the leading edge of the moon. As may be seen from the table, the trailing edge data is less definitive due to frequency response effects which vary from band to band.

TABLE 3.10-1.- EXTRACT FROM LC1 DATA (NORMALIZED)

SDO	Band	Pixel Number											
		657	658	659	660	661	662	712	713	714	715	716	717
1	3	0.02	0.02	0.05	0.13	0.24	-	0.46	0.35	0.18	0.05	0.01	-
2	3												
3	4	0.04	0.04	0.05	0.14	0.29	-	0.45	0.34	0.16	0.02	0.01	-
4	4												
5	5	0.04	0.04	0.04	0.06	0.12	-	0.47	0.37	0.19	0.07	0.04	0.05
6	5												
7	6	0.02	0.02	0.04	0.12	0.23	-	0.47	0.36	0.20	0.06	0.03	0.03
8	6												
9	7	0.04	0.03	0.06	0.14	0.25	-	0.49	0.39	0.22	0.08	0.06	-
10	7												
11	11	0.02	0.02	0.05	0.14	0.25	0.34	0.45	0.33	0.16	0.05	0.02	-
12	11												
13	12												
14	12	0.04	0.04	0.08	0.17	0.26	0.34	0.44	0.31	0.17	0.09	0.07	-
17	10	0.03	0.03	0.05	0.13	0.25	0.35	0.47	0.36	0.19	0.05	0.03	-
18	2	0.02	0.02	0.03	0.09	0.18	0.26	0.51	0.43	0.30	0.18	0.13	-
19	8	0.02	0.02	0.03	0.10	0.21	0.32	0.51	0.41	0.24	0.09	0.05	-
20	9	0.02	0.02	0.03	0.09	0.19	0.30	0.50	0.42	0.27	0.13	0.06	-
22	1	0.03	0.03	0.04	0.07	0.11	0.16	0.87	0.83	0.75	0.68	0.64	0.62

Note: The thermal band (SDOs 15, 16 and 21) was not considered, as it cannot be directly compared with the other bands.

The thermal band was not considered, as the lunar surface temperature falls off towards the edge of the nearly full moon so that thermal and reflected radiances cannot be compared in this way. Band 1, SDO 22 was not considered in LCs 1, 2, and 3 due to its very poor frequency response. However in LCs 4 and 5, when the frequency response of this band had been improved (i.e., during SL4), SDO 22 appeared to behave like an odd high-rate SDO when allowance was made for the high residual effect it contained.

Due to the large frequency response defects in the X-5 array bands 1 through 12 data, misregistration should be great. When the filtering technique is applied this problem should be greatly alleviated.

4.0 SUPPLEMENTARY ANALYSES

This section presents the results of analyses completed after the submission of the sensor performance evaluation interim report, MSC-05528, Volume III, September 6, 1974. Included in the section are an analysis of the S192 scan-related system response and a comparison of S190A, S191, and S192 radiometric performance.

4.1 Supplementary Analysis of Scan-Related System Response

Scan-related system response for S192 is the scanner response over a target of uniform radiance as a function of scan position. As implied, determination of this relationship required a data set representing scanner response to a uniform scene. The response versus scan angle functions used to reduce the S192 data were derived by averaging and normalizing the S192 response versus scan from several homogeneous scenes since uniform single scenes of the size required do not exist in nature. This technique is described in Section IV of Appendix A. The following paragraphs described an alternate technique developed by MMC for determining the S192 scan angle response from a single scene that is the most uniform available but is not in actuality uniform.

For each scene selected for analysis of the scan function, S192 data across the scan were tabulated. Data points representing the mean of 3000 samples (10 pixels times 300 scan lines) were selected for 12 points across the scan. Figure 4.1-1 illustrates a sixth-order polynomial fit to these points as the curve marked "scene data." The scan-related signal offset was determined using 12 data points of the same sample size from deep space data taken during the lunar calibration closest in time to the scene data. The true mean of the offset data points was determined using the technique described in Section III of Appendix A. The offset curve in Figure 4.1-1 illustrates the offset as a function of scan angle. This offset was subtracted from the scene data to obtain the scene data relative to zero counts. A sixth-order polynomial was fitted to the data and a normalization made to the value observed at a point 60° from the start of the scan. This point is near to the center of the S192 scan line. The normalized curves were then compared with the prelaunch scan response curves. An example, Figure 4.1-2, shows the band 3 prelaunch curve compared with the average curve for the three scenes of the Mali Desert.

The accuracy of scan response curves determined from the scene data depends on the uniformity of the averaged scenes or at least on their being statistically uniform when a large sample is taken. To assess the accuracy of the results, it was desirable to have an independent indication of how uniform the scenes were. This was accomplished by using S190A photographs.

The three Mali Desert scenes selected for S192 scan-related system response evaluation were located in the corresponding S190A frames. The black-and-white film camera stations were used (station 1, black-and-white infrared, 0.7 to 0.8 micrometers; station 2, black-and-white infrared, 0.8 to 0.9 micrometers; station 5, black-and-white Panatomic-X, 0.6 to 0.7 micrometers; and station 6 black-and-white Panatomic-X, 0.5 to 0.6 micrometers) to approximate a few of the spectral bands of the S192 scanner.

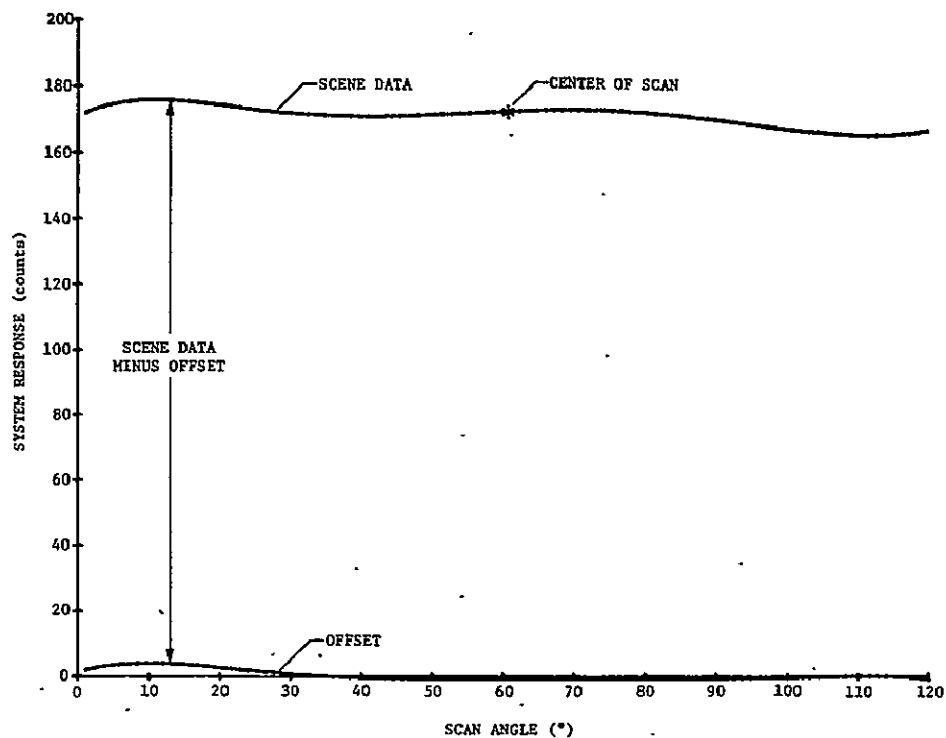


Figure 4.1-1.- Scene data minus calculated real offset.

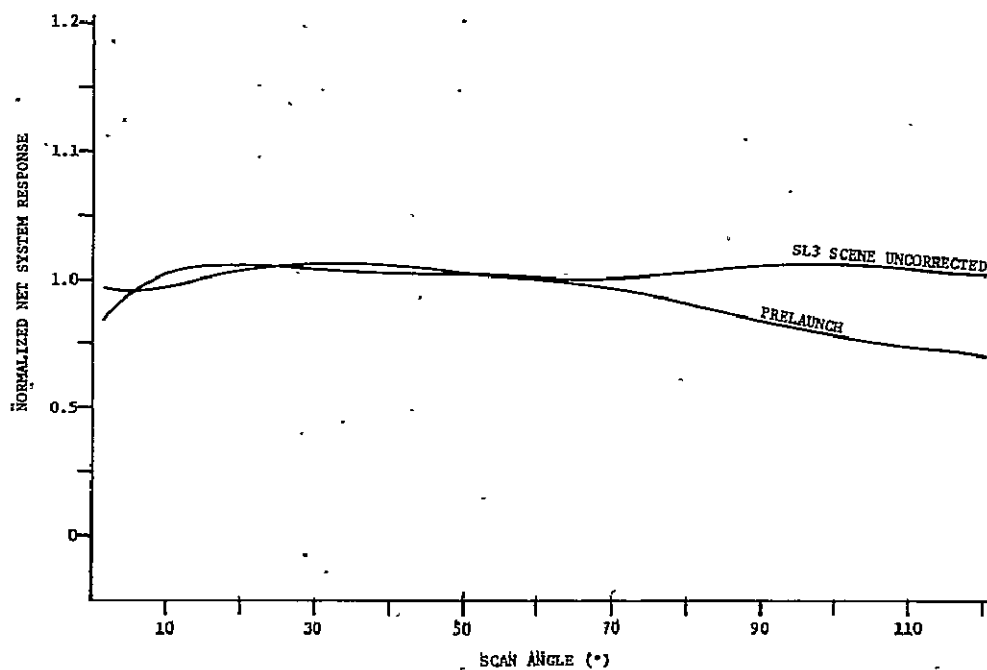


Figure 4.1-2.- Comparison of SL3 scene (Sahara Desert) with prelaunch data for band 3.

A template corresponding to 300 S192 scan lines was overlaid on the S190A frames, covering each of three selected scenes. Six film density measurements were taken at each of nine scan locations 15° apart across the field of view of the S192, as illustrated in Figure 4.1-3. These measurements were converted to original flight-film values using SL3 sensitometric data for S190A. The six corrected values for each 15° location were then averaged to obtain an average density for each of the nine scan angles.

A spectral distribution for each type of scene was needed to provide comparative calibration measurements to define spectral limits and band shape. Because ground truth was not available for these particular sites, previously determined spectral distribution values calculated by Martin Marietta Corporation in 1973 for the Great Salt Lake Desert were substituted for the Sahara Desert sites.

A density from the film, assumed scene spectral distribution, and S190A system transmittance values based on preflight test data were then used in a Martin Marietta Corporation computer program. This computed effective target radiance above the atmosphere as predicted by the S190A. These data were plotted as a function of position on the S192 scan and a sixth-order polynomial fit of the data was made. Figure 4.1-4 shows the polynomial normalized to the midpoint on the scan line for the Sahara Desert scene derived from S190A station 6.

The results from S190A indicated that the radiance of the Sahara scene was not uniform. Radiance over the last 60° of the scene increased by approximately 7% relative to the center.

This result was used to correct the S192 scan function by accounting for lack of scene uniformity. Figure 4.1-5 compares the prelaunch scan response with SL3 data from Figures 4.1-2 corrected for scene variation indicated by Figure 4.1-4.

Use of this technique demonstrated that, even without a large uniform-radiance scene, scene nonuniformity could be approximated and scan function determined in those S192 bands for which a S190A provided corresponding spectral bands. Implications as to the scene nonuniformity might then be drawn for other S192 bands.

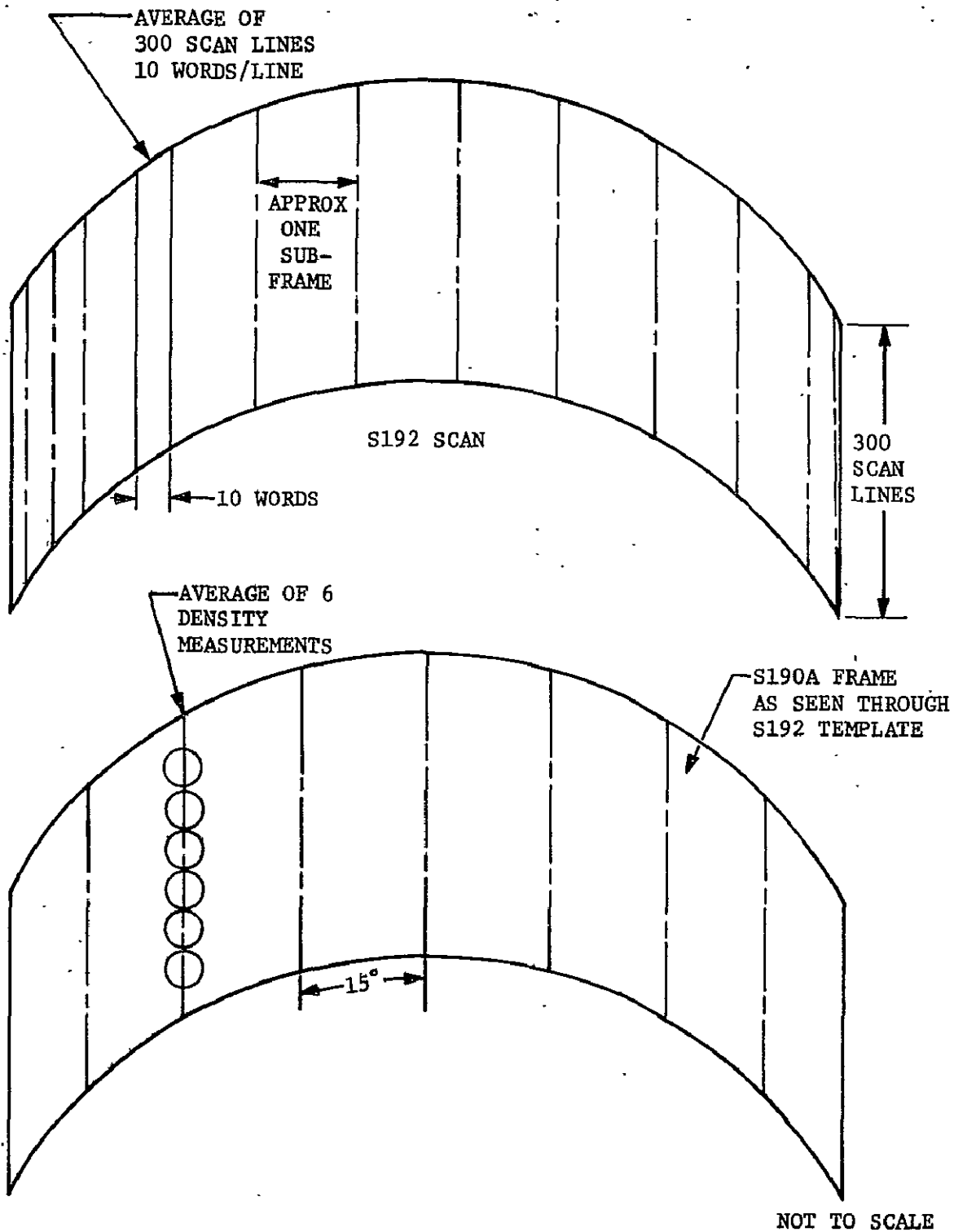


Figure 4.1-3.- Comparison of S192 data product and S190A densitometry data.

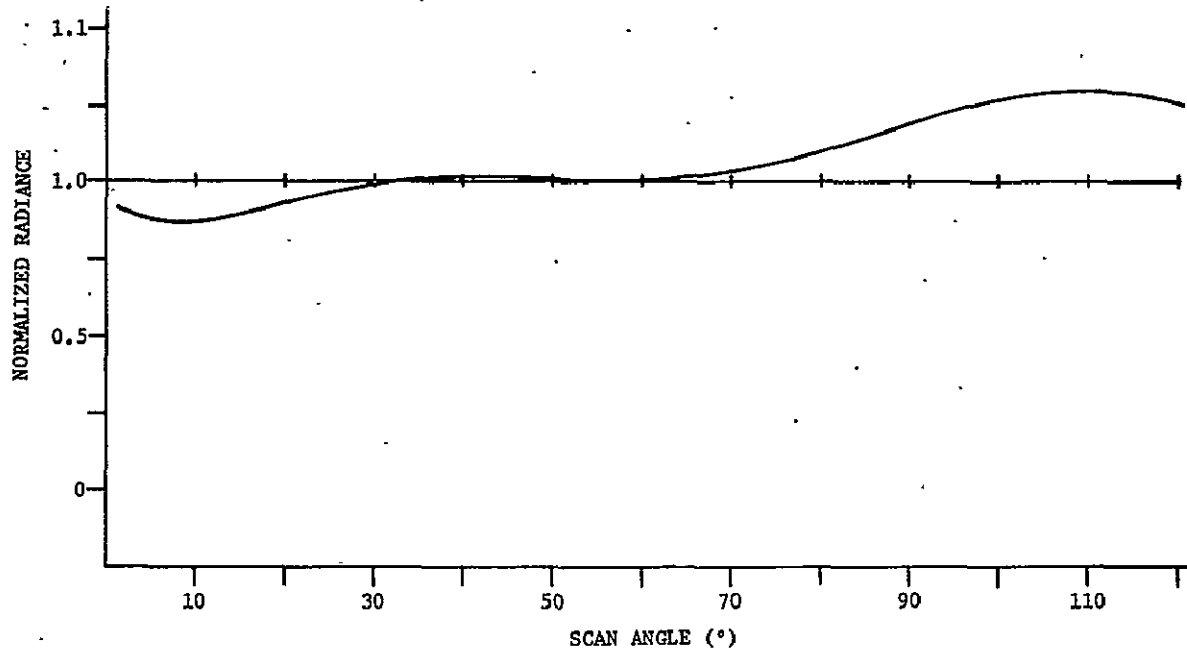


Figure 4.1-4.- S190A computed scene radiance variation for Sahara Desert.

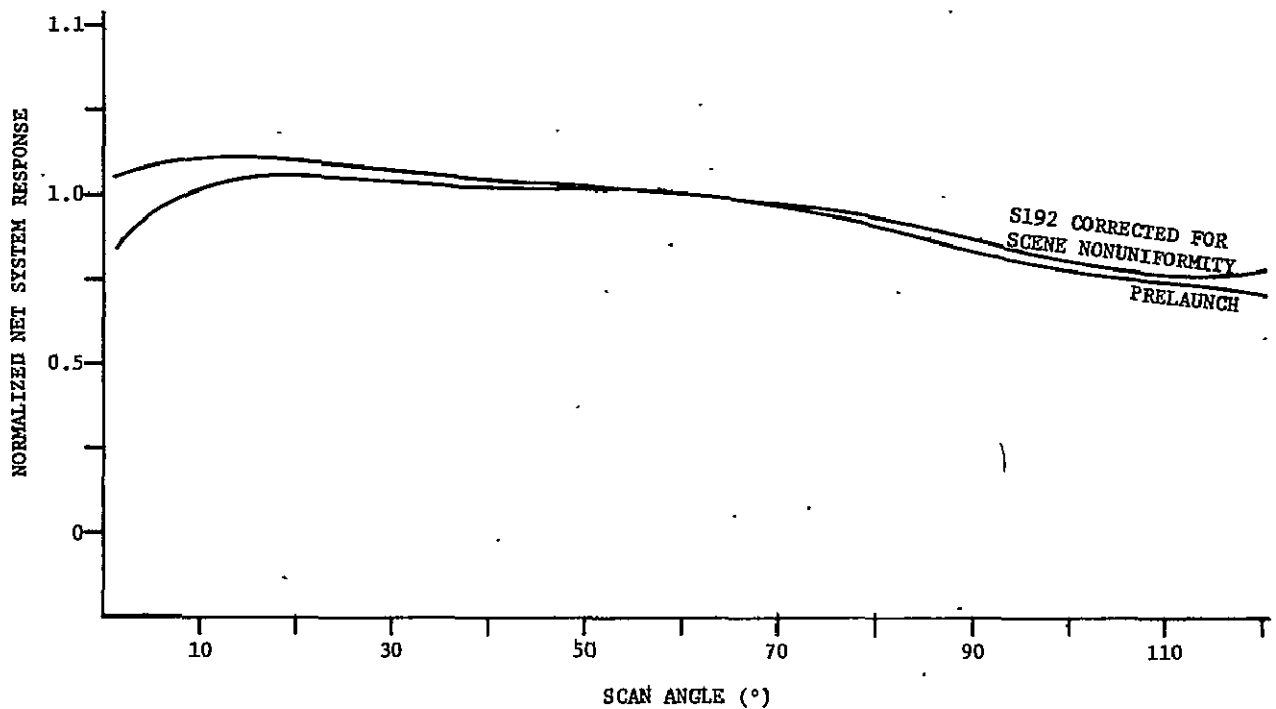


Figure 4.1-5.- Comparison of S192 data for Sahara Desert corrected for S190A scene radiance variation with prelaunch data for band 3.

4.2 Supplementary Analysis of System Noise

System noise requirements of the EIS (End Item Specification) for S192 Multispectral Scanner were stated in terms of NEAe (noise equivalent reflectance increment) and NEAT (noise equivalent temperature increment). These measures of noise level tie the system performance to the viewed scene characteristic of principal importance and, therefore, require certain viewing conditions to be defined. The scanner is always assumed to have its optical axis aligned with the local vertical axis, and the earth's surface is assumed perpendicular to it, so only the illumination conditions, and reflective properties of the scenes for bands 1 through 12 and the temperature and emissivity of the earth's surface are required to be specified. Those conditions used in the EIS were selected to be representative of average or "normal" conditions for an earth scene and are given in Table 4.2-1.

Prelaunch, both at Honeywell Radiation Center during acceptance tests and at Kennedy Space Center during integration and checkout testing, and postlaunch before the scheduled sensor performance evaluation could be performed an evaluation of the S192 noise characteristics was required. To enable direct comparison with the EIS values these noise values were generated in the form of NEAe and NEAT. The prelaunch data were obtained with the scanner viewing the uniform illuminated test target while inflight values through SL4 pass 83 (Y-3 array) were obtained from data sets taken over clear, calm (no foam) ocean free from glitter. The SL4 values after pass 83 (X-5 array) were derived from deep space σ 's for bands 1 through 12 and clear ocean σ 's for band 13 generated by ERIM in the course of developing calibration data. A tabulation of noise values for each mission is shown in Table 4.2-1 for information and as a formal record since these values were given substantial circulation -- mostly internal to NASA.

These results for the Y-3 array show that the noise levels increased inflight over the prelaunch values. The noise performance generally improved as the Skylab flights proceeded due to efforts to eliminate the causes of the increased levels. Bands 4, 5, 12, and 13 exceeded the EIS noise levels, but this condition was known to exist prelaunch for 4, 5, and 12 and values for 13 were not obtained prelaunch due to the need for performing band 13 testing in a vacuum chamber.

The X-5 array noise values in the reflective bands are higher than those for the Y-3 array in all bands except in band 4 in which case it still exceeds the EIS value. The X-5 array band 13 noise value is significantly better than for Y-3 array and is better than the EIS requirements. These results were also anticipated (even though prelaunch system tests with the X-5 array were impossible) since the dewar containing the reflective bands array was opened to replace the thermal detector. The reflective array then had to be put through a second outgassing bake-out and schedule did not permit tuning the band 1 through 12 preamps to the changed detectors.

4.3 S190A, S191, and S192 Radiometric Comparison

Each EREP optical sensor (S190A, S191, and S192) was designed and calibrated to provide absolute spectroradiometric data. These sensors also covered common wavelength regions, which facilitated a radiometric comparison. However, the spectral bands and band-widths were different and required band averaging to accomplish the comparison. The spectral bands for each sensor are given in Table 4.3-1. The radiometric values output from the sensors were converted to common units. The S190A output data were converted to units of spectral radiance ($\text{mW/cm}^2\text{-}\mu\text{m-ster}$) by dividing the S190A total radiance output ($\text{mW/cm}^2\text{-ster}$) by the bandwidth of each station. The bandwidth equaled the difference between the limits of integration used to calculate the S190A radiance output from equation A.II.12, Appendix A, Section II of Volume I.

The radiometric comparison as planned was to have compared radiance values when all three sensors were observing the same target. However, due to mission scheduling difficulties only one ground truth site suitable for radiometric evaluation was observed simultaneously by all three sensors. This site was the Willcox Playa observed during SL2 when there were small cumulus clouds near the site, and which probably influenced the results. However, common sites were available for comparing S190A to S191, S190A to S192, and a limited comparison of S191 to S192. Based on data from these sites the overall comparison of all three sensors could be made.

4.3.1 Comparison of S190A to S191

Comparison of S190A to S191 was based on the three sites:

<u>Mission</u>	<u>Date</u>	<u>Site</u>
SL2	6/3/73	Willcox Playa, Arizona
SL3	8/11/73	Katherine Playa, New Mexico
SL4	2/1/74	Katherine Playa, New Mexico

The spectral radiance of each site was first calculated from the S191 data for 13 narrow wavelength bands over the spectral range of the S190A (0.44 to 0.9 μm). These data were calculated using S191 responsivity derived from ground-based lunar mare measurements made with the S191 backup spectrometer. This responsivity is given in Volume II, Figure 4.1-1, channel A-5. The resulting spectral radiance values for the three sites are listed in Table 4.3.1-1 and plotted in Figure 4.3.1-1. These data were then averaged over each of the S190A spectral bands to obtain the average spectral radiance comparable to each S190A station. The resulting average spectral radiance for both sensors and that derived from the ground truth measurement are listed in Table 4.3.1-2. Radiance ratios were also calculated and listed to provide a basis for inter-sensor comparison.

TABLE 4.2-1.- S192 MULTISPECTRAL SCANNER SENSITIVITY (NOISE)*

Band Number	Spectral Interval (um)	Assumed Atmosphere Transmission, %	EIS	Prelaunch Y-3 Array	Y-3 Array			X-5 Array SL-4
					SL-2	SL-3	SL-4	
1	0.41 to 0.46	45	2.0	N/A**	1.4	1.3	1.1	2.2
2	0.46 to 0.51	45	2.0	0.9	1.0	1.1	0.8	2.5
3	0.52 to 0.51	55	2.0	1.0	1.5	1.2	1.0	1.6
4	0.56 to 0.61	55	2.0	2.4	3.7	2.8	2.5	2.1
5	0.62 to 0.67	60	2.0	3.0	4.2	2.5	2.5	---
6	0.68 to 0.76	65	2.0	1.3	1.6	1.5	1.3	2.6
7	0.78 to 0.88	70	2.0	1.4	1.8	1.7	1.5	3.0
8	0.98 to 1.08	80	2.0	1.3	1.5	1.5	1.6	3.0
9	1.09 to 1.19	50	2.0	0.9	0.9	1.2	0.9	2.7
10	1.20 to 1.30	80	2.0	1.8	1.9	1.7	1.7	---
11	1.55 to 1.75	70	2.0	1.5	1.6	1.8	2.0	2.6
12	2.10 to 2.35	70	2.0	2.3	2.4	1.5	2.2	2.7
13	10.2 to 12.5	90	1.5 ⁰ K	N/A***	4.0 ⁰ K	2.6 ⁰ K	2.2 ⁰ K	0.8 ⁰ K

*Bands 1 thru 12 are NEAp (% earth reflectance) while Band 13 is NEAT (⁰K), see note below.

**Band 1 attenuation removed after ground testing completed.

***Ground test of thermal band impossible outside vacuum chamber.

NOTE: NEAp's and NEAT's were computed using the atmospheric transmissions in the table, solar irradiance = 140 mw/cm² (outside the atmosphere), scene reflectance = 20% (diffuse), angle of incidence of solar radiation = 45⁰, and (for NEAT) the earth a 300⁰K blackbody.

TABLE 4.3-1.- S190A, S191, AND S192 SPECTRAL BANDS FOR RADIOMETRIC COMPARISON

S190A		S192		S191*		
Station	Wavelength Band (μm)	Band	Wavelength Band (μm)	Segment	Wavelength Range (μm)	Wavelength Resolution (μm)
6	0.48 to 0.63	1	0.41 to 0.45	1	0.39 to 0.73	0.0115
		2	0.45 to 0.51			
		3	0.50 to 0.56			
5	0.58 to 0.72	4	0.54 to 0.60	2	0.68 to 1.43	0.0185
		5	0.60 to 0.66			
		6	0.65 to 0.74			
1	0.68 to 0.78	7	0.77 to 0.89	3	1.34 to 2.50	0.015 $\times \lambda$
2	0.75 to 0.90	8	0.93 to 1.05			
		9	1.03 to 1.19			
		10	1.15 to 1.28	4	5.82 to 11.40	0.019 $\times \lambda$
		11	1.55 to 1.73			
		12	2.10 to 2.34			
		13	10.07 to 12.68	5	8.30 to 15.99	0.019 $\times \lambda$

* S191 had a continuously variable filter; definable narrow bands are given by the wavelength resolution.

This comparison shows that the spectral radiance values derived from S191 were consistently higher than those from S190A, with an average about 18% higher. The large ratios for both S190A and S191 with ground truth data for Willcox Playa indicate that local atmospheric conditions caused the S191 ground truth calculations to give erroneously low spectral radiance values, particularly in the near-infrared bands. This result supports the suspicions of that data.

The camera station operating in the visible spectral region showed better agreement with S191 data than did the infrared-sensitive stations.

4.3.2 Radiometric Comparison of S190A to S192

The comparison of S190A and S192 absolute radiometric measurements was based on four ground sites:

<u>Mission</u>	<u>Date</u>	<u>Site</u>
SL2	6/3/73	Willcox Playa, Arizona
SL3	9/2/73	Sahara Desert, Africa
SL3	9/13/73	Great Salt Lake Desert, Utah
SL3	9/17/73	Gulf of Mexico

TABLE 4.3.1-1.- S191 SPECTRAL RADIANCE FOR S190A AND S191 COMPARISON SITES

Wavelength (μm)	SPECTRAL RADIANCE VALUE ($\text{mW}/\text{cm}^2\text{-}\mu\text{m}\text{-ster}$)		
	Willcox Playa, SL2	Katherine Playa, SL3	Katherine Playa, SL4
0.448	17.63	12.05	8.542
0.475	18.64	12.50	8.975
0.500	17.09	11.45	8.853
0.552	15.40	10.1	8.828
0.600	15.04	10.0	9.267
0.657	15.78	10.9	10.286
0.675	15.65	10.5	10.199
0.700	14.61	9.21	9.866
0.725	15.58	10.04	10.468
0.741	15.29	10.65	10.474
0.800	14.46	9.86	9.920
0.850	12.42	8.75	8.454
0.901	9.28	5.97	6.418

No ground truth measurements were made at the Sahara Desert and the Gulf of Mexico sites. Unlike the S191 spectrometer, neither the S190A nor S192 had sufficiently narrow bands to define the detailed spectral distribution of the ground sites. Also, the spectral bands and response of these two systems were different. However, it was possible to obtain meaningful radiometric comparison data by calculating the average spectral radiance for each S190A station and S192 band; then computing the average of the S192 bands covering the spectral range of each S190A station. Specifically, S190A station 6 was comparable to the average of S192 bands 3 and 4; station 5 was comparable to the average of bands 5 and 6; station 1 was comparable to the average of bands 6 and 7; and station 2 was comparable to S192 band 7. The spectral ranges of these stations and bands are given in Table 4.3-1.

The average spectral radiance values and radiance ratios for the S190A, S192 and the ground truth measurements are given in Table 4.3.2-1. The S192 Willcox Playa data were recorded on pass 3 of SL2 before installation of the attenuators. The "off scale" listed in the table means the output signal was above the upper limit for bands 4 and 5. This condition was later corrected by installation of the attenuators. Review of this table shows similar error magnitude in the Willcox Playa ground truth data as in the comparison of S190A to S191. The data also indicate good agreement between S190A and S192 radiance values, with no apparent systematic error, or bias, in the comparison.

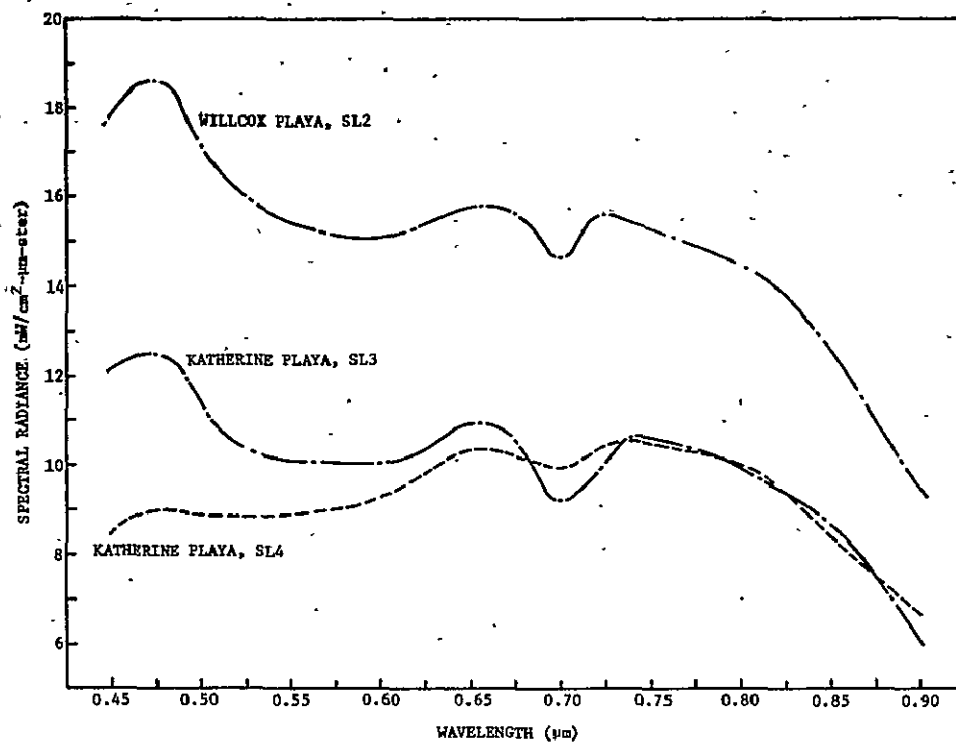


Figure 4.3.1-1.- S191 spectral radiance plot for S190A and S191 comparison sites.

TABLE 4.3.1-2.- S190A, S191, AND GROUND-TRUTH RADIOMETRIC COMPARISON

MISSION	SITE	DATE	SPECTRAL RADIANCE (mW/cm ² -μm-ster)			RADIANCE RATIO			WAVELENGTH BAND (μm)
			S190A	S191	Ground Truth	S190A/S191	S190A/Ground Truth	S191/Ground Truth	
SL2	Willcox Playa	6/3/73	11.93	16.93	10.27	0.70	1.16	1.65	0.48 - 0.63
			14.79	16.28	10.00	0.91	1.48	1.63	0.58 - 0.72
			11.21	14.95	7.16	0.75	1.57	2.09	0.68 - 0.87
			10.93	13.93	6.07	0.78	1.80	2.29	0.75 - 0.90
SL3	Katherine Playa	8/11/73	9.47	11.27	12.00	0.84	0.79	0.94	0.48 - 0.63
			10.79	10.86	11.57	0.99	0.93	0.94	0.58 - 0.72
			6.89	10.16	8.95	0.68	0.77	1.14	0.68 - 0.87
			6.40	9.60	8.20	0.67	0.78	1.17	0.75 - 0.90
SL4	Katherine Playa	2/1/74	9.27	9.67	9.93	0.96	0.93	0.97	0.48 - 0.63
			9.07	10.57	10.14	0.86	0.89	1.04	0.58 - 0.72
			No Data	10.21	8.05	--	--	1.27	0.68 - 0.87
			8.00	9.53	7.33	0.84	1.09	1.30	0.75 - 0.90

TABLE 4.3.2-1.- S190A, S192, AND GROUND-TRUTH RADIOMETRIC COMPARISON

MISSION	SITE	DATE	AVERAGE SPECTRAL RADIANCE (mW/cm ² -μm-ster)			RADIANCE RATIO			COMPARATIVE OUTPUT	
			S190A	S192	Ground Truth	S190A/S192	S190A/ Ground Truth	S192/ Ground Truth	S190A (Station)	S192 (Bands)
SL2	Willcox Playa	6/3/73	11.93	off scale	10.27	--	1.16	--	6	3,4 average
			14.79	off scale	10.00	--	1.48	--	5	5,6 average
			11.21	11.54	7.16	0.97	1.57	1.57	1	6,7 average
			10.93	11.32	6.07	0.97	1.80	1.86	2	7
SL3	Sahara Desert	9/2/73	7.75	8.10	--	0.96	--	--	6	3,4 average
			12.25	10.68	--	1.15	--	--	5	5,6 average
			No Data Available			No Data Available			1	6,7 average
			7.92	9.36	--	0.85	--	--	2	7
SL3	Great Salt Lake Desert	9/13/73	13.27	11.39	11.00	1.17	1.21	1.04	6	3,4 average
			13.21	11.12	10.43	1.19	1.27	1.07	5	5,6 average
			9.00	9.78	7.79	0.92	1.16	1.26	1	6,7 average
			8.73	9.17	6.93	0.95	1.26	1.32	2	7
SL3	Gulf of Mexico	9/17/73	4.15	3.43	--	1.21	--	--	6	3,4 average
			2.06	1.62	--	1.27	--	--	5	5,6 average

4.3.3 Radiometric Comparison of S191 to S192

Only two ground sites suitable for radiometric comparison of S191 to S192 were available. They were the SL2 Willcox Playa site discussed in paragraphs 4.3.2 and 4.3.2 and the Rio Grande Reservoir, Colorado, site observed on 8/8/73 during the SL3 mission. The absolute spectral radiance values based on S191 data for Willcox Playa are listed in Table 4.3.1-1 and plotted in Figure 4.3.1-1. The S191 spectral radiance for the Rio Grande Reservoir is given in Table 4.3.3-1 and plotted in Figure 4.3.3-1.

The comparison of S191 to S192 was achieved by taking the average of the S191 spectral radiance over each corresponding S192 band. Infrared wavelengths greater than 0.901 μm were not considered due to a lack of analysis time. The resulting comparative data are listed in Table 4.3.3-2.

A review of this table for Rio Grande Reservoir shows the S191-derived spectral radiance is higher than that for S192 by approximately 16%. The S192 results for Willcox Playa differ significantly from those of S191. No attenuators had been installed in S192 and other problems were associated with these data. The differences with Willcox Playa ground truth are again apparent.

4.3.4 Radiometric Comparison Summary

The derived spectral radiances from various targets agree closely for S190A and S192. The S191 values were about 16 to 18% higher than those for S190A and S192. The values are given in Tables 4.3.1-2, 4.3.2-1, and 4.3.3-2. The agreement among the three sensors was judged to be excellent considering that a recent study* showed the variation in radiometric calibrations made at

*Franc Grum and Joseph Cameron: "Detector Intercomparison Results,"
Electro-Optical Systems Design, Vol 6, November 1974, p 82.

TABLE 4.3.3-1.- S191 SPECTRAL RADIANCE OF RIO GRANDE RESERVOIR FOR COMPARISON OF S191 TO S192

Wavelength (μm)	Spectral Radiance ($\text{mW}/\text{cm}^2\text{-}\mu\text{m}\text{-ster}$)
0.448	4.94
0.475	4.48
0.50	3.69
0.552	2.74
0.60	1.72
0.657	1.42
0.675	1.37
0.70	1.41
0.725	1.42
0.741	1.46
0.80	1.37
0.85	1.12
0.901	0.80

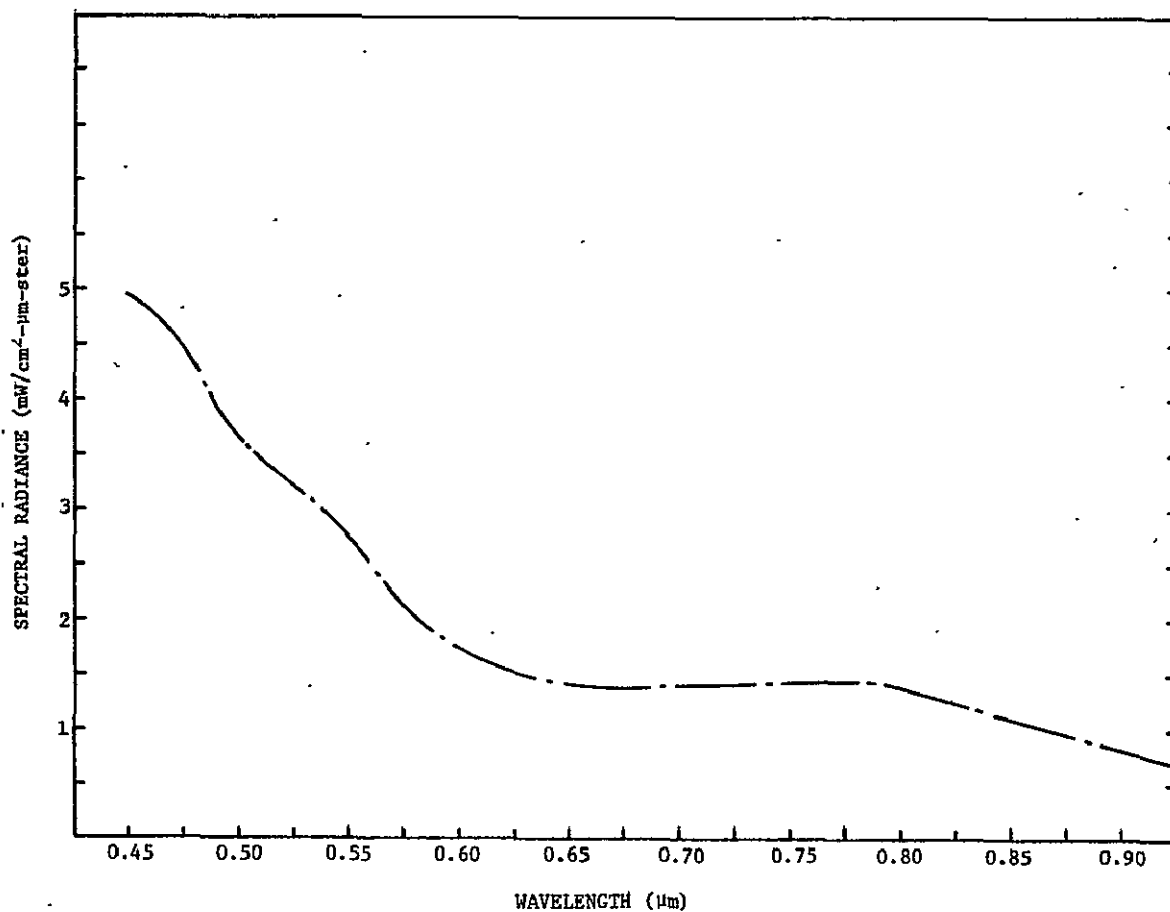


Figure 4.3.3-1.- S191 spectral radiance of Rio Grande reservoir, SL3.

TABLE 4.3.3-2.- S191, S192, AND GROUND-TRUTH RADIOMETRIC COMPARISON

MISSION	SITE	DATE	AVERAGE SPECTRAL RADIANCE (mW/cm ² -μm-ster)			RADIANCE RATIO			S192 SPECTRAL BAND
			S191	S192	Ground Truth	S192/S191	S191/ Ground Truth	S192/ Ground Truth	
SL2	Willcox Playa	6/3/73	17.8	9.51	10.8	0.534	1.648	0.881	2
			16.1	10.13	9.4	0.629	1.713	1.078	3
			15.3	off scale	9.4	---	1.628	---	4
			15.4	off scale	9.7	---	1.588	---	5
			15.3	11.54	8.6	0.754	1.779	1.342	6
			13.0	11.32	5.6	0.870	2.321	2.021	7
SL3	Rio Grande Reservoir	8/8/73	4.43	3.49	Not available	0.788	---	---	2
			3.20	2.70		0.844	---	---	3
			2.92	2.38		0.815	---	---	4
			1.51	1.60		1.060	---	---	5
			1.36	1.05		0.772	---	---	6
			1.17	1.03	Not Available	0.880	---	---	7

various standards laboratories to be approximately $\pm 10\%$ (total variation 20%) from the consensus. Considering the space environment, the variations in spectral bands, and the less-than-optimum calibration procedures available before launch, the relative radiometric absolute accuracy of these three instruments was considered excellent.

These data also showed that, based on these S190A and S192 results it appears that the lunar radiance values calculated using the Lane and Irvine data* were approximately 25% high.

REPRODUCIBILITY OF THE
ORIGINAL PAGE IS POOR

*A. P. Lane and W. M. Irvine, "Monochromatic Phase Curves and Albedos for the Lunar Disk," The Astronomical Journal, Vol 78, No. 3, 1972.

5.0 CONCLUSIONS

The sensor functioned very well indeed. The refrigerator which cooled the detectors and the dwarf which contained the detectors were considered prelaunch as the most likely source of functional problems and none materialized.

The geometric performance was excellent since the data proved to be readily registerable to maps and to LANDSAT A data.

In 9 of the 13 bands radiometric performance was very good. In most instances where the performance did not meet the EIS requirements the deficiencies were known to exist prelaunch and could have been remedied had the time and equipment been available. The principal surprise was the poor quality of the band 13 (thermal) data from the Y-3 array. This arose from the inability to complete the planned prelaunch testing in a vacuum chamber. That this could be overcome was demonstrated by the excellent quality of the band 13 X-5 array data.

Band 1 data was generally unusable for most purposes due to its poor frequency response in SL2 and SL3 and its calibration changed significantly in SL4. Bands 4 and 5 had low signal-to-noise ratio which tends to make tests of the utility of the additional bands which include comparison with LANDSAT A inconclusive.

These problems notwithstanding, the S192 Multispectral Scanner produced highly useful data in more spectral bands and in narrower spectral bands than any set of scanner data yet available for Earth Resources Survey uses.

6.0 RECOMMENDATIONS

As described throughout this report and MSC-05528, there were a number of areas in which the design and use of S192 Multispectral Scanner could have been improved upon. In most instances the deficiencies were known prelaunch and could have been cured given the opportunity. Since S192 will never be flown again there will be no attempt here to detail all the problems and recommend detailed solutions which are irrelevant. The recommendations below are those which are applicable to the whole genre of multispectral scanners and to image plane scanners in particular.

6.1 For high performance image plane scanners, provide a mechanism for in-flight determination of response versus scan angle variation. This could be a uniform test target (which can be illuminated or left dark on command) included in an enlarged objective aperture cover (this adds complexity, size, weight, and power consumption to the primary sensor). It could also be a separate, small object plane scanner with the same spectral characteristics but much lower spatial resolution (and data rate) to define the scene variation for use as described in paragraph 4.1. Either of these devices should be well calibrated and well exercised (and therefore well understood) prelaunch since they are calibration devices in themselves.

6.2 For image plane scanners used in applications requiring accurate calibration (either relative or absolute) a mechanism for inflight check of calibration, including all telescope mirrors should be provided. The near-full moon provides an excellent external source for monitoring stability of relative calibration between bands if operational constraints permit it to be viewed at appropriate times. The two mechanisms described in paragraph 6.1 would be suitable for check of either absolute or relative calibration.

6.3 For any scanner used in applications requiring accurate calibration the internal calibration sources must be uniform and stable in radiance, inset sufficiently into the dynamic range of the sensor to prevent clipping, and usable in all testing environments.

6.4 For any scanner: calibration data, data processing algorithms, and data processing computer programs should be developed in parallel with the sensor hardware so that data from Acceptance Tests, Qualification Tests, and Integration Tests can be processed and evaluated as the actual flight data will be. From this it follows that such testing should be done in "as near flight configuration as possible" with the minimum requirement to record the data in same form and format that the flight data will be recorded.

7.0 NOTES

7.1 Acknowledgements

The effort covered by this report was sponsored by the Earth Resources Program Office of the Lyndon B. Johnson Space Center. It is based on the results of a concerted effort by numerous individuals in:

Environmental Research Institute of Michigan (ERIM)
Ann Arbor, Michigan

Science and Applications Directorate
Lyndon B. Johnson Space Center

Lockheed Electronics Company, Incorporated
Lyndon B. Johnson Space Center

Martin Marietta Corporation
Denver, Colorado

Particular acknowledgement is due the late Mr. Charles K. Williams of the Skylab Program Office of the Lyndon B. Johnson Space Center. His dedication and leadership were essential to the successful completion of these evaluation studies. Alan L. Grandfield and William E. Hensley of JSC/SEAD, John G. Braithwaite and Peter Lambeck of ERIM, Earl W. Johnson and William M. Miller of MMC, and Rupp C. Malhotra and Charles C. Campbell of LEC/ASD have made substantial contributions to this effort.

7.2 Abbreviations

Abbreviations in common usage have been used for English units of measure. International units (SI) have been abbreviated in accordance with E. A. Mechtly's NASA SP-7012, The International System of Units, 2nd Rev; National Aeronautics and Space Administration, Washington, D.C., 1973—except for stera-dian, which has been abbreviated to ster.

AVG	Average
C/D/P	Cooler/Dewar/Preamplifier Assembly
DRA	Data reformatting assembly
EREP	Earth Resources Experiment Package
ERIM	Environmental Research Institute of Michigan (Formerly Willow Run Laboratories, University of Michigan)
FOV	Field of view
JSC	Lyndon B. Johnson Space Center
KSC	Kennedy Space Center
LC	Lunar calibration
LEC/ASD	Lockheed Electronics Corporation, Aerospace Systems Division
MMC	Martin Marietta Corporation
MSC	Manned Spacecraft Center
MTF	Modulation transfer function
N/A	Not available
NEAT	Noise-equivalent temperature difference
NESR	Noise-equivalent spectral radiance
NOAA	National Oceanic and Atmospheric Administration
OFCE	Optical functional checkout equipment
PASS XX	Pass numbers used in this document are EREP Skylab consecutive pass numbers
PRT-5	Barnes precision thermal radiometer, Model PRT-5
PSD	Power spectral density

MSC-05546

RPMI	Radiant-power measuring instrument, Bendix Model 100
S&AD	Science and Applications Directorate, JSC
SKYBET	Skylab Best Estimate of Trajectory Ephemeris Data
SL2	First Manned Skylab Flight
SL3	Second Manned Skylab Flight
SL4	Third Manned Skylab Flight
SPE	Sensor performance evaluation
X-5	C/D/P installed between EREP passes 83 and 84 during SL4
Y-3	Primary C/D/P used during SL2 and SL3 and through pass 83 during SL4

APPENDIX A

TECHNIQUES ADDENDUM

This appendix describes in detail the techniques used to evaluate S192 performance as presented in the Sensor Performance Evaluation Report, MSC-05528, Volume III, dated September 6, 1974. These descriptions of the techniques include both the theoretical approach and the mechanics of application.

I. SPECTRORADIOMETRIC CALIBRATION OF S192 BASED ON GROUND TRUTH MEASUREMENTS

Spectroradiometric calibration of the S192 required that the relationship between output of the instrument (in counts) and a known input spectral radiance ($N_{S\lambda}$) be determined. One means of obtaining this relationship was the use of ground truth measurements made by Martin Marietta concurrently with EREP overpasses. The detailed results of these ground truth measurements were reported for each Skylab mission.*

The expression relating $N_{S\lambda}$ to the quantities measured on the ground is

$$N_{S\lambda} = \frac{\rho}{\pi} H e^{-\tau \sec \theta} + N_{a\lambda} \quad [A.I.1]$$

where

$N_{S\lambda}$ = apparent spectral radiance from the target area at the spacecraft

H = total (direct and diffuse) spectral radiance incident on the target

ρ = target reflectivity (as a function of wavelength)

τ = atmospheric optical depth

θ = sensor view angle with respect to the normal

$N_{a\lambda}$ = atmospheric path spectral radiance

The methods used to measure H , ρ , τ , and $N_{a\lambda}$ are:

1) Total solar radiance, H , (direct and diffuse) incident on the target. A spectral scanning spectroradiometer covering the wavelength range from 400 to 1300 nm was used to measure the total solar radiation incident on the target.

* MSC-05531 Ground Truth Data for Test Sites (SL2), August 15, 1973

MSC-05537 Ground Truth Data for Test Sites (SL3), March 29, 1974

MSC-05543 Ground Truth Data for Test Sites (SL4), April 30, 1974

2) Target reflectivity, ρ , (as a function of wavelength). The same spectroradiometer used to measure H was used to measure the radiance reflected from the target area. The ratio of these two values gives the target reflectivity.

3) Atmospheric optical depth, τ . This quantity is calculated by using measurements of the direct solar radiance as functions of the solar incidence angle.

The instrument used was a pyrheliometer, which is a spectral scanning spectroradiometer equipped with a collimator. In use, it is pointed directly at the sun, and produces a meter reading, M , that is proportional to the direct solar radiance at the surface. Using the expression

$$M = M_0 e^{-\tau \sec \theta_0} \quad [A.I.2]$$

where

M_0 = the value of M that would be observed by the pyrheliometer if it were above the atmosphere

θ_0 = solar incidence angle (with respect to the normal),

rewriting the equation by taking logs of both sides and transposing,

$$\tau \sec \theta_0 = \log M_0 - \log M \quad [A.I.3]$$

By measuring values of M at various values of θ_0 , simultaneous equations can be written and solved for τ and M_0 . In practice, the solution technique used is to plot values of M versus $\tau \sec \theta$ (which gives the relative air path length with respect to a vertical path) on a semilog plot. The slope of the line is $-\tau$, and the extrapolated line intercept with the vertical axis gives the value of M_0 . This technique allows a convenient least squares fit of the data to determine M_0 .

4) Atmospheric path spectral radiance $N_{a\lambda}$. This is a calculated quantity derived from an atmospheric radiative transfer computer model**.

** W. A. Malila, et.al: Studies of Spectral Discrimination, Report No. NAS CR-WRL 31650-22-T, Contract NAS9-9784, May 1971.

Required inputs to the computer program are:

- a) altitude of the sensor;
- b) target reflectivity;
- c) target background reflectivity;
- d) solar zenith angle;
- e) solar-sensor azimuth angle;
- f) sensor view angle;
- g) atmospheric visual range.

These values were available from field observations, Skylab Best Estimate of Trajectory Ephemeris Data (SKYBET), mission tapes and ephemeris data.

Radiance at the S192 aperture determined from ground truth measurements and the path radiance program were presented as a curve of apparent spectral radiance $[N_s(\lambda)]$ versus wavelength (λ) . For example, results of SL3 measurements of the Great Salt Lake Desert ground truth site are presented in Figure A.I-1.

S192 response to this input radiance was determined as follows.

For a constant input radiance, $I d\lambda$, from λ to $\lambda + d\lambda$, where I is a constant spectral radiance independent of λ , detector output is $S_x(\lambda) d\lambda$, for each S192 band, $x = 1, 2, 3, \dots, 12$. For an input spectral radiance, i , over the frequency range λ_{x1} to

λ_{x2} , the detector output is $\int_{\lambda_{x1}}^{\lambda_{x2}} S_x(\lambda) d\lambda$. S192 response should

be equal to the input spectral radiance, i . Therefore, a conversion factor, A , is applied to the detector output so that

$$i = A \int_{\lambda_{x1}}^{\lambda_{x2}} S_x(\lambda) d\lambda \quad [A.I.4]$$

Solving for A , the conversion factor required is given by

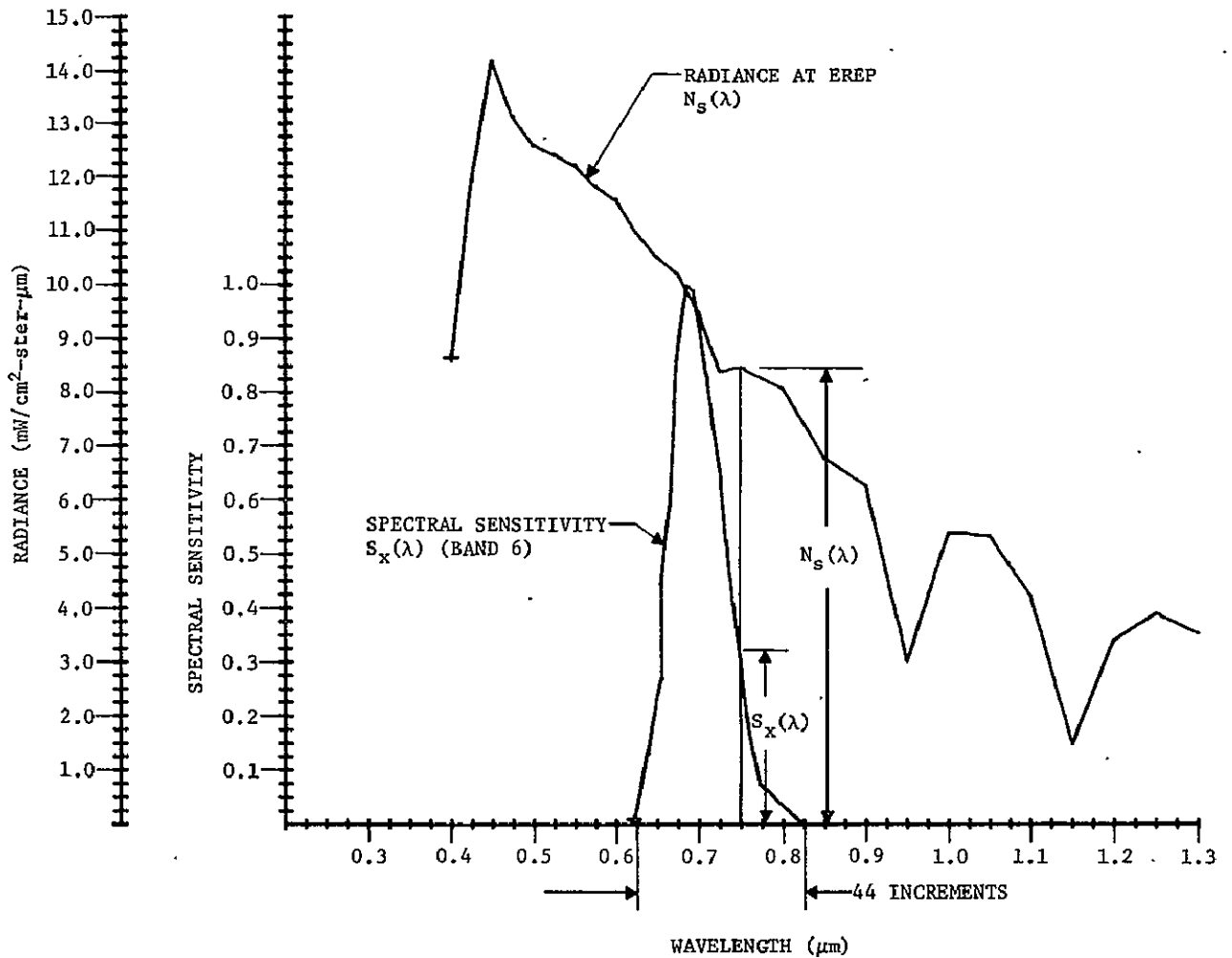


Figure A.I-1.- Sample determination of ground-truth atmospheric and target radiance for an S192 band.

$$A = \frac{I}{\int_{\lambda_{X1}}^{\lambda_{X2}} S_X(\lambda) d\lambda} \quad [A.I.5]$$

For a ground target input spectral radiance that is a function of λ , from λ to $\lambda + d\lambda$, $N_s(\lambda) d\lambda$, and the related S192 output for band X, $r(\lambda) d\lambda$

$$\frac{r(\lambda)d\lambda}{N_s(\lambda)d\lambda} = \frac{A S_X(\lambda) d\lambda}{I d\lambda} \quad [A.I.6]$$

solving for $r(\lambda)d\lambda$

$$r(\lambda)d\lambda = \frac{A S_X(\lambda) N_S(\lambda) d\lambda}{I} \quad [A.I.7]$$

substituting for A and integrating, where $R = \int r(\lambda)d\lambda$

$$RAD_X = \frac{\int_{\lambda_{X1}}^{\lambda_{X2}} S_X(\lambda) N_S(\lambda) d\lambda}{\int_{\lambda_{X1}}^{\lambda_{X2}} S_X(\lambda) d\lambda} \quad [A.I.8]$$

where

RAD_X = S192 average input spectral radiance for band X,
accounting for spectral sensitivity

$S_X(\lambda)$ = instrument spectral sensitivity for each band X
(X = 1, 2, 3, . . . 12)

$N_S(\lambda)$ = input spectral radiance.

Equation A.I-8 was used for determining S192 response to ground truth spectral radiance. The integrals were evaluated by using a curve multiplication program that performed a point-to-point multiplication and summation:

$$R_{GTX} = \frac{\sum_{i=1}^{44} S_{Xi}(\lambda) N_{Si}(\lambda)}{\sum_{i=1}^{44} S_{Xi}(\lambda)} \quad [A.I.9]$$

where

R_{GTX} = ground truth spectral radiance for each band X
(X = 1, 2, 3, . . . 9), accounting for the spectral
sensitivity of that band

$S_{Xi}(\lambda)$ = S192 spectral sensitivity for each band X
 (X = 1, 2, 3, . . . 9) for each segment, i, where
 a maximum of 44 segments were used over the band
 so that $\Delta\lambda$ = a constant

$N_{Si}(\lambda)$ = spectral radiance at the S192 aperture determined
 from ground truth measurements for each segment, i,
 whose value was determined to coincide with each
 $\Delta\lambda$ increment of the band X spectral sensitivity
 (X = 1, 2, 3, . . . 9)

This operation is illustrated in Figure A.I-1.

S192 digital output in counts corresponded to the ground truth radiance. The counts were obtained by selecting the instantaneous fields of view (picture elements or pixels) corresponding to the ground truth site and determining average counts for each band. In most cases, the size of the ground truth site limited the sample size to between 50 and 100 pixels.

S192 response in counts per unit of spectral radiance could then be determined.

$$\text{Response for band X} = \frac{\text{Average counts over ground truth site for band X (counts)}}{R_{\text{GTX}} (\text{mW/cm}^2\text{-ster-}\mu\text{m})}$$

Assuming the response was linear, it is the slope of a line for counts (0 to 255) versus radiance whose dynamic range was determined by the slope and count limits.

However, this calibration varied with the low-frequency noise on the output. To account for this effect, the response determined was used to find the equivalent calibration-lamp radiance for each band by using the output counts when viewing the calibration lamp for each scan line of the ground truth target.

$$ECR_X = \frac{1}{RESP_X} (\overline{CLC}_X) \quad [A.I.10]$$

where

ECR_X = equivalent calibration lamp spectral radiance for band X (X = 1, 2, 3, . . . 12)

$RESP_X$ = response for band X ($X = 1, 2, 3, \dots, 12$)

\overline{CLC}_X = average calibration lamp counts for band X
($X = 1, 2, 3, \dots, 12$) of the scan lines used in
obtaining $RESP_X$

This equivalent calibration-lamp spectral radiance is then independent of the low-frequency noise and can be used to obtain the slope of the calibration curve [counts versus radiance (mW/cm^2 -ster- μm)] applicable to a target of interest when the calibration lamp counts are known, i.e.,

$$\left(\text{Radiance of target of Interest}_X \right) = \frac{ECR_X}{\left(\begin{array}{c} \text{Target of} \\ \text{interest} \\ \text{calibration} \\ \text{counts}_X \end{array} \right)} \left(\begin{array}{c} \text{Target of} \\ \text{Interest Counts}_X \end{array} \right) \quad [A.I.11]$$

II. USE OF TOTAL LUNAR IMAGE TO DETERMINE ABSOLUTE RADIOMETRIC RESPONSE

In the S192 Production Data Processing System defined in PHO-TR524* the difference in signal output between a high (bright) and low (black) calibration source is used as an internal calibration reference. Thus to calibrate the several bands it is necessary to find the difference in radiance between two external sources which give rise to the same change in output signal as in generated by this internal reference. The mean signals from the moon and space have been used in this way. Assuming that the output is linear with radiance, one can obtain the calibration constant for band j :

$$L_j = L_{cj} \left(\frac{\bar{C}_{Hj} - \bar{C}_{Lj}}{\bar{C}_{cj} - \bar{C}_{Sj}} \right)$$

where \bar{C}_{Hj} is the mean count output on the high calibration source

\bar{C}_{Lj} is the mean count output on the low calibration source

\bar{C}_{cj} is the mean count output on the moon

\bar{C}_{Sj} is the mean count output on deep space at the same scan angle

j indicates the j th band

In order to make these results compatible with those obtained by others participating in the S192 performance evaluation, \bar{C}_H and \bar{C}_L were taken as the mean value of all six recorded values available for each SDO except for those bands with active Automatic Gain Control for which $(\bar{C}_H - \bar{C}_L)$ was put equal to 255. The steps used to obtain values for L_{cj} and $(\bar{C}_{cj} - \bar{C}_{Sj})$ will be described in the following subsections.

THE SPECTRAL RADIANT INTENSITY OF THE MOON

While there is an extensive literature on the photometry and radiometry of the moon, a search revealed only two programs whose results were relevant. (The remaining papers were too limited in spectral coverage, spatial coverage or lacked absolute calibration, or more often suffered from two or three of these

*Philco-Ford Corporation, Earth Resources Production Processing Requirements for EREP Sensors, NASA Report No. PHO-TR524 Rev. A, Change 2, Johnson Space Center, Houston, Texas, 1974.

defects.) The most useful results are those of W. M. Irvine and his co-workers** (and a series of earlier papers).

This article gives spectral magnitudes and spectral geometrical albedos for the moon as a function of lunar phase angle. Unfortunately the results only cover the spectral region from $0.36\mu\text{m}$ to $1.063\mu\text{m}$. However the region from $0.36\mu\text{m}$ out to $2.50\mu\text{m}$ is covered by the work of McCord and Johnson***. Over the spectral region ($0.36\mu\text{m}$ to $1.06\mu\text{m}$) common to both programs the results are inconsistent by up to about 10%. This, and inconsistencies between measurements made by the Irvine group at different times, are commented on in the referenced Irvine paper. The possibility of a variable moon is discussed but discarded, and the authors find no firm reason for the discrepancies. Further, the McCord and Johnson results are not given in absolute radiometric units and were made on relatively small areas of the moon, though a reasonable estimate for the entire moon can be made from the results given. Such an estimate has been used here.

The Irvine results are given in terms of spectral magnitudes and spectral geometric albedos together with the change in spectral magnitudes as a function of lunar phase. The albedos and the changes in magnitude with phase were used, as these two concepts are well defined in the paper whereas the concept of spectral magnitude was not. Since the albedo is a measure of reflectance rather than radiation this course involves using a measure of the solar spectral irradiance at the moon derived from some other source. Suitable results for the solar irradiance at the moon derived from some other source. Suitable results for the solar irradiance at the mean earth-sun distance are given in the Air Force Cambridge Research Laboratories Handbook of Geophysics and Space Environments*.

The spectral geometric albedo results from the Irvine paper are given in Figure A.II-1. Superimposed are the results from McCord normalized to fit the Irvine results as well as possible. The solid line is a best estimate and represents the values used. The scatter of the points suggests that the line lies within 10% of the true value and probably within 5%.

**A. P. Lane and W. M. Irvine, "Monochromatic Phase Curves and Albedos for the Lunar Disc," *Astronomical Journal*, Vol. 78, No. 3, April 1973, p. 267.

***T. B. McCord and T. V. Johnson, "Lunar Spectral Reflectivity (0.30 to 2.50 Microns)," *Science*, No. 169, 28 August 1970, p. 833.

*S. L. Valley, ed., *Handbook of Geophysics and Space Environments*, Air Force Cambridge Research Laboratories, Bedford, Massachusetts, 1963, pp. 16-5.

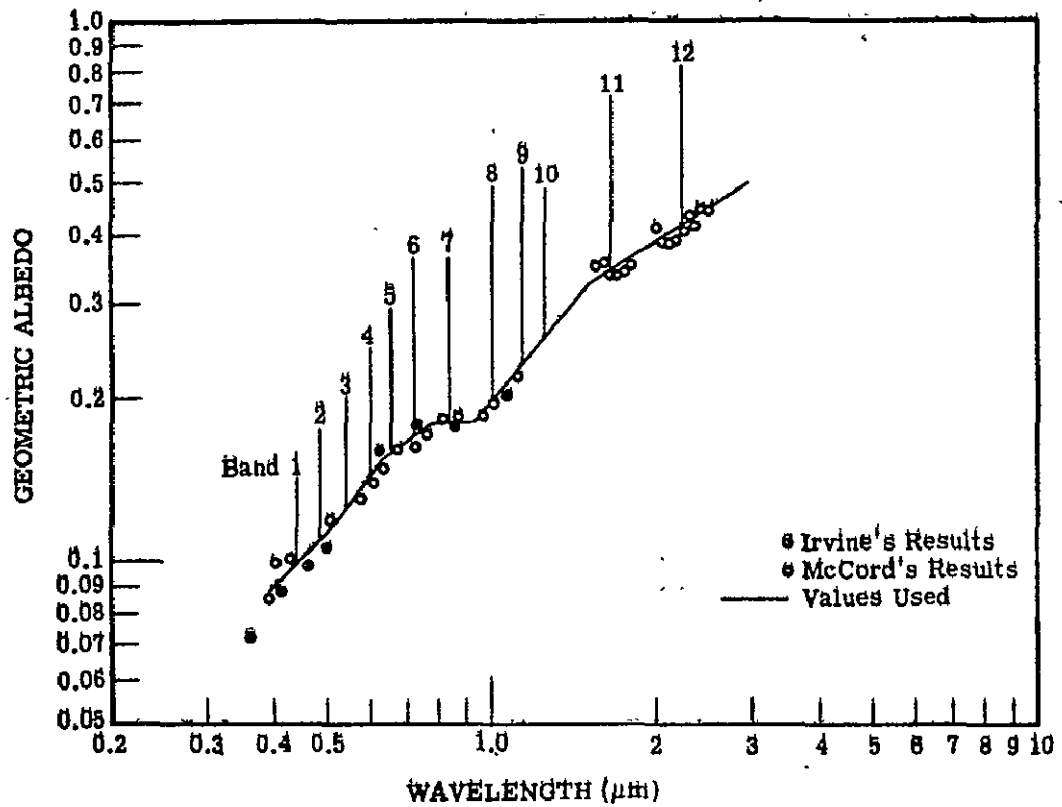


Figure A.11-1.- Geometric albedo of the moon.

The radiant intensity of the moon is a function of the phase angle (i.e., the angle between the lines joining the center of the moon to the observer and to the center of the sun). This phase function arises partly from the change in projected area of illuminated lunar surface visible to the observer but to a greater extent from the large changes in bidirectional reflectance of the lunar surface as a function of illumination and viewing angles. (The bidirectional reflectance increases dramatically as the phase angle is reduced from 5° to 0° . It was therefore decided during the planning of the EREP SPE to avoid very small phase angles during lunar calibration passes. Phase angles of about 15° were in fact used.)

As explained earlier it was decided to use the (spectral) geometric albedos given in Table VIII of the Irvine paper. It is a straightforward procedure to apply relative changes of spectral magnitude with lunar phase to these results. To obtain the absolute spectral radiance of the moon, solar spectral irradiance values at the mean earth-sun distance were taken from the Air Force Cambridge Handbook. The procedures used are outlined below.

According to Irvine, et al, the geometric albedo ρ of the full moon is given by the relationship:

$$\log \rho = 0.4(m_\odot - m_\epsilon) - \log \sin \sigma$$

where σ = the angular radius of the moon at the observer m 's are magnitudes defined by:

$$m = -2.5 \log E$$

$$E_\odot = \text{irradiance at the moon due to sun}$$

$$E_\epsilon = \text{irradiance at the earth due to moon}$$

Substituting in Eq. A.II-1 we obtain

$$\log \rho = -\log E_\odot + \log E_\epsilon - \log \sin^2 \sigma$$

or

$$\rho = \frac{E_\epsilon}{E_\odot \sin^2 \sigma} \quad \text{A.II-2}$$

Now

$$E_c = L_c \frac{\text{Area of Moon}}{(\text{Earth-Moon Dist})^2} = L_c \pi \sin^2 \sigma$$

where L_c is the mean radiance at the moon.

Substituting in Eq. A.II-2 we obtain

$$L_c = \frac{\rho E_\odot}{\pi}$$

It is convenient to consider the unprimed quantities as representing the case of zero lunar phase (i.e., full moon) and mean sun-moon distance, and then to write

$$L' = \frac{\rho' E'_\odot}{\pi} \quad \text{A.II-3}$$

where primes indicate values at the time of the lunar calibration period. Then, by the inverse square law, we can put

$$E'_\odot = E_{\odot\odot} \left(\frac{R^2}{R'^2} \right) \quad \text{A.II-4}$$

where $E_{\odot\odot}$ = irradiance due to sun at the mean sun to earth distance

R = mean sun to earth distance

R' = sun to moon distance at the time of the lunar calibration

Then, in order to correct for phase angle variation Δm we put

$$\Delta m = m' - m = -2.5 \log \left(\frac{\rho' E'_\odot}{\pi} \right) + 2.5 \log \left(\frac{\rho E_\odot}{\pi} \right)$$

or

$$\rho' = \rho \operatorname{antilog} \left[\frac{-\Delta m}{2.5} \right] \quad \text{A.II-5}$$

Substituting Eqs. A.II-4 and A.II-5 into Eq. A.II-3 we obtain

$$L'_{\text{c}} = \frac{1}{\pi} E_{\odot} \left(\frac{R^2}{R^2 + 2} \right) \rho \operatorname{antilog} \left[\frac{-\Delta m}{2.5} \right]$$

Rearranging and putting in terms of spectral quantities,

$$L'_{\text{c}(\Delta\lambda)} = \frac{R^2}{\pi R^2 + 2} E_{\odot(\Delta\lambda)} \rho_{\Delta\lambda} \operatorname{antilog} \left[\frac{-\Delta m}{2.5} \right]_{\Delta\lambda} \quad \text{A.II-6}$$

Appropriate values for Δm for each LC were obtained by interpolation and extrapolation from the results of Irvine's Table V. Figure A.II-2 illustrates this process for the phase angles of LC_s 1 and 2, 12°44' and 15°57' respectively. (The phase angles for LC_s 3, 4 and 5 were intermediate: 13°09', 14°33' and 13°18' respectively.) It will be seen that Bands 1 through 8 are well covered by the available results and that the extrapolation to Bands 9 and 10 seems unlikely to be in serious error. However, for Bands 11 and 12 a considerable extrapolation has to be made so the results for these bands are suspect, particularly those for Band 12.

Returning to Eq. A.II-6, $L'_{\text{c}(\Delta\lambda)}$ is the mean spectral radiance of the lunar disc facing the observer with the unilluminated area included in the average. All the terms on the right can be derived from the references cited or from the Astronomical Ephemerides and the appropriate EREP Postpass Summary Reports. As explained, the phase angle correction is found by interpolation from Table V of Irvine's paper. This however requires a knowledge of the phase angle of the moon at the time of measurement. The phase of the moon referred to the center of the earth is given as a function of time in Hartung's Lunar Ephemeris.* The phase angle referred to the SKYLAB at the time of the lunar calibration differed from this value by less than one half degree. A relatively elaborate calculation was used to obtain the true phase angle to the nearest minute of arc, though in retrospect the additional accuracy this gave to the phase angle correction was hardly necessary.

*Ann D. Hartung, Lunar Ephemeris and Selenographic Coordinates of the Earth and Sun for 1973 and 1974, NASA Report No. BP-3058, Scientific and Technical Information Office, Washington, D.C., 1972.

The spectral radiances found using Eq. A.II-6 were weighted by the spectral response (R) of the several S192 bands using the formula

$$\frac{\int L_i R_i d\lambda}{\int R_i d\lambda} = \frac{\sum L_i (\Delta\lambda_j) R_i (\Delta\lambda_j)}{\sum R_i (\Delta\lambda_j) \cdot \Delta\lambda_j} \quad \text{A.II-7}$$

Here 'i' is the band number and $\Delta\lambda_j$ is a series of adjacent wavelength intervals over which L and R had been tabulated. Generally the $\Delta\lambda_j$ were the intervals for which the solar irradiance was tabulated in the Air Force Cambridge Handbook. However at the longer wavelengths these intervals become wider than the structure of the R. For these, therefore, suitable narrower intervals were selected and interpolation was used to obtain the necessary values of E_0 . This particular method of weighting was used to make our results directly comparable with terrestrial scene results presented in Figure 3.4.1-1 and Section I of this Appendix.

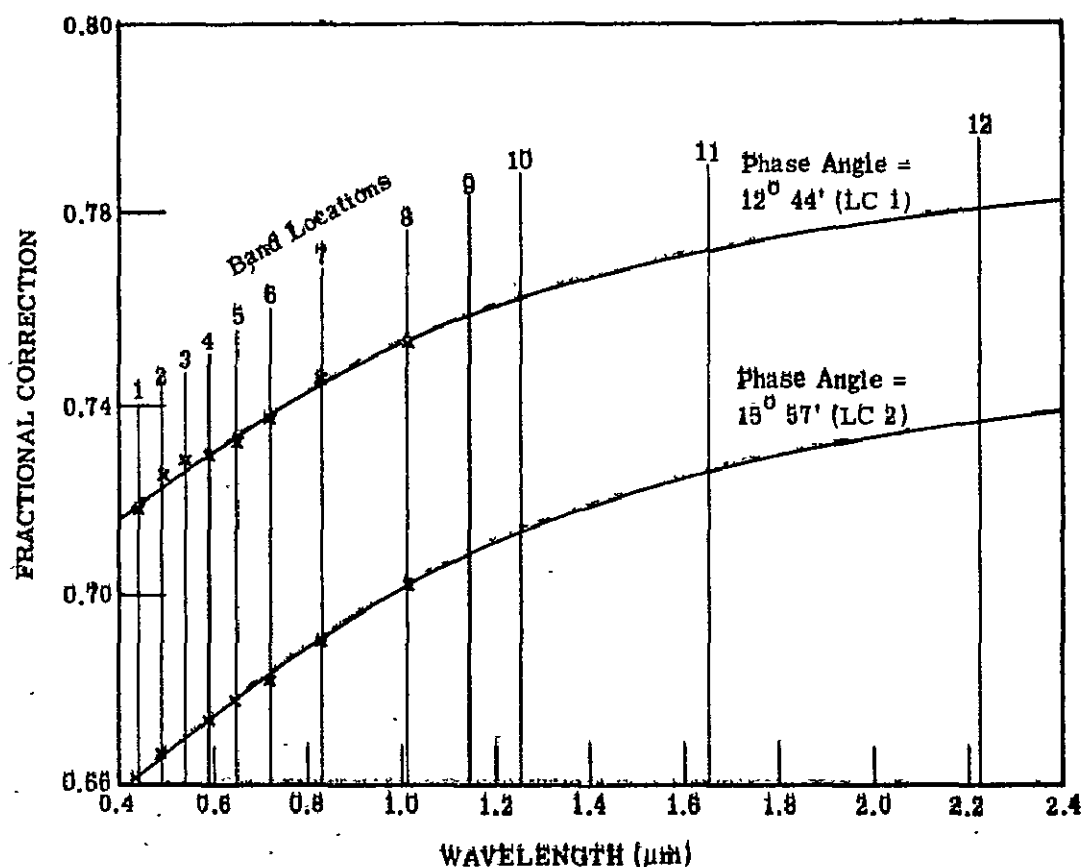


Figure A.II-2.- Correction for lunar phase angle.

The input data for Eq. A.II-7 was tabulated as illustrated in Table A.II-1. The contents of the tables were punched onto paper tape and the integration carried out on the computer. New phase corrections and ranges were calculated for each lunar calibration, punched onto a tape used to correct the earlier tape, and a new integration carried out. This exercise was also carried out for LC 6 but the complications introduced by the large phase angle, $72^{\circ}25'$, and the severe frequency distortion in most S192 bands have prevented completion of a calibration for this LC. The resulting estimated lunar radiances normalized by band may be seen in Table A.II-2.

MEAN SIGNAL LEVELS FROM THE LUNAR DISK

Having obtained the mean radiances of the moon it remains to find the corresponding mean S192 outputs and calibration levels.

During each LC the SKYLAB was rotated about an axis parallel to the middle of the scan line in such a way that the scan lines moved onto and across the moon with about 95% overlap. Thus when an image of the moon is developed in the ordinary way from the recorded data the moon appears elongated by about 20:1.

For each LC a block of data was selected in which the first scan line was about 20 lines in front of the moon and the last one about 20 lines after it, as shown in Figure A.II-3. The same section was used from each scan line. This was about 250 pixels in length, so that every section started at least 20 pixels before the moon. As the diameter of the moon in the scan line direction was about 55 pixels, this left at least 175 pixels of deep space after the trailing edge of the moon. This was done so that the signal overshoot and decay following the moon could be taken into account. As the moon lay approximately in the middle of the scan in each LC the effects of scan line curvature were very small and were ignored. The block of data selected was processed in the computer to give the mean count level for each column of pixels and also a cumulative total to facilitate manual data manipulation. The mean count value for each word of the high and low calibration signals was printed out at the same time.

In principle the mean count value over the moon can be found by multiplying the mean count value for a block of data enclosing the moon by the number of pixels in this block of data divided by the number of pixels falling inside the lunar circumference. In practice a series of uncertainties were encountered.

(1) There is uncertainty regarding the extent to which the frequency response of the several bands changes with the radiance being reviewed. The detectors used in the S192 proved to be nonlinear. The frequency response of the amplifiers was shaped so that the resulting detector-plus-electronics frequency response was optimum for typical terrestrial scene levels and the degraded response at other levels accepted. Thus it was not surprising when examination of plots of scan lines crossing the moon showed, in most bands, a considerable negative overshoot immediately following the lunar trailing edge followed by a recovery and then a slow decay. A typical example is shown in Figure A.II-4.

TABLE A.II-1.- SAMPLE OF TABLE CONSTRUCTED TO FACILITATE
CALCULATION OF MEAN LUNAR RADIANCE BY BAND

Interval No.	$\Delta\lambda$ (μm)	$E_{\Delta\lambda}$ ($\text{Wm}^{-2}\Delta\lambda^{-1}$)	R_1	R_2	R_3	R_4	R_5 to R_{12}	$\rho_{\Delta\lambda}$	$\theta_{\Delta\lambda}$
21	0.500-0.505	9.80	0.01	0.50	0.93	0.07	0	0.116	0.717
22	0.505-0.510	9.80	0.01	0.43	0.98	0.12	0	0.117	0.717
23	0.510-0.515	9.65	0.01	0.36	0.998	0.21	0	0.118	0.718
24	0.515-0.520	9.60	0.01	0.26	0.99	0.33	0	0.120	0.718
25	0.520-0.525	9.65	0.01	0.15	0.93	0.56	0	0.121	0.718

R_i is the relative spectral response of Band i.

$\rho_{\Delta\lambda}$ is the lunar albedo extrapolated to zero phase angle.

$\theta_{\Delta\lambda}$ is the fractional correction for phase angle which must be re-entered for each lunar calibration.

TABLE A.II-2.- ESTIMATED LUNAR RADIANCE NORMALIZED BY BAND, I
milliwatts $\text{cm}^{-2} \text{sr}^{-1}$ per bandpass

Band	KSC* Panel Radiance	LC1 12 ⁰⁴⁴ ' $0.400 \times 10^6 \text{ km}^{**}$	LC2 15 ⁰⁵⁷ ' 0.395 km^{**}	LC3 13 ⁰⁰⁹ ' 0.384 km^{**}	LC4 14 ⁰³³ ' 0.355 km^{**}	LC5 13 ⁰¹⁸ ' 0.352 km^{**}
1	0.92	3.99	3.70	4.02	4.05	4.19
2	1.52	5.02	4.65	5.06	5.09	5.27
3	2.34	5.31	4.93	5.36	5.40	5.58
4	3.02	5.68	5.27	5.73	5.78	5.97
5	4.13	5.74	5.34	5.80	5.85	6.04
6	5.24	5.40	5.03	5.46	5.50	5.69
7	6.54	4.30	4.02	4.35	4.40	4.54
8	6.46	3.35	3.16	3.38	3.42	3.53
9	6.09	3.07	2.88	3.10	3.15	3.25
10	5.57	2.78	2.62	2.81	2.86	2.94
11	3.39	1.62	1.53	1.64	1.67	1.72
12	1.51	0.74	0.70	0.75	0.76	0.78

*Values derived from Optronic Laboratories Letter Report to Mr. Richard Juday/TF3, NASA, Johnson Space Center, Houston, Texas, 17 January 1974.

**Phase angles and sun-moon ranges given are those which existed at the time of each LC.

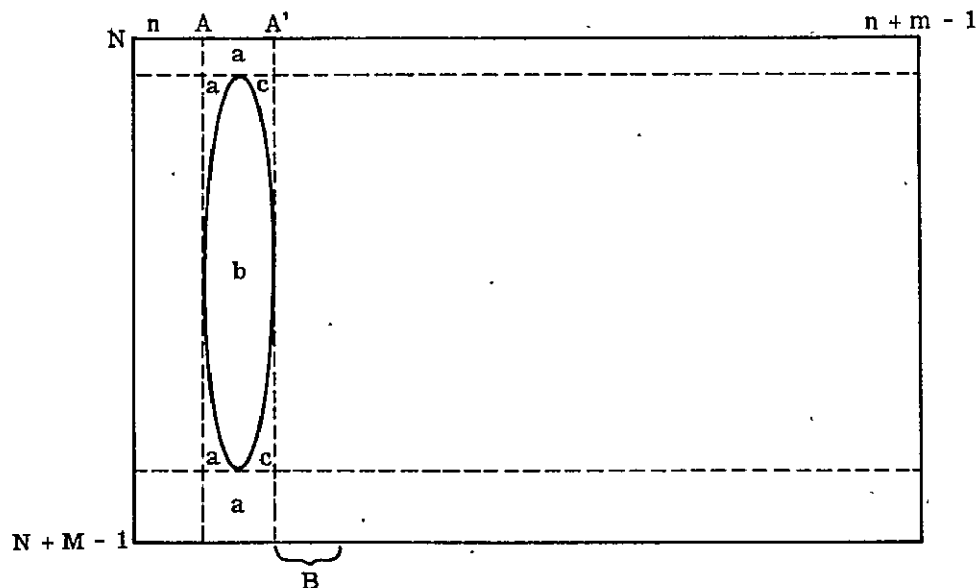
Limited investigation of frequency response effects based on the SL2 data suggested that frequency response, except for Band 1, was much better for normal scene radiances than for the darkness of deep space. Under these circumstances the lagging signals are an artifact of the system nonlinearities and should be excluded from the mean signal calculated for the moon.

To follow the way in which this was done refer to Figure A.II-3. The block of data from scan lines N to $(N + M - 1)$ and from pixels A to A' was used. A and A' were the pixel traces judged to overlap the edge of the moon. The total of the outputs for each pixel in this rectangle can easily be formed from the printout referred to above. From this total must be subtracted the residual signals in areas a and b and the residual plus lagging signals in areas c . From areas a the contribution of the raw residual signals is removed. For the lunar area b residual signals corrected for clipping are removed. For areas c corrections for the lagging lunar signals must be made. These corrections for the lagging lunar signals must be made. These corrections were estimated by inspection of the printout values for columns of pixels immediately following the moon (the region indicated by B). While this last is not a very exact procedure, the corrections for area c are typically about 1% of the total count so even an unlikely 30% error in its estimation would not be very significant.

To investigate the size of errors which might be introduced by these assumptions on frequency response, the mean signals from the moon were calculated from the same computer printouts in an alternative way. Then the average of all pixels from A to $(n + m - 1)$ (Figure A.II-3) was formed, corrected for residual effects by subtracting the mean of all pixels from N to $(A-1)$. The result was then multiplied by the area of the rectangle bounded by pixels A and $(n + m - 1)$ divided by that of the lunar image to give the mean lunar signal. This was equivalent to assuming that each band has constant frequency response and therefore the counts due to the lagging signals following the moon were included in the count. However, as will be seen, the differences between the results given by the two methods are not too significant.

(2) The area of the lunar image was found by inspection from traces of scan lines and pixels crossing orthogonal lunar diameters. Small corrections ($\pm 1\%$) were made for the areas of the moon in shadow at the time of observation. In the scan line direction this could be done with fair accuracy and checked by comparison with an estimate based on the scanning parameters of the S192, and ephemerides and Skylab data from which the size of the moon and the moon-to-SKYLAB distance can be determined. The results are believed accurate to ± 0.25 pixels or $\pm 1/2\%$. As the lunar image was always close to the center of a scan line and occupied less than 65 pixels, effects of scan line curvature were small and have been ignored.

For the long (pixel-trace) diameter the situation was awkward due to the scan line overlap of about 95%. If the moon appeared uniformly bright a pixel trace along the long diameter would appear as a regular trapezoid and it would be a straight-forward matter to estimate the length of the lunar image, which is the distance between the half-down points of the sloping ends of the trapezoid. As the brightness of the moon is quite irregular however, the shoulders



The printout gives the mean count for all pixels in columns n , $n + 1$, $n + 2$, \dots , $n + m - 1$ consecutively. Thus the sum of these values multiplied by M gives the total of all counts in the rectangle of size $m \times M$ pixels.

Figure A.II-3.- Selection of lunar data.

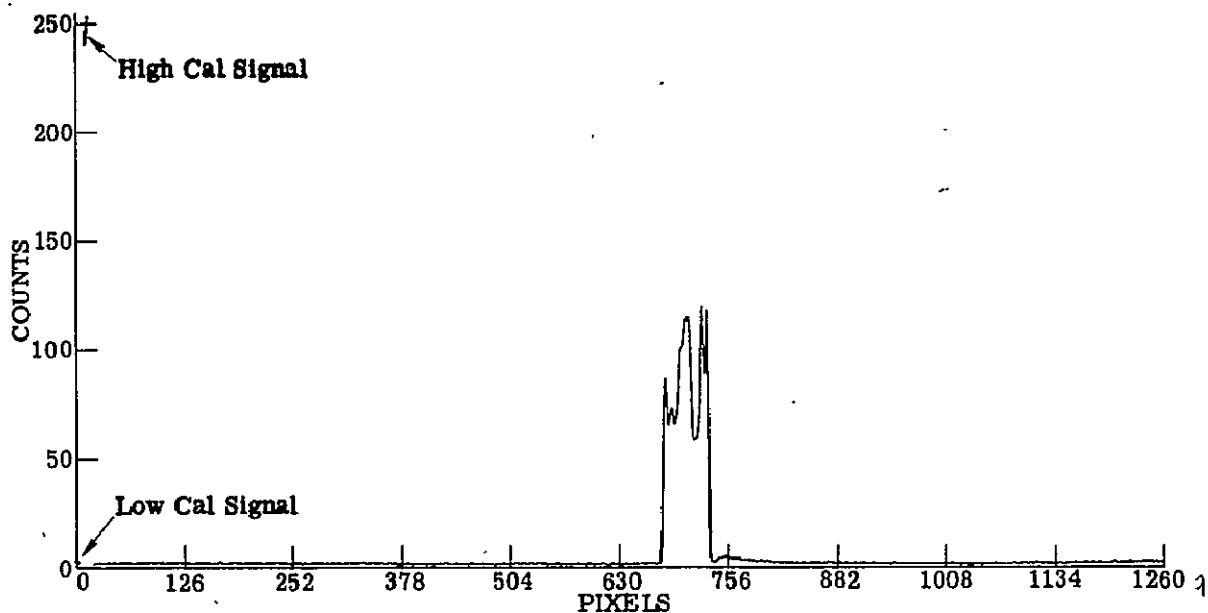


Figure A.II-4.- A-trace of averaged scan line centered on lunar diameter (LC 1, band 6).

of the trapezoid are so poorly defined that it is not possible to determine the half-down points with any accuracy. Consideration was given to solving the problem geometrically, but some formidable coordinate transforms would have been required and it appeared that the SKYLAB ephemeris data was too infrequent (20-second intervals) to allow unambiguous determination of the SKYLAB rotation rate for the 12 to 14 seconds of the observations. However it can be shown that the overall length of the trapezoid L_T is related to the true length L by the expression

$$L = \frac{L_T}{1 + \theta/\Theta}$$

where θ = angular width of scan line

Θ = angular diameter of the moon

This method was used because as θ is known, Θ can be calculated from ephemerides data and L_T can be estimated from appropriate pixel traces to better than $\pm 0.5\%$. Again, corrections were made for the shadowed area of the moon.

III. DETERMINATION OF TRUE MEAN VALUES FROM CLIPPED MEAN VALUES

One of the S192 performance characteristics, scan related system offset, was its response as a function of scan angle to zero radiance input. Deep space was used as a scene with essentially zero radiance. The digital output of S192 ranged from 0 to 255 counts. For low input radiance values, many digital output values were zero. These zero digital values corresponded to any input radiance values that were equal to or less than the input threshold radiance (0.5 equivalent counts) corresponding to the digital output of zero. A mean of the output values, some of which are zero, was designated a clipped mean, while an unclipped, or true, mean was one taken over values that were not constrained to be zero or greater. The relationship between a clipped mean and its corresponding true mean was obtained in the following manner.

It was assumed that a signal X not constrained to be zero or greater has a true mean and standard deviation of μ and σ , respectively, and a Gaussian noise distribution. The relationship between μ_c , the clipped mean, and μ , σ , and X is given by

$$\mu_c = \int_{0.5}^{255} X e^{-\left(\frac{X-\mu}{\sigma}\right)^2 \frac{1}{2}} \frac{dX}{\sigma\sqrt{2\pi}}$$

The units are the equivalent counts for the analog signal. The integral's lower limit is 0.5 because the action of the analog-to-digital converter was to set all values of the signal X equal to or less than 0.5 equal to zero. This, expressed for μ_c in terms of μ and σ , results in the family of curves shown in Figure A.III-1.

By using the Figure, given a value of the standard deviation, σ , it was possible to convert clipped mean values, μ_c , to true mean values, μ , and thereby determine the S192 response to a zero-radiance scene.

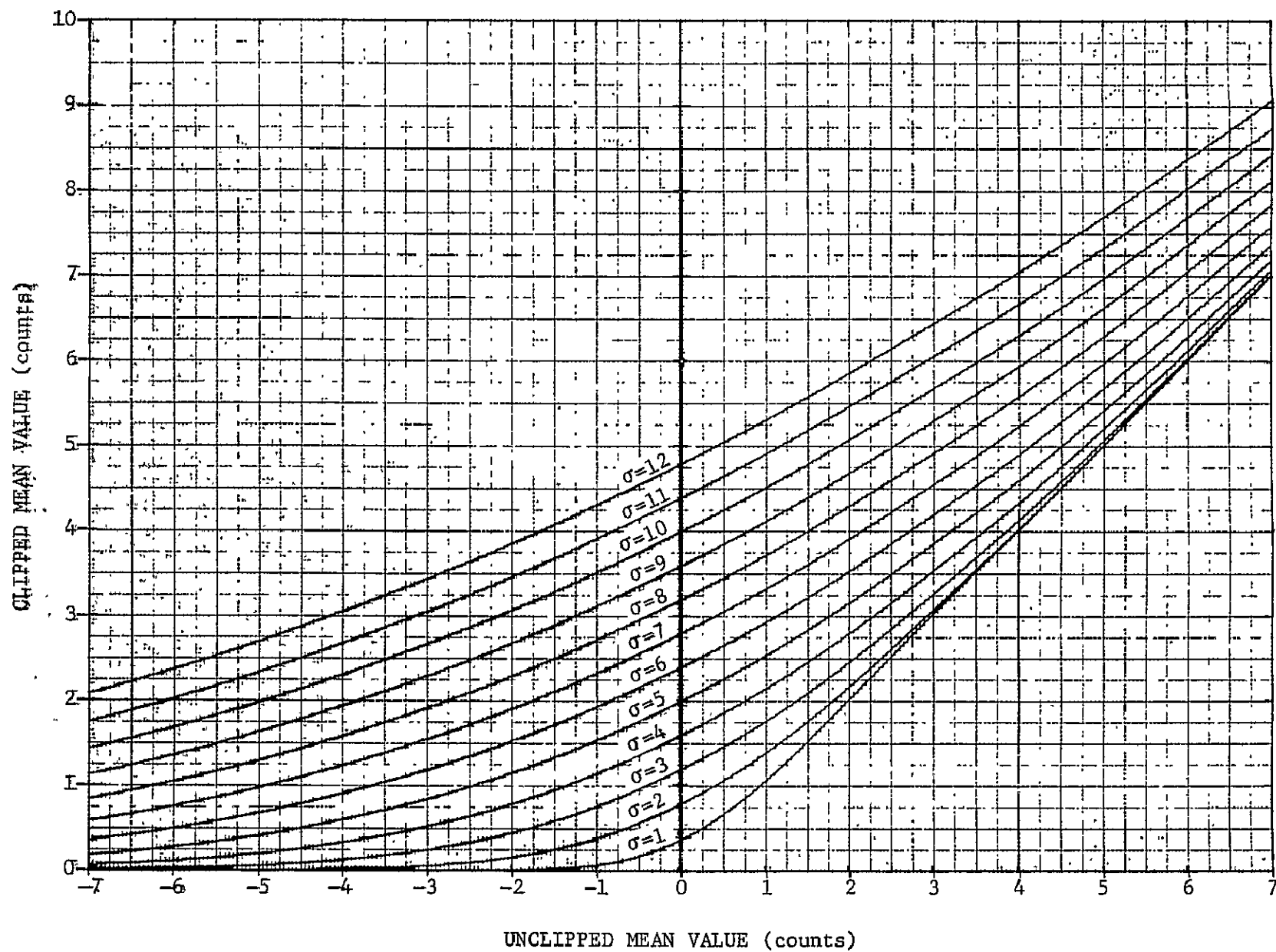


Figure A.III-1.- Correction curves for clipped mean values.

IV. DETERMINATION OF RESPONSE VERSUS SCAN ANGLE CORRECTIONS METHOD FOR BANDS 1 THROUGH 12

To correct raw S192 outputs for scan angle effects an additive and a multiplicative effect are required. These are defined in PHO-TR524* by an equation of the form

$$C'_{ij} = R_{ij} [C_{ij} - Z_{ij} - \bar{C}_L] \quad \text{A.IV-1}$$

where i is the band number

j is the pixel number

C_{ij} are raw data in counts

C'_{ij} are the corrected data in counts

\bar{C}_L is the average count value for the Low Calibration Source

R_{ij} is referred to as the Response vs Scan Angle function and Z_{ij} is referred to as the Residual Effect. In an ideal system they would be identically unity and zero respectively. In practice they are not and must be found experimentally.

Z can be found easily by viewing a black scene for which C is zero so that

$$Z_{ij} = C_{ij} - \bar{C}_L \quad \text{A.IV-2}$$

Before launch a test panel in total darkness was used. In orbit, deep space viewed during the lunar calibration (LC) periods provided an ideal scene for this purpose. Tapes of raw data were obtained for each LC. Usually one sample before and one after the moon were used, both being spaced as far from the moon as possible, using available data.

However a major problem arose in using this data, in that the S192 digital system translates negative numbers as zeros. Thus the noise and negative values occurring in the residual signals cause many negative output values to be recorded as zeros. As a result each pixel value in an averaged scan line tends to be offset by this clipping of the negative values. The method described in Section III of this Appendix was used to "unclip" the clipped values.

*Philco-Ford Corporation, Earth Resources Production Processing Requirements for EREP Sensors, NASA Report No. PHO-TR524 Rev. A, Change 2, Johnson Space Center, Houston, Texas, 1974.

A computer program was written which implemented the "unclipping" scheme on a pixel by pixel basis. All the results given here have been corrected using this "unclipping" program.

Having found Z using Eq. A.II-2, R can then be found using data from a uniform scene, for which C is constant.

To obtain results for flight conditions, S192 screening films were searched for uniform or at least homogeneous scenes. These proved more difficult to find than had been expected. Most of the data used was of agricultural areas which appeared homogeneous, though inspection of averaged scan lines formed from this data led us to reject some samples. In the rejected samples the averaged scan lines appeared much less smooth than those generated from pre-launch data. A few ocean scenes were used for Bands 1 through 5. Unfortunately these scenes, though often appearing highly uniform, give outputs which are too low to be of any value for Bands 6 through 12. One desert and one cloud scene were used but otherwise such scenes were never uniform on the scale (40 miles) required. In some scenes an apparent scan angle effect may occur due to changes in the bidirectional reflectance of the scene as the azimuth of the viewing angle changes throughout the scene. To reduce the effects of gradients introduced in this way or by other scene anomalies, the results for several scenes were used.

In the use of Eq. A.IV-1 in this way the scale of G' is defined by putting the average value of $1/R_1$ equal to unity. Averaged curves for R and Z were formed for each mission or mission section when a change in the system configuration of the instrument made this desirable. These averaged curves were then fitted by least squares techniques, by sixth order polynomials, or for some of the Z 's, by two such polynomials pieced together to give a smooth junction between the two parts of the curve. Curve fitting in this way proved a satisfactory way of smoothing the noise and small scene artifacts left after the averaging processes described above.

METHOD - BAND 13

As explained previously deep space data can be used in a straightforward way to obtain residual effects results (Z_1) for the visible near-IR, Bands 1 through 12.

Unfortunately, for Band 13 this cannot be done as the low end of the recorded dynamic range corresponds to a radiance high enough that the deep space data is completely clipped.

Explained below is the alternative method which has been used with Band 13 flight data to obtain estimates of the scan response function and residual effects correction.

As explained previously the scale of R is fixed by normalizing R_{ij} so that for each Band (i), $(\overline{I/R_j})$ is unity. Thus by averaging Eq A.IV-1 over j we can write for a uniform scene

$$C'_{ij} = \overline{C}_{ij} - \overline{Z}_{ij} - \overline{C}_{iL} \quad \text{A.IV-3}$$

Substituting back into Eq. A.IV-1 gives

$$\overline{C}_j - \overline{Z}_j - \overline{C}_L = R_j [C_j - \overline{C}_L - Z_j] \quad \text{A.IV-4}$$

where we have dropped the subscript i as we are only considering Band 13.

Then if we have data from two uniform scenes with significantly different \overline{C}_j as denoted by subscripts 1 and 2, we can rewrite Eq. A.IV-4 as a pair of simultaneous equations.

$$\overline{C}_{1j} - \overline{Z}_j - \overline{C}_{1L} = R_j [C_{1j} - \overline{C}_{1L} - Z_j] \quad \text{A.IV-5}$$

$$\overline{C}_{2j} - \overline{Z}_j - \overline{C}_{2L} = R_j [C_{2j} - \overline{C}_{2L} - Z_j] \quad \text{A.IV-6}$$

Subtracting and rearranging we obtain

$$R_j = \frac{\overline{C}_{1j} - \overline{C}_{2j} - \overline{C}_{1L} + \overline{C}_{2L}}{C_{1j} - C_{2j} - \overline{C}_{1L} + \overline{C}_{2L}} \quad \text{A.IV-7}$$

which gives R_j in terms of quantities which can readily be derived from the data. As R_j is now known we can rearrange Eq. A.IV-5 to give Z thus

$$Z_j = C_{1j} - C_{1L} - \frac{1}{R_j} [C_{1j} - C_{1L}] + \frac{\overline{Z}_j}{R_j} \quad \text{A.IV-8}$$

The terms in Eq. A.IV-8 are known except for \overline{Z} . Inspection of Sections 5.3.9.1 and 5.3.9.2 of PHO-TR524 shows that the origin of the C' scale for Band 13 must be selected so that scene elements for which $C' = 0$ have the same radiance as the low calibration source.

Thus we must have

$$C'_j = k_1 (L_{Sj} - L_L) \quad \text{A.IV-9}$$

where k_1 = a constant which determines the scale of C

L_{Sj} = radiance of scene element j

L_L = radiance of the low calibration source

Combining this with Eq. A.IV-1 we obtain

$$\frac{L_{Sj}}{R_j} = \frac{1}{k_1} (C_j - \bar{C}_L) - \frac{Z_j}{k_1} + \frac{L_L}{R_j} \quad \text{A.IV-10}$$

For uniform scenes we can average over j obtaining

$$L_{Sj} = \frac{\bar{C}_j - \bar{C}_L}{k_1} - \frac{\bar{Z}_j}{k_1} + L_L \quad \text{A.IV-11}$$

Thus we see that if data from uniform scenes of known radiance are used to find L_L it will not be possible to separate it from the constant term in

Eq. A.IV-11, viz:

$$-\frac{\bar{Z}_j}{k_1} + L_L$$

Thus if Band 13 is to be calibrated in this way we are free to assign any value we may choose to \bar{Z}_j . We have chosen to assign the value zero to \bar{Z}_j partly for convenience and partly because in the absence of a valid calibration this is the most probable value for this constant, as in an ideal scanner Z_j would be zero for all j .

In practice we used the scene (or an average of two scenes) which appeared to be most uniform in Band 13 as scene 1 and derived R_j using this together with each of the remaining scenes. The average for each j of the R_j found in this way was then formed and plotted as the best available values of R_j and was also used with the scene data to give Z_j with the assumption $\bar{Z}_j = 0$.

We can however demonstrate that Eq. A.IV-3 provides an accurate description of the way a thermal scanner actually operates and thereby find a value for \bar{Z}_j in terms of system parameters.

For such a scanner a non-uniform scan angle response implies that the optical transmission is a function of scan angle. However, when the transmission is less than unity the optics must have emissivity and/or reflectivity in complement:

$$t + r + e = 1$$

where t = transmissivity

r = reflectivity

ϵ = emissivity

Thus assuming that the S192 optics and its surroundings have a uniform temperature T we can write the apparent radiance of the scene as modified by the optical train

$$L = tL_s + (r + \epsilon)P(T)$$

where L_s is the scene spectral radiance integrated over Band 13 and $P(T)$ is the corresponding radiance of a black body with a temperature T . If the system is not at uniform temperature we can find an effective P_j for each scan angle provided the temperature distribution does not change with time.

Adding the subscript j to those terms which may be dependent on scan angle, adding a term E_j for electro-magnetic pick up, and using Eq. A.IV-12 we obtain

$$L_j = t_j L_{sj} + (1 - t_j)P_j + E_j \quad \text{A.IV-13}$$

L_j is thus the radiance presented to the detector when the scanner views the scene. If L'_L is the radiance presented to the detector when the scanner views the cold black body used as the internal AOC reference and assuming that the detector is linear we have

$$C_j - \bar{C}_L = k_2(L_j - L'_L) \quad \text{A.IV-14}$$

where k_2 is a constant to be determined experimentally. Substituting from Eq. A.IV-13 we obtain

$$C_j - \bar{C}_L = k_2[t_j L_{sj} + (1 - t_j)P_j + E_j - L'_L] \quad \text{A.IV-15}$$

Substituting in Eq. A.IV-9 gives

$$\frac{C_j - \bar{C}_L}{k_1} = t_j \frac{C'_j}{k_1} + (1 - t_j)P_j + E_j - L'_L + t_j L_L$$

Rearranging, we obtain

$$C'_j = \frac{k_1}{t_j k_2} \left\{ C_j - \bar{C}_L - k_2[(1 - t_j)P_j + E_j - L'_L + t_j L_L] \right\} \quad \text{A.IV-16}$$

This equation is identical in form to Eq. A.IV-1 indicating that Eq. A.IV-1 is valid for band 13 provided the temperature distribution and optical constants of the scanner optics and their surroundings do not change. By comparing coefficients we see that

$$R_j = \frac{k_1}{t_j k_2} \quad \text{A.IV-17}$$

and

$$Z_j = k_2 [(1 - t_j)P_j + E_j - L'_L + t_j L] \quad \text{A.IV-18}$$

While these equations give physical meanings to R_j and Z_j they do not provide means for determining these parameters as several of the terms are unknown in practice.

Thus we are unable to determine the true value of \bar{Z}_j . As demonstrated this is of no moment if an external calibration can be carried out. Putting estimated values into the righthand side of Eq. A.IV-18 we obtained $\bar{Z}_j = 2.6$ counts. However, in doing this it became apparent that this effect was caused by the finite emittance of the primary and secondary minors. In fact, the PDP system makes corrections for this effect when the raw data is converted to radiometric units. Thus, in the absence of an external calibration, $\bar{Z}_j = 0$ is the best estimate we can use for such data. However gradients in transmissivity and emissivity across the optics may produce errors of a few counts.

V. DETERMINATION OF FREQUENCY RESPONSE AND OFF-AXIS REJECTION

Data gathered by S192 when scanning the moon and surrounding deep space were used in determining two sensor performance characteristics. The sharp radiance cutoff at the edge of the moon was used to determine system spatial frequency response. The relatively small solid angle subtended by the moon approximated the ideal point source required to check off-axis rejection, which is a measure of system sensitivity to undesired light scattering or reflecting from S192 surfaces.

A. Frequency Response

A measure of a system's frequency response is its modulation transfer function (MTF), which is the amplitude of the output sine wave divided by the amplitude of the corresponding input sine wave. The MTF is normalized so that its numerical value is one at zero frequency.

One method used to determine a system's MTF is based on its response to an input step function, which instantaneously changes from one constant value to another. Such step function inputs for S192 were approximated during each of the six lunar passes. First, as the S192 scanned from deep space past the leading edge of the moon, and again, in the opposite sense, as the scan went off the trailing edge of the moon and returned to deep space. Because the surface of the moon is not uniform in radiance, its trailing edge provided a more suitable step function for determining MTF than the leading edge.

The image of the moon produced by S192 was a very elongated ellipse because the along-track motion of the S192 field of view was too slow to provide an accurate reconstruction of the lunar image. Because of this characteristic, an average scan line could be obtained from 100 consecutive scan lines chosen so that the moon's trailing edge occurred at essentially the same point in each of them. The scanner output averages from deep space were corrected for clipping as described in Section III of this appendix.

The MTF was obtained from the average scan line by first taking its derivative with respect to scan angle, then a fast Fourier transform of the negative of this derivative, and finally normalizing the transform to one at zero frequency.

B. Off-Axis Rejection

Off-axis rejection is the rejection of undesired light scattering or reflecting from S192 surfaces. It was checked by looking for the presence of a ghost or halo near the edge of the moon.

Two edge geometries were examined. The first was the leading edge of the moon, as discussed in subsection V.A. One hundred consecutive scan lines were averaged, pixel by pixel, along the flight path to determine an average scan line. A plot of these averages as a function of scan angle revealed the presence or absence of a ghost or halo near this edge of the moon. The other lunar edge considered was that encountered when the moon first appeared in the scan, or, in other words, at 90° to the first edge. In this case, 10 consecutive output values centered on the moon were averaged. These averages were determined for consecutive scan lines, starting when S192 scanned only deep space and ending when the scan was well into the moon. A plot of these averages as a function of scan line revealed the presence or absence of a ghost or halo near this edge of the moon.

VI. USE OF POWER SPECTRAL DENSITY PLOTS FOR NOISE EVALUATION

One noise characteristic of concern in S192 data was the noise frequency distribution as represented by power spectral density plots. Let $X(t)$ represent the S192 output as a function of time when scanning a uniform scene. If $X(t)$ is thought of as a voltage applied to a unit resistor, the average noise power P during the time interval from $t = 0$ to T would be

$$P = \frac{1}{T} \int_0^T [X(t) - \bar{X}]^2 dt \quad [\text{A.VI.1}]$$

$$\text{where } \bar{X} = \frac{1}{T} \int_0^T X(t) dt$$

While P would have provided a measure of the noise in the S192 output, it was more useful to determine the power spectral density $S(f)$, where f denotes frequency. $S(f)$ was found by squaring the absolute value of the f^{th} Fourier component of $S(t)$, i.e.,

$$S(f) = \left| \int_0^T e^{j2\pi ft} [X(t) - \bar{X}] dt \right|^2 \quad [\text{A.VI.2}]$$

where

$$j = \sqrt{-1}$$

e = natural log base

$$f = \frac{n}{T} \text{ where } n = 0, \pm 1, \pm 2, \dots, \pm \infty$$

$S(f)$ = power associated with the component of noise whose frequency is f .

P and $S(f)$ are related by

$$P = \sum_{n=-\infty}^{\infty} S\left(\frac{n}{T}\right) \quad [\text{A.VI.3}]$$

The usefulness of the power spectral density, $S(f)$, stemmed from this relationship in that it provided the frequency distribution of the total noise power, P .

It should be noted that false peaks were introduced into the power spectral density plots by the periodic interruptions in the values for $X(t)$ caused by the instrument scanning characteristics. $X(t)$ was only known for that third of the time when the scan was actually occurring. These bogus peaks must be discounted when evaluating the power spectral density plots.

VII. DETERMINATION OF GEOMETRIC DISTORTION

Analysis of S192 geometric distortion used a three-dimensional mathematical model, based on the geometry of the S192 dynamic data acquisition system. The model performed absolute spatial registration of the S192 data. The theory and the mathematical details of the data reduction techniques are given in LEC/ASD Technical Report "Absolute Spatial Registration of the Skylab S192 Conical Scanner Imagery by Means of Dynamic Modeling", August 1973 (LEC #0801). An "S192" computer program in FORTRAN V source language was developed and used for data reduction in accordance with the theory given in LEC #0801 for the S192 sensor geometric performance evaluation. The procedure is given below.

A set of topographic detail points were selected on topographic maps (1:250,000 or larger scale) and also located on the S192 digital image display of the scene being evaluated. The map provided the object space coordinates (geographic, geocentric, geodetic, or local vertical) of these points; whereas, the digital display provided the scan line and sample number counts to locate the same points. The line and sample counts were converted to elapsed time relative to a predefined reference time and were used to obtain the scan direction in the S192 image coordinate system. For each topographic detail point, two observational equations, one each for X and Y coordinates, were then established by the mathematical model, which was based on collinearity between the scan direction and the vector defined by the scanner location and ground point being scanned.

Additional observational equations were written for each of the parameters being solved for by using previous knowledge of the parameters. A weighted least squares solution resulted in the best fit between the set of points in the imagery and on the ground, which resulted in residuals (ΔX , ΔY) in the X and Y coordinates of the points used in the solution. Residuals were also computed at several check points over the entire scene.

Salient features of the mathematical model and the data reduction technique included:

- 1) The earth was considered an ellipsoid of revolution.
(Fishers': Major axis = 6,378,166.00 meters,
Minor axis = 6,356,784.28 meters)
- 2) The rotation of the earth was accounted for.

- 3) Solution for the parameters for absolute registration of data was based on a rigorous least squares method. There were 18 parameters solved for:
 - a) Position vector (X, Y, Z) of the sensor at the reference time for a frame of "data-take";
 - b) Velocity vector ($\dot{X}, \dot{Y}, \dot{Z}$) of the sensor at that time;
 - c) Acceleration vector ($\ddot{X}, \ddot{Y}, \ddot{Z}$) of the sensor at that time;
 - d) Attitude vector (W, ϕ, K) of the sensor at that time;
 - e) Rotational velocity vector ($\dot{W}, \dot{\phi}, \dot{K}$) of the sensor at that time;
 - f) Rotational acceleration vector ($\ddot{W}, \ddot{\phi}, \ddot{K}$) of the sensor at that time.
- 4) The SKYBET (Skylab Best-Estimate Trajectory) information was used to approximate initial values of the parameters in the solution, and in the formation of observational equations from previous knowledge of the parameters, while solving for these by the method of weighted least squares. However, the solution did not depend on SKYBET information, but used it only for an initial approximation of the parameters.
- 5) The mathematical model considered the elevations of the control points, which provided a means to consider terrain topography in resampling to generate a registered data tape. As an extension of the sensor performance evaluation, the technique can be used to generate a registered data tape of a scene.
- 6) Assuming no abrupt discontinuity (due to thrust) in Skylab (or sensor) motion defined by the parameters, the limitation of the mathematical model was the length of the time slice for which data could be registered. However, modifications could be made in the mathematical model to consider any desired time slice of data.

The following products were needed to prepare input data for the computer run to solve the parameters of the mathematical model for registration of S192 scanner data:

- 1) A computer-compatible digital tape to display a selected band (band 7 or 8) that gives the best topographic details in a scene;
- 2) A hard copy of the scene from the Data Analysis Station (DAS) of NASA, Houston, Texas, with an overlay grid of 100 lines X 100 samples over the scene. This product was used to obtain scan line and sample number counts to locate a topographic detail in the scene;
- 3) Topographic maps at 1:250,000 or large scale for the scene. Geographic coordinates of the selected topographic detail points were obtained;
- 4) Relevant SKYBET information needed in the solution.

VIII. USE OF LAKES AS THERMAL CALIBRATION TARGETS

The use of lakes as infrared calibration targets for the thermal band was especially useful because for measurements made at normal incidence their emissivity is greater than 0.98 over most of the spectral region. Figures A.VIII-1 and A.VIII-2 show that the emissivity remains high and the reflectivity low at incident angles up to 60°.

For lakes viewed by Skylab, the radiometric surface temperatures were measured using a PRT-5 radiation thermometer.

When viewing any target less than 4000 meters above sea level (99% of all targets) corrections for atmospheric absorption and re-emission must be made at wavelengths longer than 0.82 micrometers. Therefore, a correction for atmospheric constituent absorption was made.

Atmospheric transmission was calculated using a computer program developed by R. F. Calfee, NOAA, Boulder, Colorado. This program calculated atmospheric transmission by dividing the atmosphere into layers. The required inputs are average temperature, atmospheric pressure, and total water content for each layer. These inputs for most S192 targets were derived from temperature/humidity profiles measured with radiosondes that were balloon launched or dropped from a helicopter at the time of Skylab overflight. These radiosonde data were supplemented by adjacent NOAA network radiosonde data. The NOAA data, as well as the ground-truth team's radiosonde data, were then plotted on skew T log P diagrams. The ground-truth radiosonde data were most heavily weighted in the meteorological analysis performed to arrive at a "composite" water-vapor temperature profile for a particular Skylab observation, but weather features such as cold fronts were also taken into account in developing the "composite" curves. The atmosphere was then divided into convenient layers based on the "composite" profile. Water amounts and representative temperatures were then selected for each layer.

The layer temperature, water amount, and layer thicknesses were used as input parameters to the Calfee atmospheric transmission program, which uses the "compressed line" data* but

* R. McClatchy et.al.: AFCRL Atmospheric Absorption Line Parameter Compilation, AFCRL Environmental Research Laboratory Publication Number 434, Bedford, Massachusetts.

R. F. Calfee & R. Schweisow: Nu Averaged Infrared Absorption Coefficients of Water Vapor, NOAA Technical Report #ERL 274-WPL24, Boulder, Colorado.

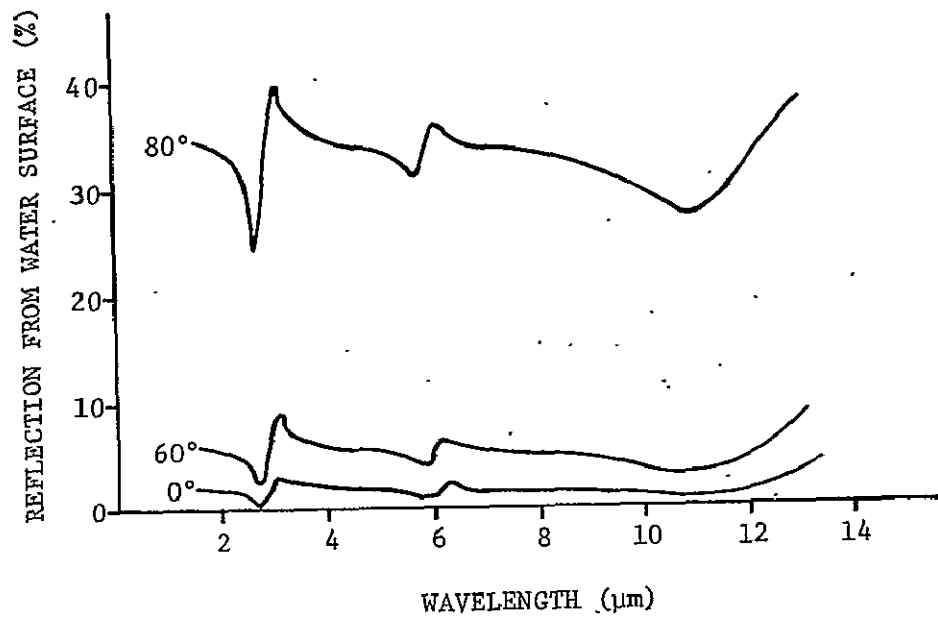


Figure A.VIII-1.- Reflection from water surface at 0, 60, and 80° incidence angles.

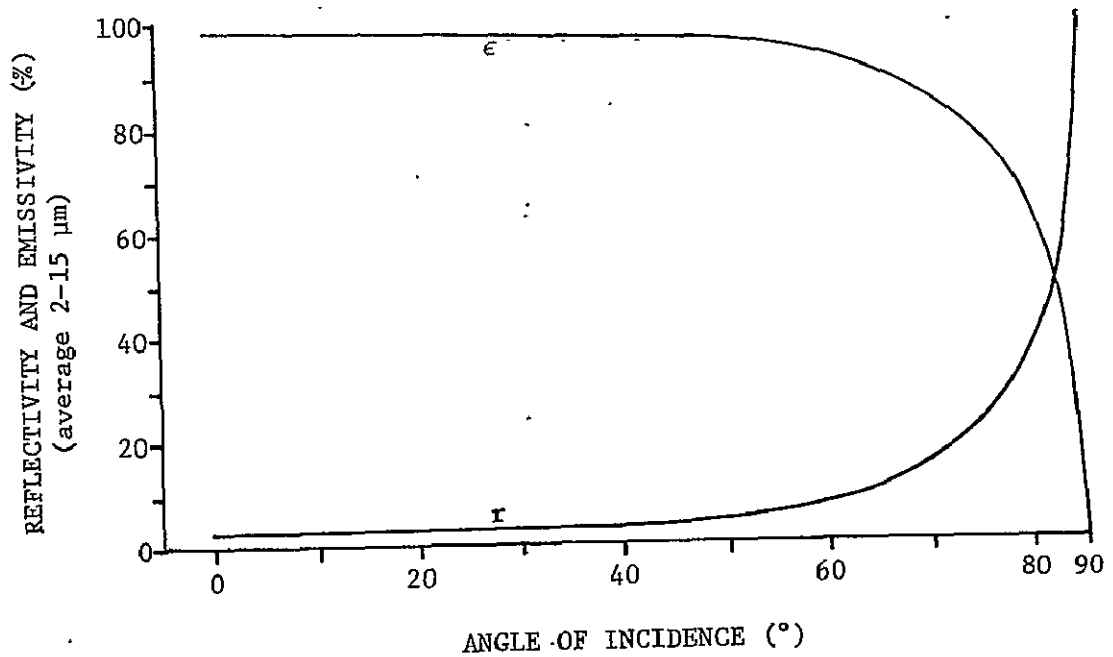


Figure A.VIII-2.- Reflectivity and emissivity of water versus incidence angle.

did not take into account the magnitude of radiation from the target nor the upwelling radiance from each layer. The Calfee program was therefore modified according to the following equation, as illustrated in Figure A.VIII-3:

$$R_{\lambda} = (\tau_1 - 1) B_1 + (\tau_2 - \tau_1) B_2 \tau_1 + \dots + (\tau_n - \tau_{n-1}) B_n \tau_{n-1} + B_t \tau_n$$

where

R_{λ} = radiance above atmosphere at a particular wavelength, λ

B_n = blackbody radiance of nth layer (starting at the top atmosphere layer)

B_t = blackbody radiance of target

τ_n = transmission from space through nth layer.

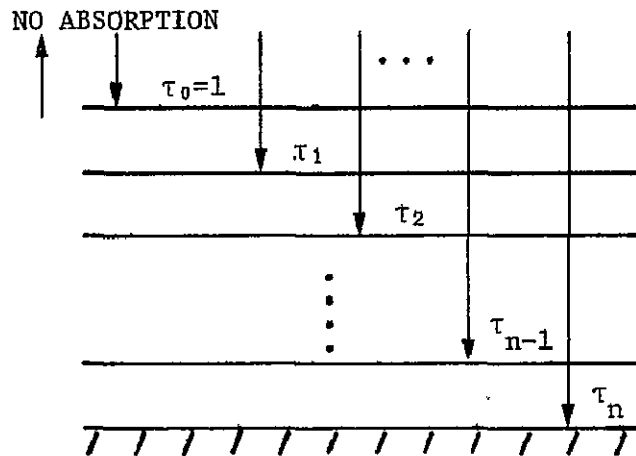


Figure A.VIII-3.- Upwelling radiance calculation.

The radiance at the spacecraft was then adjusted for the thermal-band spectral sensitivity by the technique described for bands 1 through 12 in Section I of this appendix.

The radiances of the two temperature calibration sources were also adjusted for the thermal-band spectral sensitivity. These two calibration source radiances plotted versus their respective S192 output counts defined a straight line that was the thermal-band calibration line. The deviation from this calibration line of the point resulting from the radiance computed above and the corresponding observed S192 output counts was used as a measure of the accuracy of the calibration.